

DYNAMICALLY-CROSSLINKED SELF-ASSEMBLED SMART
MICROGELS FOR DRUG DELIVERY

DYNAMICALLY-CROSSLINKED SELF-ASSEMBLED SMART
MICROGELS FOR DRUG DELIVERY

By

EVA MUELLER, B.ENG.BIOSCI.

A Thesis
Submitted to the School of Graduate Studies
In Partial Fulfillment of Requirements
For the Degree
Master of Applied Science

McMaster University

©Copyright by Eva Mueller, July 2018

Master of Applied Science (2018)

McMaster University

Chemical Engineering

Hamilton, Ontario

TITLE: Dynamically-Crosslinked Self-Assembled Smart Microgels for Drug
Delivery

AUTHOR: Eva Mueller, B.Eng.Biosci. (McMaster University)

SUPERVISOR: Dr. Todd Hoare

NUMBER OF PAGES: i-xiii, 121

Acknowledgements

Throughout my undergraduate and Masters studies here at McMaster, I have been extremely fortunate to be surrounded by the most wonderful people. I owe every single person I have met during this journey a big thank you. A special thank you goes out to the following people who have made my year as a Masters student so memorable:

To my supervisor, Todd Hoare, thank you for going above and beyond with your guidance and support, and for allowing me to grow into an independent researcher. I'm looking forward to the next chapter of exciting research.

To the entire department of chemical engineering at McMaster, thank you for your continuous support.

To Daryl, thank you for introducing me to the world of research and for being the best mentor.

To the entire Hoare Lab, to the ones graduated, to the new members, to Madeline, Nicola, Kelli, Jon, Ali A, Ali B, Fei, Rabia, Trevor, thank you for being the most supportive group, for your countless laughs, allowing me to play the Sunshine Playlist on repeat, and for always helping me out whenever I needed it. You guys are awesome, and I know you will excel in grad school and beyond.

To the Winston family, to Kushal, Angus, Marié, Katya, Uma, thank you for being the best of the best, for always being there during both the good and bad times and for dealing with my silliness every day (that one's for you, Kushal). I couldn't have done it without you.

To my parents, Klaus and Carmen, thank you for your unconditional love and support that have shaped me into the person I am today. Mom, I owe you everything; from driving me to music lessons three times a week, to allowing me to play every sport possible, to being my biggest rock in life. Dad, you are the reason I strive to be a better person each and every single day; thank you for making it possible to live in two of the best countries in the world.

To my brother, Tim, and sister-in-law Brittany, thank you for always supporting me and being the voice of reason during this crazy life of mine. You have no idea how much I appreciate it all.

To everyone, my friends and teammates, thank you from the bottom of my heart and I can't wait to do it all again. Here's to the next chapter full of memories and smiles!

Table of Contents

Acknowledgements	iv
Table of Contents	v
List of Abbreviations	xii
Declaration of Academic Achievement	xiii
Lay Abstract	1
Abstract	2
Chapter 1: Introduction	4
Hydrogels	4
Microgels	4
Microgel Fabrication Techniques	5
Microgel Applications	7
Drug Delivery	8
Sustained Drug Release	9
On-Demand Drug Release	9
Microgel-Based Drug Delivery	11
Hydrophobic Drug Delivery	11
Temperature/pH Specific Cancer Drug Delivery	12
Objectives	14
Chapter 2: Structural Analysis and Direct Drug Loading of Uncharged PNIPAM	
Microgels	15
Summary	15
Literature Review	17
Objectives	23
Experimental Section	24
Materials	24
Prepolymer Synthesis	24
Microgel Particle Size Measurements	25
Microgel Fabrication	26
Small-Angle Neutron Scattering (SANS)	27
Ultra-small Angle Neutron Scattering (USANS)	29
Neutron Scattering Data Analyses	29
Langmuir Trough	30
Drug loading and Release Experiments	31
High Performance Liquid Chromatography	32
Results	33
Microgel Particle Size	33
SANS of PNIPAM-Hzd Nanoaggregates	34
SANS of Self-Assembled PNIPAM Microgels	35
Contrast Matching Experiment	40

SANS of Self-Assembled Layered PNIPAM Microgels	43
Langmuir Trough	45
Drug Loading Efficiencies	47
Drug Release Study	48
Discussion	50
Conclusion	52
Chapter 3: Fabrication and Characterization of Charged and Amphoteric Self-Assembled PNIPAM Microgels	54
Summary	54
Literature Review	55
Objective	60
Experimental Section	61
Materials	61
Prepolymer Synthesis	62
Prepolymer Characterization	64
Microgel Particle Size and Charge	64
LCST Measurements	65
Microgel Fabrication	65
Results and Discussion	66
Polymer Characterization	66
Single Charged Microgels	68
Amphoteric Microgels	72
Conclusion	76
Chapter 4: Conclusion and Future Outlook	77
Conclusions	77
Future Experiments	79
References	85
Appendices	93
Appendix A: Chapter 2 Supplementary Information	93
Appendix B: Chapter 3 Supplementary Information	104

LIST OF FIGURES

- Figure 1.1:** Thermally-driven self-assembly approach for fabricating degradable PNIPAM microgels. Adapted from Mueller et al.²⁶ 7
- Figure 1.2:** (a) Comparison between conventional drug release profile and controlled release with respect to the drug therapeutic concentration range, and (b) The difference between controlled release and on-demand (pulsatile) release. Reproduced from Santini et al.⁴⁰ 9
- Figure 1.3:** Chemical structure of dexamethasone 11
- Figure 2.1:** Schematic of precipitation/self-assembly process used to fabricate degradable microgels from functional PNIPAM oligomers and anticipated structures of resulting microgels depending on the diffusibility of the PNIPAM-Ald crosslinker and the permanence of the crosslinks formed. The homogeneous morphology is consistent with the structural characterization results. 27
- Figure 2.2:** Neutron scattering intensity $I(q)$ as a function of the scattering vector (q) as a function of temperature for: (A) 0.05 Ald:Hzd microgel (1 wt% PNIPAM-Hzd); (B) 0.20 Ald:Hzd microgel (1 wt% PNIPAM-Hzd); (C) 0.05 Ald:Hzd microgel (2 wt% PNIPAM-Hzd). Solid black lines represent the fits, and standard deviations of the fits are plotted as error bars. 37
- Figure 2.3:** Key fitting parameters of the SANS analysis on bulk self-assembled PNIPAM microgels: (A) microgel radius versus temperature; (B) correlation length versus temperature. 38
- Figure 2.4:** Combined SANS and USANS intensity versus q profiles (and fits) for index-matched d7-PNIPAM-Hzd (black curve) and index-matched PNIPAM-Ald (orange curve) in self-assembled microgels as a function of temperature (0.20 Ald:Hzd ratio, 1 wt% d7-PNIPAM-Hzd). USANS data are highlighted with a dotted black box. Note that while standard deviations of the fits are plotted as error bars, most error bars are too small to be visible on the graph. 41
- Figure 2.5:** Normalized compression isotherms of self-assembled PNIPAM microgels (A) 0.05 Ald:Hzd (1 wt% PNIPAM-Hzd) and (B) 0.20 Ald:Hzd (1 wt% PNIPAM-Hzd) at the n-decane/water interface. 46
- Figure 2.6:** Cumulative drug release profile of dexamethasone from 0.05 Ald:Hzd microgels (n=3) with a first order-fit ($R^2 = 0.91$) 49

Figure 2.7: Cumulative drug release of dexamethasone from 0.05 Ald:Hzd microgels (n=3) as a function of sample number; linear regression plotted with $R^2 = 0.98$	49
Figure 3.1: Schematic for amphoteric self-assembly, illustrating the blending technique. The different colors represent cationic and anionic PNIPAM-Hzd polymers.	66
Figure 3.2: Diameter as a function of pH for single-charged cationic self-assembled PNIPAM microgels with (+)-PNIPAM-Hzd and (0)-PNIPAM-Ald	69
Figure 3.3: Diameter as a function of pH for single-charged anionic self-assembled PNIPAM microgels at 0.10 Ald:Hzd	70
Figure 3.4: Diameter as a function of pH for single-charged anionic self-assembled PNIPAM microgels at 0.20 Ald:Hzd	71
Figure 3.5: Electrophoretic mobility versus pH measurements for cationic, anionic and amphoteric self-assembled PNIPAM microgels at 0.20 Ald:Hzd (in 10 mM NaCl)	73
Figure 3.6: Electrophoretic mobility versus pH measurements for amphoteric self-assembled PNIPAM microgels at 0.20 Ald:Hzd (in 10 mM NaCl) using different ratios of (+)-PNIPAM-Hzd to (-)-PNIPAM-Hzd	74
Figure 3.7: Hydrodynamic diameter as a function of pH for amphoteric self-assembled PNIPAM microgels prepared in 10 mM NaCl with pH adjusted to either acidic (pH 4) or basic (pH 10) conditions in the seed polymer solution.	75
Figure S1.1: Scattering intensity as a function of the scattering vector of hydrazide-functionalized PNIPAM precursors (PNIPAM-Hzd) dissolved in water at (A) 1 wt% and (B) 2 wt%, measured at 70°C (the temperature used for microgel self-assembly based on these PNIPAM-Hzd nanoaggregates). The homogeneously crosslinked model fits are shown as black lines (up to $q=0.2 \text{ nm}^{-1}$). The dotted black lines represent aggregation and are fit to a $M \cdot X^{-4.5}$, where M (amplitude of intensity in arbitrary units) is 3.5×10^{-5} for (A) and 6.5×10^{-5} for (B).	93
Figure S1.2: Neutron scattering intensity $I(q)$ as a function of the scattering vector (q) as a function of temperature for: (A) 0.05 Ald:Hzd microgel (1 wt% PNIPAM-Hzd); (B) 0.20 Ald:Hzd microgel (1 wt% PNIPAM-Hzd); (C) 0.05 Ald:Hzd microgel (2 wt% PNIPAM-Hzd), using the Stieger model. Solid black lines represent the fits and standard deviations of the fits are plotted as error bars.	94
Figure S1.3: Hydrodynamic radius obtained from dynamic light scattering versus temperature for 0.05 Ald:Hzd and 0.20 Ald:Hzd microgels	95

Figure S1.4: Particle size distributions from dynamic light scattering measurements of (A) 0.05 Ald:Hzd (▲) and (B) 0.20 Ald:Hzd (•), fabricated and measured in D ₂ O, as a function of temperature: black (25°C), red (32°C), blue (37°C), green (45°C)	95
Figure S1.5: Scattering intensity as a function of the scattering vector for 0.05 Ald:Hzd (1 wt% PNIPAM-Hzd) self-assembled microgels subsequently mixed with additional PNIPAM-Hzd and/or PNIPAM-Ald polymers (treatment sequences as indicated in legend). Scattering profiles were measured in D ₂ O at 25°C. Solid black lines represent the fits, while the standard deviations of the fits are plotted as error bars.	96
Figure S1.6: Surface pressure as a function of un-normalized area for (a) 0.05 Ald:Hzd (1 wt% PNIPAM-Hzd) and (b) 0.20 Ald:Hzd (1 wt% PNIPAM-Hzd) self-assembled microgels	97
Figure S2.1: Reaction mechanism for PNIPAM-Hzd-AA	104
Figure S2.2: NMR Spectra for acrylate hydrazide monomer: (A) ¹ H NMR (600 MHz; DMSO): δ 9.79 (s, 1H), 8.84 (s, 1H), 6.21-6.16 (m, 2H), 5.71 (dd, <i>J</i> = 9.2, 3.1, 1H), 1.41 (s, 9H), (B) ¹³ C NMR (150 MHz; DMSO): 164.19, 155.20, 129.34, 126.75, 79.17, 28.03.	105
Figure S2.3: ¹ H NMR for (+)-PNIPAM-Hzd	106
Figure S2.4: ¹ H NMR for (-)-PNIPAM-Hzd	106
Figure S2.5: ¹ H NMR for (+)-PNIPAM-Ald	107
Figure S2.6: ¹ H NMR for (-)-PNIPAM-Ald	107
Figure S2.7: Isoelectric point as a function of % cationic charge in amphoteric self-assembled PNIPAM microgels	108

LIST OF TABLES

Table 2.1: Dynamic light scattering size and polydispersity measurements on microgels in solvents used for SANS/USANS analysis	34
Table 2.2: Best fit parameters for fuzzy sphere model fit of PNIPAM-Hzd nanoaggregates at 70°C; see Supporting Information Fig. S1.1 for raw data and fit curves.	35
Table 2.3: Best-fit parameters from homogeneous network fits of the combined USANS/SANS data for self-assembled microgels fabricated with d7-PNIPAM-Hzd and PNIPAM-Ald examined using contrast matching experiments sequentially hiding (A) the d7-PNIPAM-Hzd polymer and (B) the PNIPAM-Ald polymer	41
Table 2.4: Best-fit parameters from homogeneous network fits of the SANS data for layer-by-layer self-assembled microgels based on a 0.05 Ald:Hzd (1 wt % PNIPAM-Hzd) microgel core (solvent = D ₂ O), measured at 25°C	44
Table 2.5: Drug loading efficiency for <i>in situ</i> dexamethasone loading during self-assembly	47
Table 3.1: Chemical structures of charged co-monomers in PNIPAM polymerizations	62
Table 3.2: Charged PNIPAM polymer characterization	66
Table 3.3: LCST for PNIPAM polymers at different pH values	67
Table 4.1: Drugs to be tested in future drug loading and release experiments	80
Table 4.2: Samples to be measured and analyzed using SANS and uSANS	82
Table S1.1: Chi squared (χ^2) goodness of fit parameters for the homogeneously cross-linked model and the Stieger model for three bulk self-assembled PNIPAM microgels, measured at 25°C. The similarity between the χ^2 values for both fits suggests the additional complexity of the Stieger model is not necessary to fit the data accurately, suggesting that the self-assembled microgels are internally homogeneous.	98
Table S1.2: Chi squared (χ^2) goodness of fit parameters for the homogeneously cross-linked model and the Stieger model for four layered self-assembled PNIPAM microgels, measured at 25°C. As in Table S1, no significant difference exists between the quality of the model fits using the two models, suggesting the added complexity of the core-shell model is unnecessary to fit.	99

Table S1.3: Summary of fitting parameters for bulk self-assembled PNIPAM microgels using the homogeneous sphere model ($\sigma_{fuzzy} = 0$): (a) 0.05 Ald:Hzd (1 wt% PNIPAM-Hzd); (b) 0.20 Ald:Hzd (1 wt% PNIPAM-Hzd); (c) 0.05 Ald:Hzd (2 wt% PNIPAM-Hzd)	100
Table S1.4: Fitting parameters for bulk self-assembled PNIPAM microgels using the homogeneous sphere model ($\sigma_{fuzzy} = 0$), using IDL for analysis: (a) 0.05 Ald:Hzd (1 wt% PNIPAM-Hzd); (b) 0.20 Ald:Hzd (1 wt% PNIPAM-Hzd); (c) 0.05 Ald:Hzd (2 wt% PNIPAM-Hzd)	100
Table S1.5: Fitting parameters for contrast-matched self-assembled PNIPAM microgels using the homogeneous sphere model ($\sigma_{fuzzy} = 0$), using IgorPro for analysis: (a) index-matched d7-PNIPAM-Hzd; (b) index-matched PNIPAM-Ald	101
Table S1.6: Fitting parameters for layered self-assembled PNIPAM microgels using the homogeneous sphere model ($\sigma_{fuzzy} = 0$), using IDL for analysis: (a) 0.05 Ald:Hzd microgel + PNIPAM-Hzd; (b) 0.05 Ald:Hzd microgel + PNIPAM-Ald; (c) 0.05 Ald:Hzd microgel + PNIPAM-Hzd + PNIPAM-Hzd; (d) 0.05 Ald:Hzd microgel + PNIPAM-Hzd + PNIPAM-Ald	102

List of Abbreviations

AA	Acrylic Acid
DLS	Dynamic light scattering
DMAEMA	2-dimethylaminoethylmethacrylate
EDC	N'-ethyl-N-(3-dimethylaminopropyl)-carbodiimide
HCl	Hydrochloric acid
HPLC	High-performance liquid chromatographic
LCST	Lower critical solution temperature
log P	Octanol-water partitioning coefficient
MW	Molecular weight
NaCl	Sodium chloride
NaOH	Sodium hydroxide
PBS	Phosphate-buffered saline
PDI	Polydispersity index
PEG	Polyethylene glycol
PNIPAM	Poly(N-isopropylacrylamide)
PNIPAM-Hzd	Hydrazide functionalized PNIPAM
PNIPAM-Ald	Aldehyde functionalized PNIPAM
POEGMA	Poly(oligoethylene glycol methacrylate)
VPTT	Volume phase transition temperature

Declaration of Academic Achievement

The work presented in this thesis was written by the author, in consultation of Dr. Todd Hoare, with the exception of the following:

Chapter 2: Richard J. Alsop and Andrea Scotti assisted with the neutron scattering analysis. Markus Bleuel conducted the uSANS measurements at the National Institute of Standards and Technology in Gaithersburg, Maryland. Maikel C. Rheinstädter and Walter Richtering helped with the progression of the project through useful discussions. Nadine Daleiden at RWTH Aachen assisted with the Langmuir Trough experiments.

Chapter 3: Ali Affar assisted with NMR measurements. Lukas Sadowski synthesized and characterized the hydrazide acrylate monomer. Madeline Simpson helped with the progression of the project.

Lay Abstract

Medications can exist in many different forms. From pills to injections, existing drug delivery systems require a high frequency of drug administration and often result in low efficacy of drug once administered to the human body. Polymer-based drug delivery systems have the potential to improve this delivery. In particular, microgels, water-filled crosslinked polymer networks with a size less than one micron, offer promise as a drug delivery vehicle. The size and chemical composition of microgels can be tailored to enable their use in a wide array of drug delivery applications. In addition, microgels can be loaded with a therapeutic agent and transported in the blood stream to deliver drug at a rate and/or location tunable based on the internal structure of the microgel. “Smart” microgels have the particularly attractive ability to change their properties in response to certain environmental stimuli (i.e. temperature or pH). However, current smart microgel systems are non-degradable and would accumulate in the body, causing undesired side-effects. In this thesis, a new self-assembly approach has been used to produce degradable microgels with the potential to switch properties in response to both temperature and pH. Water-insoluble drugs can be encapsulated more efficiently with this method, and the dual-responsive behaviour is expected to improve our capacity to deliver drug at the rate and location desired in the body.

Abstract

Microgels, colloidal networks of crosslinked water-soluble polymers with dimensions < 1 μm , have been demonstrated to be useful materials in a wide range of biomedical and environmental applications. In particular, temperature-responsive microgels based on poly(N-isopropylacrylamide) (PNIPAM) have attracted significant research interest in drug delivery applications. However, conventional precipitation-based PNIPAM microgels are functionally non-degradable, problematic for biomedical applications. To resolve this issue, a thermally-driven self-assembly approach based on hydrazide and aldehyde functionalized PNIPAM oligomers to form an acid-labile hydrazone bond was developed in the Hoare Lab to produce thermoresponsive, colloidally stable, monodisperse and degradable microgels.

In this thesis, the internal structure of these self-assembled microgels was investigated using small and ultra-small angle neutron scattering and surface force experiments. Contrary to expectations based on the assembly technique, all these characterization strategies suggested that self-assembled microgels have a homogeneously cross-linked internal structure. It is anticipated that these well-defined degradable and homogeneous nanoscale gel networks offer opportunities for addressing challenges in drug delivery, biosensing, and optics by exploiting the predictable diffusive and refractive properties of the homogeneous microgel networks. In addition, the co-self-assembly of a moderately hydrophobic anti-inflammatory drug (dexamethasone) during the microgel self-assembly process was demonstrated to enable five-fold higher drug encapsulation (75-80%) relative to the conventional partition/diffusion-based drug loading processes. This result addresses a key challenge in delivering hydrophobic drugs using conventional precipitation-based microgel systems due to the inherent hydrophilicity of the crosslinked network.

The potential of the self-assembly approach to fabricate multi-responsive smart microgels was demonstrated by incorporating pH-ionizable functional groups (via the copolymerization of acrylic acid and 2-dimethylaminoethylmethacrylate to introduce anionic and cationic charges respectively) into the hydrazide and aldehyde-functionalized precursor polymers prior to self-assembly. The self-assembled charged microgels showed the same pH-responsive swelling behaviours of conventional microgels, including amphoteric microgels that can be formed at any desired cationic:anionic charge density by simply mixing different ratios of cationic and anionic precursor polymers. Such microgels offer significant potential to improve the performance of microgels in applications demanding dual pH/temperature specific drug delivery.

Chapter 1: Introduction

Hydrogels

Hydrogels are water soluble polymer networks that swell (but do not dissolve) in an aqueous environment and have been heavily investigated as a potential drug delivery vehicle in literature¹. Hydrogels can be fabricated with a variety of different water-soluble polymers, including both natural polymers (dextran, carboxymethylcellulose)² and synthetic polymers (chitosan³, PNIPAM⁴ and POEGMA⁵). Depending on the polymer and the type of crosslinking used, the networks can be designed to be stable over extended periods or exhibit controllable degradation rates. Hydrogels have several advantages over other polymeric drug delivery systems as they are generally cytocompatible (owing to their high water content as well as physical, mechanical, and often chemical similarity to cells) and offer tunable porosities that can regulate both the encapsulation and controlled release of drugs¹.

Microgels

In general, materials at the micro or nanoscale offer an even wider range of potential properties and thus applications compared to their macroscopic counterparts. Microgels are colloidal hydrogels with at least one dimension less than 1 μm and have demonstrated promising results in a wide range of drug delivery applications⁶. The micro- or nanoscale dimensions of microgels provide the ability to control and design drug delivery mechanisms and/or specific binding affinities for a host of therapeutic or environmental targets. In addition, in comparison to their bulk hydrogel analogues, microgels offer the advantages of higher surface areas to maximize drug loading or sorption, easier injection into the body at room temperature, and significantly faster stimulus responses¹. Such behaviour facilitates the “smart” drug or target-specific uptake and subsequent release properties of microgels that has motivated significant attention in literature⁷⁻⁸.

Poly(N-isopropylacrylamide) (PNIPAM) microgels are perhaps the best-known smart drug delivery system. PNIPAM was first synthesized in the 1950s⁹ and has attracted considerable research interest since given its lower critical solution temperature (LCST) of 32°C, at which point it switches from a soluble state at lower temperatures to an insoluble state above this temperature⁷. Pelton and Chibante prepared the first microgels based on PNIPAM in 1986 that exploit the LCST behaviour of PNIPAM to generate volume phase transitions (VPT) in microgels, by which PNIPAM microgels decrease in size above this temperature, but can reversibly re-swell to their original size at room temperature¹⁰. This phase transition is commonly related to the competition between hydrogen bonding between water and amide bonds in PNIPAM relative to the hydrophobic interactions between the isopropyl groups, the latter of which (as an entropic interaction) more strongly influences the free energy balance at higher temperatures. Furthermore, PNIPAM-based microgels can be easily functionalized using free-radical polymerization to engineer the phase transition temperature to other desired values for different applications¹¹. The internal structure of the microgels plays an important role when determining the swelling properties and the transition temperature response of the microgels as well as the capacity of the microgels to uptake and release small molecules¹²⁻¹³. PNIPAM microgels have been widely investigated as drug delivery vehicles because of their capacity for deformation while staying intact (allowing for improved penetration through biological barriers), controlled porosity and controllable drug-polymer affinities⁷.

Microgel Fabrication Techniques

Conventional PNIPAM microgels are made by a precipitation polymerization process¹⁰ in which NIPAM monomers are copolymerized with N,N'-methylenebisacrylamide (MBA) crosslinker using a water-soluble free radical initiator (i.e. potassium sulfate) at a temperature above the lower critical solution temperature (LCST) of PNIPAM to drive particle

formation¹⁴⁻¹⁵. Other monomers may be copolymerized to obtain microgels with desired phase transitions and “smart” properties. For example, acrylic acid and 2-dimethylaminoethylmethacrylate can be co-polymerized to obtain anionic and cationic PNIPAM microgels respectively, while N-alkylacrylamide monomers with less hydrophobic (higher VPT temperature) or more hydrophobic (lower VPT temperature) alkyl end groups can shift the critical temperature for microgel swelling/deswelling¹⁶⁻¹⁷. NIPAM has been successfully copolymerized with acrylic acid, methacrylic acid, maleic acid, vinylacetic acid, allyl-acetic acid, and dimethylaminoethyl methacrylate, among many others¹⁸. The copolymerization of pH-ionizable monomers (such as those in the previous list) are of special interest as they introduce charges into the polymer network, allowing for (1) increased microgel swelling when the charges are ionized due to Donnan equilibrium effects and (2) coupled pH and temperature responses at $\text{pH} \sim \text{pK}_a$ of the comonomer¹⁹.

While the conventional precipitation polymerization method is highly effective at preparing monodisperse microgels, the microgels produced are non-degradable particles, significantly limiting their potential use in the body and in environmental applications²⁰. Even if a degradable crosslinker is used (i.e. disulfides²¹, diesters²², diacyls²³), there is no direct way to control the molecular weight of degradation products to ensure the ultimate clearance of the materials. To provide a solution to this degradability issue, a novel thermally-driven self-assembly has been developed in the Hoare Lab²⁰. This method utilizes well-defined hydrazide and aldehyde-functionalized PNIPAM oligomers as the microgel building blocks instead of PNIPAM monomers, inherently controlling the length of the C-C bonded backbone in the degradation products from the microgels. Mixing these oligomers results in the formation of hydrazone crosslinks, which are hydrolytically degradable (via hydrazone bond hydrolysis) over the course of weeks to months and cleavable with a strong acid within hours. Hydrazone chemistry provides an ideal solution because it occurs within seconds to minutes,

no additional catalyst is needed, and it can be used with a variety of potential payloads (cell, proteins, drugs)^{5, 24-25}. By ensuring that the molecular weights of the starting oligomers are below the kidney clearance limit, the degradation products directly represent these oligomers and can be processed by the kidney. A schematic of the self-assembly approach can be seen in Figure 1.1.

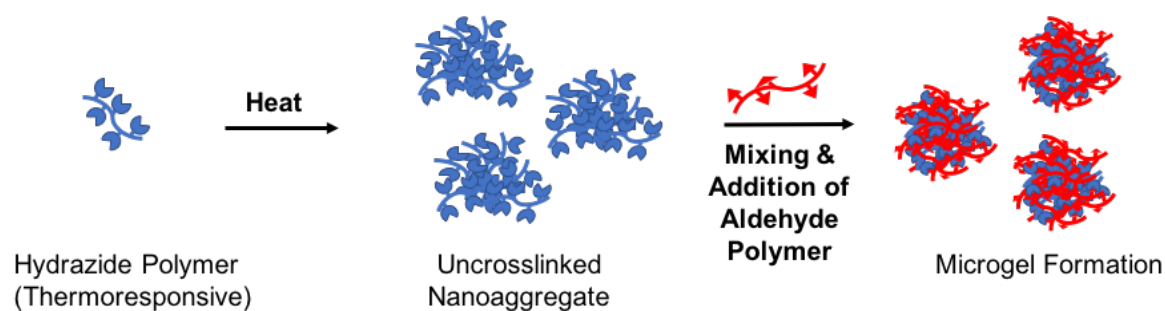


Figure 1.1: Thermally-driven self-assembly approach for fabricating degradable PNIPAM microgels. Adapted from Mueller et al.²⁶

The novelty of this self-assembly approach is based on (1) the potential for degradation via hydrolysis and (2) the ability to react upon contact or upon sequential mixing within seconds. More recently, the self-assembly process has also been adapted successfully to poly (oligoethylene glycol methacrylate) (POEGMA) to fabricate stable, covalently cross-linked, degradable POEGMA microgels. This recent paper also highlights that the self-assembly process can be successfully scaled up to produce microgels for a range of biomedical and biosensing applications²⁷.

Microgel Applications

Microgels have been demonstrated to be useful in a wide range of biomedical and environmental applications. In particular, the thermally-switchable properties of PNIPAM microgels can be leveraged in bioseparations²⁸⁻²⁹ (to reversibly adsorb/desorb a target molecule), membranes³⁰⁻³¹ (to open or close pores), nanoswitches³² (to oscillate on/off

responses in microfluidic channels), and other applications³³⁻³⁴. Each of these applications works due to some combination of the reduced hydrophilicity and/or the reduced pore size observed upon heating.

Drug Delivery

One of the most relevant applications of microgels in the biomedical field is their role as a drug delivery vehicle¹. Drug delivery has become the main focus of modern drug therapy. Though there will always be a continuous need in developing new drugs due to the rise of rare diseases and/or changing activity patterns of existing drugs (e.g. antibiotic resistance³⁵), the main challenge of modern drug therapy lies in improving ways of delivering our current drugs inside the body³⁶. In particular, drugs often need to be delivered to a specific site within the body and be released in small doses at controlled time intervals. Over the past few decades, various drug formulations and drug delivery methods have been developed and implemented in the healthcare sector.

One way to improve drug delivery is through the use of polymers. Recent advances in polymeric materials have been instrumental in the development of drug delivery vehicles that allow for a long-term controlled release of drug, significantly improving patient quality of life³⁷. Common oral medications require a high frequency of drug administration and often result in low efficacy of drug administered because they are subject to degradation within the gastrointestinal tract³⁸. Polymers have been widely used in the pharmaceutical industry as excipients for these oral medications to protect drugs in the stomach and prolong the release of drug in the intestine³⁹. Polymeric drug delivery systems including polymersomes, gels and nanoparticles have been widely used to change the pharmacokinetics of drugs and provide an easily controllable platform for delivering these drugs to the target site. The release of drug

from the polymer matrix can be tuned depending on the physical properties of the drug and the polymer. In general, there are two types of drug release: sustained drug release and on-demand drug release (Figure 1.2).

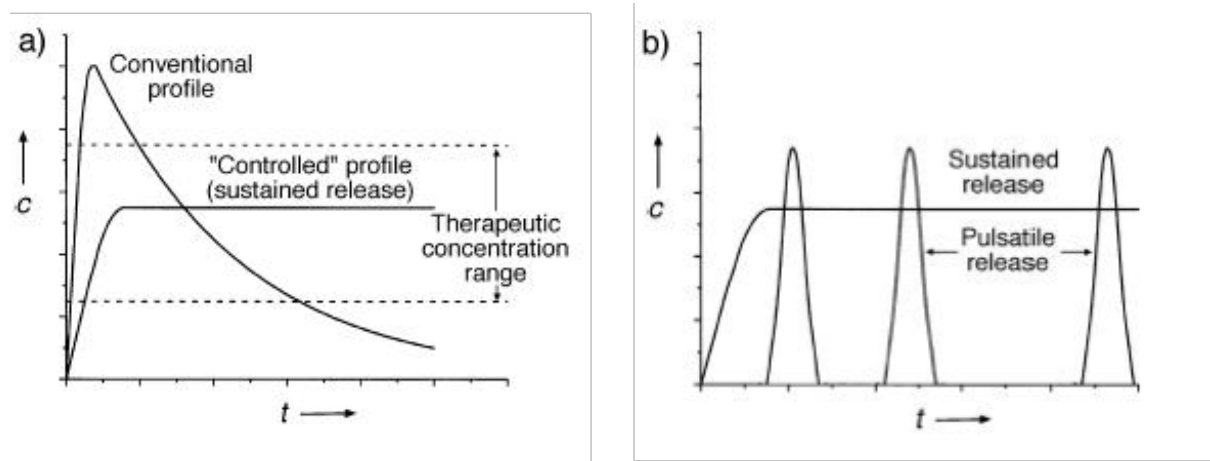


Figure 1.2: (a) Comparison between conventional drug release profile and controlled release with respect to the drug therapeutic concentration range, and (b) The difference between controlled release and on-demand (pulsatile) release. Reproduced from Santini et al.⁴⁰

Sustained Drug Release

Each drug has a therapeutic concentration range above which it becomes toxic to the patient and below which it is clinically ineffective. In traditional delivery systems, once the drug is administered, the drug concentration in the blood stream increases rapidly (above the therapeutic window) and is followed by a decline (below the therapeutic window)³⁷. Once the drug concentration reaches a low concentration in the blood, the drug needs to be re-administered for the patient's symptoms to be effectively treated. In sustained release systems, the goal is to avoid these frequent administrations, by extending the decline in drug concentration to be within the therapeutic window for a longer time period.

On-Demand Drug Release

On-demand drug release systems can be triggered to allow for repeated doses of drug according to the patient's needs⁴¹. The main advantage of these systems includes having full

control over where and when a specific amount of drug is released in the body. It reduces the frequency of drug administration and thus improves patient compliance. Examples of clinical situations in which on-demand drug release may be most beneficial include post-surgical pain control medications⁴² (dose as required by the patient), treatment of infections or inflammatory conditions⁴³ (release only when infections are present), and hormonal therapy⁴⁴ and chemotherapy⁴⁵ (both of which have shown benefits associated with chronotherapeutic drug release).

On-demand drug delivery systems can be divided into three categories⁴⁶: (1) time-controlled, (2) stimuli-induced and (3) externally-triggered. Time controlled drug delivery systems include polymeric systems with coatings that erode or rupture over time and/or have a controlled degradation profile that precisely predicts the release of drug from the polymeric matrix⁴⁶. Stimuli-induced drug delivery systems respond to changes in their local environment, such as changes in temperature, pH and/or chemical concentrations³³. Such smart materials can dynamically control the delivery and dosage of drug as needed in response to internal changes (i.e. the higher temperature and lower pH values associated with rapidly-metabolizing infection or tumour sites⁴⁷⁻⁴⁸). Externally-triggered drug delivery systems respond to externally-applied *ex vivo* signals such as electrical fields, mechanical forces, or ultrasound waves⁴⁶. By combining external signals such as near-infrared irradiation, radiofrequency waves, or alternating magnetic fields⁴⁹ with inherently temperature-responsive materials, release can be induced by using the external signal to generate heat and drive a stimulus-induced thermal response. Using any of these approaches, alone or in combination, would allow patients in the future to control drug intake and allow healthcare professionals to directly target areas of interest within the body without invasive surgery.

Microgel-Based Drug Delivery

Microgels have the ability to be used in both sustained drug release and on-demand drug release, as mentioned in the previous section. Two specific drug delivery applications that can benefit from the use of microgels and are of interest to healthcare professionals include (1) the controlled delivery of hydrophobic drugs and (2) the delivery of anti-cancer therapeutics to specific temperature/pH environments within the body:

Hydrophobic Drug Delivery

Hydrophobic drugs can range from slightly soluble compounds to completely insoluble in aqueous solutions. A drug is considered insoluble if its solubility in water is $< 0.1 \text{ mg/L}$ ⁵⁰. Dexamethasone is one example of a moderately hydrophobic drug ($\sim 0.1 \text{ mg/mL}$ solubility in 10 mM PBS⁵¹), that has the ability to reduce inflammation and calms an overactive immune system by mimicking the effect of cortisol, a hormone released by the adrenal glands that controls metabolism and stress⁵². Dexamethasone is commonly used in the treatment of arthritis as well as various skin, blood, kidney, eye, thyroid, and intestinal disorders such as colitis⁵².

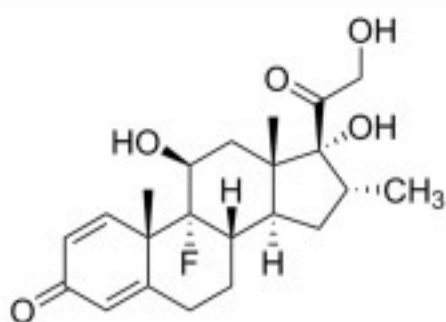


Figure 1.3: Chemical structure of dexamethasone

Due to their inherent hydrophilicity, both microgels and hydrogels typically experience challenges with the loading and release of hydrophobic drugs. For conventional precipitation-

based PNIPAM microgels, the only available method of loading hydrophobic drugs is via passive diffusion, which results in low encapsulation efficiencies¹. Through the novel self-assembly method for microgel fabrication, loading can occur either *in situ* (directly co-assembling the drug with the precursor polymer) or via passive diffusion. This attribute is a distinct advantage of self-assembled PNIPAM microgels over conventional precipitation-based PNIPAM microgels, as a significantly higher amount of drug can be encapsulated (particularly drugs like dexamethasone, which have some degree of aqueous solubility but would prefer to partition inside the hydrophobic nanoaggregate formed during the self-assembly process).

The delivery of dexamethasone is important for the treatment of ocular diseases including macular degeneration and glaucoma⁵¹. Specifically, dexamethasone delivery to the posterior segment of the eye is required to treat these diseases. Conventional treatments are applied at the front of the eye, resulting in very low doses of drug (typically <5% of the administered dose) reaching the back of the eye due to lachrymal drainage; as such, the drug needs to be re-administered frequently to effectively treat the symptoms⁵³, inconvenient and uncomfortable for the patients. As a potential alternative, a one-time injection to the back of the eye could be performed using a drug delivery system (i.e. the self-assembled PNIPAM microgels) loaded with dexamethasone to release small amounts of drug over an extended period of time and thus avoid frequent drug administrations.

Temperature/pH Specific Cancer Drug Delivery

Site-specific drug delivery to cancerous tissues would significantly address the serious side-effects related with chemotherapeutic drugs. While multiple biological targeting approaches have been attempted, they have been relatively ineffective at improving tumour localization of delivered drugs⁵⁴. One potential opportunity for improving current targeting is to exploit

the small changes in temperature (increased) and pH (decreased) characteristic of areas of enhanced metabolism and/or decreased vascularization^{47-48, 55}, like tumours. Introducing charged co-monomers into the PNIPAM backbone allows for pH tunability in addition to the already inherent temperature responsiveness due to the PNIPAM polymer. With both temperature and pH responsiveness, the swelling behavior and/or drug affinity of microgels may be precisely tuned to target the cancer microenvironment, driving improved localized drug delivery. A similar approach may also be useful for targeting infection sites in the body, which have similar characteristic physical properties due to enhanced local inflammatory/immune responses⁵⁶.

Objectives

The novel thermally-driven self-assembly offers an alternative and advantageous synthesis method of fabricating PNIPAM microgels compared to the conventional precipitation-based PNIPAM microgels that lack full control over the degradation products. The aim of this research is thus to leverage the previously demonstrated successful fabrication of monodisperse, colloidally stable and degradable self-assembled PNIPAM microgels **to develop a platform of smart self-assembled dynamically cross-linked PNIPAM microgels to improve drug delivery**. The thesis is divided into two distinct chapters:

- (1) The first chapter “Structural analysis and direct loading of self-assembled uncharged PNIPAM microgels” was adapted from a recent publication in *Langmuir*²⁶. This chapter analyzes the internal structure of the uncharged PNIPAM microgels and investigates their ability to encapsulate and release a moderately hydrophobic drug.
- (2) The second chapter “Fabrication and characterization of charged and amphoteric self-assembled PNIPAM microgels” is unpublished (expected to be submitted by August 2018) and takes a closer look at single charged and amphoteric self-assembled PNIPAM microgels with applications in dual temperature/pH drug delivery.

Overall, this thesis makes significant contributions to understanding the fundamental physics of the thermal self-assembly process as well as expanding the chemical flexibility of the self-assembled microgels to better address key opportunities in drug delivery.

Chapter 2: Structural Analysis and Direct Drug Loading of Uncharged PNIPAM Microgels

Adapted from: Dynamically-Crosslinked Self-Assembled Thermoresponsive Microgels with Homogeneous Internal Structures

Eva Mueller, Richard J. Alsop, Andrea Scotti, Markus Bleuel, Maikel C. Rheinstädter, Walter Richtering, Todd Hoare

Reference: Mueller, E.; Alsop, R. J.; Scotti, A.; Bleuel, M.; Rheinstadter, M. C.; Richtering, W.; Hoare, T., Dynamically Cross-Linked Self-Assembled Thermoresponsive Microgels with Homogeneous Internal Structures. *Langmuir* **2018**, *34* (4), 1601-1612.

Summary

The internal morphology and the ability to efficiently encapsulate moderately hydrophobic drugs of temperature-responsive degradable poly(N-isopropylacrylamide) (PNIPAM) microgels formed via an aqueous self-assembly process based on hydrazide and aldehyde-functionalized PNIPAM oligomers are investigated. A combination of surface force measurements, small angle neutron scattering (SANS), and ultra-small angle neutron scattering (USANS) was used to demonstrate that the self-assembled microgels have a homogeneously cross-linked internal structure. This result is surprising given the sequential addition process used to fabricate the microgels, which was expected to result in a densely crosslinked shell-diffuse core structure. The homogeneous internal structure identified is also significantly different than conventional microgels prepared via precipitation polymerization, which typically exhibit a diffuse shell-dense core structure. The homogenous structure is hypothesized to result from the dynamic nature of the hydrazone crosslinking chemistry used

coupled with the assembly conditions chosen that promote polymer interdiffusion. Furthermore, a five-fold increase in drug loading efficiency was measured when loading dexamethasone directly during the self-assembly process instead of allowing the drug to passively diffuse into the system over time, the only method by which conventional precipitation-based PNIPAM microgels can encapsulate hydrophobic drugs. Consequently, fabricating microgels using the self-assembly process not only yields homogenous internal structures (interesting from a physical chemistry perspective) but also facilitates high drug loading (interesting from a more applied chemical engineering perspective).

Literature Review

Microgels, colloidal networks of crosslinked water-soluble polymers with dimensions < 1 μm , have been demonstrated to be useful materials in a wide range of biomedical and environmental applications. In particular, temperature-responsive microgels and nanogels based on poly(N-isopropylacrylamide) (PNIPAM) have attracted significant research interest due to their ability to change their diameter^{20, 33, 57-58}, hydrophobicity⁵⁹, pore size¹², and surface charge⁶⁰⁻⁶¹ as a function of temperature, the so-called volume phase transition temperature (VPTT) behavior. These thermally switchable properties have been applied in drug delivery¹ (to target locally hotter areas in the body, such as poorly vascularized but quickly metabolizing cancerous sites⁶²⁻⁶³), bioseparations²⁸⁻²⁹ (to reversibly adsorb/desorb a target molecule), membranes³⁰⁻³¹ (to open or close pores), nanoswitches³² (to oscillate on/off responses in microfluidic channels), and other applications³³⁻³⁴. Each of these applications works due to some combination of the reduced hydrophilicity and/or the reduced pore size observed upon heating, with the former governing the strength of interactions between the microgel and more hydrophobic molecules^{7, 64} and the latter governing the diffusivity of molecules through the gel network⁶⁵.

The swelling properties and the transition temperature responses of microgels are governed by not only the chemistry but also the internal microgel structure. The internal structure regulates the speed/degree of swelling⁶⁶⁻⁶⁸, the breadth of the volume phase transition (less internally heterogeneous particles have narrower transitions)^{14, 69}, the rate of intraparticle diffusion⁷⁰, the ease of microgel functionalization⁷¹ and the capacity of the microgels for the uptake/release of small molecules¹²⁻¹³. This latter property is widely leveraged to apply microgels as a drug delivery vehicle that allows therapeutic agents to be localized at the site of interest for extended periods of time at safe but clinically relevant concentrations^{1,37}. The

uptake and release of drug from the interior of a microgel depends on the property of the drug (hydrophilic or hydrophobic), the tendency of the drug to interact with the individual polymer chains, the degradation profile of the crosslinked networks (i.e. in acidic conditions for hydrazone bonds), and the internal structure of the polymer network, the latter of which regulates the diffusion coefficient of drug through the microgel network.

Hydrophobic drug delivery, in particular, remains a challenge for conventional precipitation-based microgel systems due to the hydrophilicity of the crosslinked network and required use of diffusion/partitioning-based processes for loading drugs with conventional microgels¹. The hydrated gel network typically has low affinity for hydrophobic drugs, resulting in low drug uptakes. Current strategies to address this problem include modifying the chemical structure of the hydrophobic drug itself (which typically decreases the overall effectiveness of the drug and at minimum changes its pharmacokinetics⁵⁰), increasing the solubility of the hydrophobic drug by increasing the pH or introducing organic co-solvents (not feasible under physiological conditions) or stabilizing the drug with surfactant⁵⁰.

The internal structure of microgels is most commonly studied using small-angle neutron scattering (SANS) in dilute suspensions, although static light scattering can also give some insight⁷². Direct modeling expressions for the scattering intensity distribution have been developed to describe structural changes induced by changes in temperature⁷³⁻⁷⁵, cross-linking density⁷⁶, or particle size⁷²⁻⁷³ as well as inherent compositional gradients resulting from the synthetic conditions used (e.g. batch, semi batch or controlled monomer feed)⁷⁷. The internal structure of microgels is directly related to the method by which the microgels are synthesized. Conventional PNIPAM microgels are made by a precipitation polymerization process¹⁰ in which NIPAM monomers are polymerized with N,N'-methylenebisacrylamide

(MBA) crosslinker using a water-soluble free radical initiator (i.e. potassium sulfate) at a temperature above the lower critical solution temperature (LCST) of PNIPAM to drive particle formation¹⁴⁻¹⁵. Other monomers may be copolymerized to obtain microgels with desired properties and the process may be carried out in batch, semi-batch or continuous modes¹⁴. The resulting microstructure of the microgels produced using this conventional technique has been shown to relate directly to the copolymerization ratios between the constituent monomers and crosslinkers used to prepare the microgel⁷⁸. For example, since the MBA crosslinker typically used to prepare microgels reacts faster than NIPAM, the core of the resulting microgel is more densely cross-linked than the shell, resulting in a “fuzzy sphere” nanostructure⁵⁷. The fuzzy sphere internal structure of conventional PNIPAM microgels was further studied and formally quantified with a small angle neutron scattering (SANS) model by Stieger et al.⁷³. Additionally, Geisel et al. investigated and indirectly confirmed the core-corona structure of PNIPAM-copolymerized with methacrylic acid (MAA) microgels using interface/surface force measurements⁷⁹. This inhomogeneous structure makes the prediction of drug binding⁶⁴, swelling responses⁸⁰, and other key microgel properties challenging, although also offering opportunities to leverage these structures in specific applications (e.g. bioconjugation⁵⁸).

Given that copolymerization kinetics govern the microgel morphology via precipitation polymerization, it is possible to manipulate the feed rate of the monomers/crosslinkers within the scope of the conventional precipitation process to create uniformly crosslinked particles. For example, Acciaro et al. have prepared homogeneous PNIPAM microgels by using a continuous reactor to maintain the concentrations of monomer and cross-linker constant⁶⁶, Du's group copolymerized an unprotected catechol monomer that could self-crosslink to create a more homogeneous internal structure⁸¹, and we have demonstrated the capacity to

create uniform functional group distributions in microgels using semi-batch delivery of the functional monomer⁸². In all cases, the homogeneously cross-linked or functionalized microgels showed significantly different optical and swelling properties relative to conventional batch polymerized microgels, showing the importance of controlling and understanding the internal morphology of microgels in designing particles for applications.

Alternately, to avoid the dominance of free radical copolymerization kinetics on the morphology of the resulting microgels, two-step microgel fabrication techniques have been reported in which a pre-formed PNIPAM polymer or oligomer is heated above its LCST to form a nanoaggregate followed by crosslinking to stabilize that aggregate into a microgel. Multiple post-crosslinking strategies including UV irradiation⁸³⁻⁸⁴ and self-condensation of pendant methoxysilyl groups⁸⁵ have been reported to create microgels from the nanoaggregates, with the distribution of crosslinking sites governed by UV light penetration and/or the surface activity of the precursor polymer(s) in the former case and the self-association of the hydrophobic methoxysilyl groups in the latter case.

However, particularly in the context of biological applications and for these self-assembled microgels to be used as potential drug delivery vehicles in the human body, controlling degradability remains a challenge with both the conventional synthesis approach as well as these nanoaggregation stabilization strategies. In the former case, there is no direct way to control the molecular weight of degradation products (even if degradable crosslinkers are used) to ensure the ultimate clearance of the materials; in the latter case, the bonds formed are non-degradable. Alternate methods such as pre-polymer crosslinking inside inverse emulsions allows for both homogeneous internal morphologies as well as degradation into well-defined products⁸⁶; however, this approach typically results in non-uniform particle size

distributions⁸⁷. Microfluidics can be utilized to produce more uniform microgels with specific flow-focusing techniques⁸⁸ but typically results in larger particle sizes in the micron size range instead of the nanoscale.

Recently, we have developed a novel method to create degradable and monodisperse microgels using a thermally-driven self-assembly approach mimicking the conventional microgel fabrication process but using well-defined hydrazide and aldehyde-functionalized PNIPAM oligomers instead of the monomers as the building blocks. Mixing the hydrazide (PNIPAM-Hzd) and aldehyde (PNIPAM-Ald)-functionalized oligomers results in the formation of degradable hydrazone crosslinks²⁰; by maintaining the molecular weight of those oligomers below the kidney clearance limit, we can facilitate renal clearance of the synthetic polymer-based microgel network following degradation of the hydrazone crosslinks. These degradable analogues of conventional thermoresponsive microgels can be fabricated rapidly (<10 minutes) using a highly scalable method to generate colloiddally stable, non-cytotoxic microgels with sizes in the 200-300 nm range, high monodispersity, and controllable swelling responses²⁰. Furthermore, given that the stoichiometry and sequence of addition of PNIPAM-Hzd and PNIPAM-Ald are asymmetric during the assembly process, residual functional groups are available in the microgel to enable *covalent* “layer-by-layer” (LbL) assembly of the reactive pre-polymers templated from the initially fabricated microgel, previously only demonstrated on microgels via polyelectrolyte interactions⁸⁹. Interestingly, in such previous microgel studies, the soft and porous nature of microgels enabled significant interpenetration of lower molecular weight polyelectrolyte into the microgels⁹⁰, with the reversible ionic interactions between the charged additive polymer and the oppositely charged microgel enabling the transport of the polymer into the microgel core⁹¹. We have previously demonstrated the efficacy of the proposed covalent LbL approach for fabricating

thin film hydrogels with tunable thicknesses⁹², but have not yet demonstrated a similar effect on the nanoscale.

Given that our new microgel fabrication method involves controlled thermoaggregation of the hydrazide-functionalized pre-polymer at a temperature above its LCST followed by the addition of the aldehyde-functionalized pre-polymer, we hypothesized that mass transfer considerations would limit the diffusion of PNIPAM-Ald into the collapsed PNIPAM-Hzd aggregate prior to hydrazone bond formation (which is rapid in aqueous conditions⁵) to result in a dense shell/disperse core structure, the inverse of the conventional microgel morphology. However, to-date, we do not have evidence supporting this hypothesized microstructure. In addition, the dynamic nature of the hydrazone bond means that initial crosslinks formed during synthesis may be broken and re-formed over time, such that a homogenization of the crosslink distribution at room temperature at $T < VPTT$ is theoretically possible even if the interdiffusion of the two polymers during the $T > VPTT$ fabrication step is indeed rate-limited. Similarly, for the covalent LbL surface modification steps performed on pre-fabricated microgels at $T > VPTT$, the dynamic crosslinking chemistry may permit interdiffusion of the added polymer into the gel structure over time (as observed with the polyelectrolyte LbL assemblies⁹⁰) despite the fast and multidentate covalent crosslinking anticipated between the added functional polymer and residual surface or near-surface complementary functional groups.

Objectives

Herein, we investigate (1) the internal morphology of these self-assembled PNIPAM microgels, with or without subsequent LbL modification, using a combination of surface force measurements, small angle neutron scattering (SANS), and ultra-small angle neutron scattering (USANS), and (2) the encapsulation (and preliminary release studies) of a moderately hydrophobic drug (dexamethasone) in uncharged self-assembled PNIPAM microgels. Dexamethasone is a type of corticosteroid that has the ability to reduce inflammation and calms an overactive immune system by mimicking the effect of cortisol, a hormone released by the adrenal glands that controls metabolism and stress⁵². Dexamethasone is used in the treatment of arthritis as well as various skin, blood, kidney, eye, thyroid, and intestinal disorders such as colitis⁵², and it is moderately hydrophobic (~ 0.1 mg/mL in 10 mM PBS⁵¹). We anticipate that this low but not insignificant water solubility will facilitate high drug loading directly in the microgel during the self-assembly process. We demonstrate that the oligomeric self-assembly approach not only leads to degradable microgels but also highly homogeneous microgel structures which may be of significant benefit in drug delivery and other applications in which uniform crosslink densities should yield more uniform properties (e.g. optics).

Experimental Section

Materials

N-isopropylacrylamide (NIPAM, 99%), acrylic acid (AA, 99%), thioglycolic acid (98%), aminoacetaldehyde dimethyl acetal (99%), sodium cyanoborohydrate (95%), 2,2,6,6-tetramethyl-1-piperidinyloxy (TEMPO, 98%), methacryloyl chloride (purum), and dexamethasone (>98%) were purchased from Sigma Aldrich (Oakville, Canada). NIPAM was purified by dissolving 1 g/mL in toluene at 60°C, adding a 2:3 ratio of hexane to toluene, placing the solution in an ice bath for 1-2 hours, filtering/rinsing with hexanes, and drying the recrystallized NIPAM monomer under N₂ overnight. Adipic acid dihydrazide (ADH, Alfa Aesar, 98%), *N*⁷-ethyl-*N*-(3-dimethylaminopropyl)-carbodiimide (EDC, Carbosynth, Compton CA, commercial grade), 2,2-azobisisobutyric acid dimethyl ester (AIBMe, Wako Chemicals, 98.5%), and ethanol (Commercial Alcohols, Brampton, Ontario) were purchased and used without further purification. Milli-Q grade distilled deionized water (DIW) was used for all experiments. Deuterium oxide (99.9 atom% D) was purchased from Sigma Aldrich (Oakville, Canada) for use in neutron scattering experiments. N-decane (Sigma Aldrich, 99%) was purchased and triple-columned with aluminum oxide prior to use.

Prepolymer Synthesis

Hydrazide-functionalized (PNIPAM-Hzd) and aldehyde-functionalized (PNIPAM-Ald) prepolymers were synthesized using the previously reported protocols²⁰. Briefly, PNIPAM-Hzd was prepared via free radical copolymerization of NIPAM (4.5 g) and acrylic acid (0.5 g) in 20 mL of ethanol using thioglycolic acid (TGA, 80 µL) as the chain transfer agent and 2,2-azobisisobutyric acid dimethyl ester (AIBME, 0.056 g) as the initiator (reaction temperature = 60°C). Gel permeation chromatography (GPC) using a Waters 590 HPLC pump, three Waters Styragel columns (HR2, HR3, HR4; 30 cm x 7.8 mm (ID); 5 µm particles) at 40°C, a

Waters 410 refractive index detector operating at 35 °C, and DMF as the solvent indicated that the resulting polymer had a molecular weight of 21.6 kDa, while base-into-acid conductometric titration indicated a stoichiometric incorporation of acrylic acid (~15 mol%) into the polymer. Subsequently, the acrylic acid residues were conjugated using carbodiimide chemistry with a 5-fold excess of adipic acid dihydrazide, resulting in an overall conversion of 95% of acrylic acid residues to hydrazide functionalities (i.e. ~14 mol% of the total monomer residues were functionalized with a hydrazide group). Deuterated PNIPAM-Hzd (d-PNIPAM-Hzd) was similarly prepared by substituting NIPAM with d7-PNIPAM (Polymer Source, Montreal, PQ) in the recipe, with base-into-acid conductometric titration indicating the same stoichiometric (~15 mol% total monomer) incorporation of acrylic acid into the polymer and ~95% conversion of those acrylic acid residues into hydrazide groups following carbodiimide coupling.

PNIPAM-Ald was prepared by copolymerizing NIPAM (4.5 g) with N-(2,2-dimethoxyethyl)methacrylamide⁴ (DMEMAm, 0.95 g) using the same polymerization conditions used for the hydrazide polymer, resulting in a polymer with a molecular weight of ~15.1 kDa via GPC. Subsequently, acid hydrolysis of the pendant acetal groups in DMEMAm into aldehyde groups was performed by dissolving the initial polymer in 1 M HCl and hydrolyzing over 24 hours, resulting in 12 mol% of total monomer residues in the polymer bearing aldehyde groups. All polymers were dialyzed against Milli-Q water for 6 cycles of at least 6 hours and lyophilized for storage.

Microgel Particle Size Measurements

Dynamic light scattering measurements were performed using a Brookhaven 90Plus particle analyzer running Particle Solutions Software (Version 2.6, Brookhaven Instruments

Corporation), using a 659 nm laser and a 90 degree detection angle. Each measurement was performed at a count rate between 200-500 kilocounts/s for 2 minutes and repeated at least six times. The intensity-weighted particle sizes and polydispersities were reported as averages of these six replicate measurements, with the reported error representing the standard deviation of these replicates.

Microgel Fabrication

Oligomer self-assembled microgels were prepared following our previously reported self-assembly/precipitation protocol (Figure 2.1)²⁰. Both PNIPAM-Hzd and PNIPAM-Ald were dissolved at 1 wt% in D₂O or a mixture of D₂O/H₂O appropriate for index matching (see the SANS section for details on how this ratio was chosen). The PNIPAM-Hzd solution (5 mL) was then heated to a temperature above its lower critical solution temperature (LCST) to create stable nanoaggregates, after which the PNIPAM-Ald solution was added dropwise (~1-2 drops per second) at either 5 or 20% mass PNIPAM-Ald/mass of PNIPAM-Hzd to stabilize the nanoaggregate via a hydrolytically-labile hydrazone bond. All self-assemblies were performed at a reaction temperature of 70°C, well above the LCST of PNIPAM-Hzd (~56°C) to ensure efficient nanoaggregate formation. The mixture was magnetically stirred (350 RPM) at 70°C for 15 minutes following PNIPAM-Ald addition to ensure crosslinking prior to cooling.

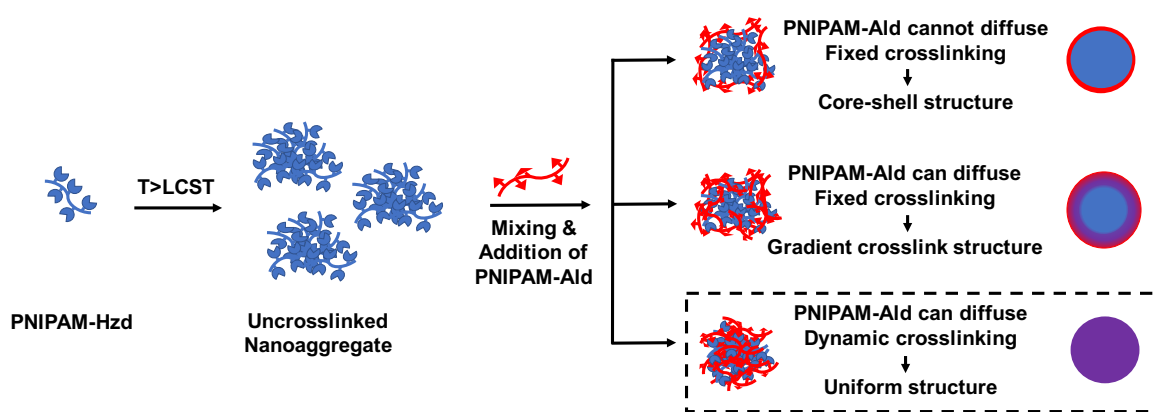


Figure 2.1: Schematic of precipitation/self-assembly process used to fabricate degradable microgels from functional PNIPAM oligomers and anticipated structures of resulting microgels depending on the diffusibility of the PNIPAM-Ald crosslinker and the permanence of the crosslinks formed. The homogeneous morphology is consistent with the structural characterization results.

To assess the impact of adding additional functional polymer following the initial assembly process (i.e. “layer-by-layer” self-assembly), the pre-formed microgel suspensions were cooled overnight and then re-heated to 70°C. Either PNIPAM-Hzd or PNIPAM-Ald at a concentration of 5 or 20% mass/mass of initial PNIPAM-Hzd was then added as described above for the initial PNIPAM-Ald crosslinking step, with the process repeated as desired to add additional “layers” to the assembly.

Small-Angle Neutron Scattering (SANS)

SANS experiments were conducted using the 30 m SANS NGB30 at the NIST Center for Neutron Research (NCNR, Gaithersburg, MD). Sample-to-detector distances of 1, 4 and 13 m were used in conjunction with neutrons of wavelength 6 Å, while the lens geometry was also used at the 13 m detector distance with 8.4 Å wavelength neutrons to expand the accessible q range. The microgels were self-assembled in D₂O as described in the previous section and loaded into NCNR’s custom titanium/quartz sample holders (diameter 19 mm and path length 2 mm) without further dilution. The internal gap thickness of the sample cell

was 2 mm, which corresponds to $\sim 800 \mu\text{L}$ of test solution. Three microgels were assessed at four temperatures (25, 32, 37 and 45°C) spanning the volume phase transition temperature (VPTT) of PNIPAM-based microgels: (1) 0.05 Ald:Hzd microgels (prepared with a 1 wt% PNIPAM-Hzd starting solution), (2) 0.20 Ald:Hzd microgels (1 wt% PNIPAM-Hzd starting solution) and (3) 0.05 Ald:Hzd microgels (2 wt% PNIPAM-Hzd starting solution). In addition, four layer-by-layer microgels were assembled in the sequences listed below and measured at 25°C only to assess the mass distribution in each microgel as a result of the layer-by-layer assembly process: (1) 0.05 Ald:Hzd microgel + PNIPAM-Hzd, (2) 0.05 Ald:Hzd microgel + PNIPAM-Ald, (3) 0.05 Ald:Hzd microgel + PNIPAM-Hzd + PNIPAM-Hzd and (4) 0.05 Ald:Hzd microgel + PNIPAM-Hzd + PNIPAM-Ald. Note that each “+ Polymer” addition step listed above involves cooling the sample overnight, re-heating to the assembly temperature of 70°C , and adding the next polymer in sequence at the concentrations listed above. Additional measurements were also performed on PNIPAM-Hzd precursor polymer solutions at the same concentration and temperature used for microgel self-assembly, allowing for direct correlation between the structure of the nanoaggregate before and after crosslinking. The low q range data were acquired by counting for ~ 20 min using the 13 m distance, the medium q range data were acquired by counting for ~ 15 min using the 4 m distance, and the high q range data were acquired for ~ 5 min using the 1 m detection distance. The three ranges were merged using the DAVE on-site data reduction tool and standard Igor Pro macros⁹³⁻⁹⁴.

The contrast matching experiment on the self-assembled PNIPAM microgels was performed by fabricating microgels using d7-PNIPAM-Hzd as the seed polymer and (hydrogenated) PNIPAM-Ald as the crosslinking polymer (0.2 Hzd:Ald polymer mass ratio), with the ratio of $\text{D}_2\text{O}:\text{H}_2\text{O}$ in the suspending solvent changed in order to match one of the two constituent

polymers. The match points were first calculated based on the atomic composition to predict the theoretical scattering length density for each of the polymers, corresponding to theoretical match points 67:33 (v:v) D₂O:H₂O for d7-PNIPAM-Hzd and 21:79 (v:v) D₂O:H₂O for hydrogenated PNIPAM-Ald. These values were refined by conducting scattering experiments both at the calculated match point as well as $\pm 10\%$ solvent mixtures from this calculated match point, with the experimental D₂O:H₂O ratio producing zero scattering determined by regression to be 63:37 D₂O:H₂O for d7-PNIPAM-Hzd and 22:78 D₂O:H₂O for PNIPAM-Ald. Microgels were then self-assembled as described in the previous section in the matched solvents to ensure the total microgel concentration was constant for each experiment. SANS experiments were conducted as previously described for the non-contrast matched samples.

Ultra-small Angle Neutron Scattering (USANS)

USANS experiments were conducted on the contrast-matched microgels using the BT5 USANS at the NIST Center for Neutron Research (NCNR, Gaithersburg, MD)⁹⁵. The neutron wavelength used was $2.4 \text{ \AA} \pm 6\%$, with the q range spanning between $\sim 0.00003 \text{ \AA}^{-1}$ to 0.002 \AA^{-1} to slightly overlap the lower end of the accessible q range from SANS (0.001 \AA^{-1}) and allow for efficient stitching/scaling of the data using the DAVE on-site data reduction tool. Samples were loaded into the same sample holder used for SANS analysis.

Neutron Scattering Data Analyses

The SANS analysis on the bulk microgels and the contrast-matched microgels was done using Interactive Data Language (IDL) and Igor Pro, using the fuzzy sphere model shown in Equation [1].

$$I(q) = \frac{scale}{V} (\Delta p)^2 \langle A^2(q) \rangle S(q) + \frac{I_{lor}(O)}{1 + (\xi * q)^m} + bkg \quad [1]$$

$$\text{where } A(q) = \frac{3[\sin(qR) - qR\cos(qr)]}{(qR)^3} \exp\left(\frac{-(\sigma_{fuzzy}q)^2}{2}\right) \text{ and } q = \frac{4*\pi}{\lambda} \sin\left(\frac{\theta}{2}\right)$$

Note that the $\langle \rangle$ brackets denote an average over the size distribution, where $\langle A^2(q) \rangle$ represents the form factor $P(q)$, $S(q)$ is the structure factor (for dilute solutions, $S(q) = 1$ for all q), ξ is the correlation length (roughly representing the mesh size of the gel network), σ_{fuzzy} denotes the width of the smeared or “fuzzy” particle surface (which, when set to 0, reduces the expression to that of a homogeneous sphere), m is the Lorentzian exponent, and q is the scattering vector, related to the neutron wavelength (λ) and the scattering angle (θ). Since the instrument resolution causes a smearing of the data, the intrinsic desmearing function in IgorPro (the convolution of $P(q)$ with a Gaussian function) was used to account for smearing effects⁹⁶.

Langmuir Trough

Compression isotherms were recorded and analyzed on the oil-water interface using a KSV-NIMA Langmuir trough with two barriers operating at a speed of 108 mm/min and a platinum Wilhelmy plate to measure the change in interfacial tension from the clean interface to the interface covered with microgel particles. Distilled water (200 mL) was used as the aqueous phase and triple-columned n-decane (200 mL) was used as the oil phase. Low crosslink ratio (0.05 Ald:Hzd polymer mass ratio) or high crosslink ratio (0.20 Ald:Hzd polymer mass ratio) self-assembled microgels were dispersed in the aqueous phase. As the particles were compressed, the change in interfacial tension was measured with the platinum Wilhelmy plate, with the measurement converted to a surface pressure using the KSV-NIMA software.

Drug loading and Release Experiments

Two methods of loading dexamethasone into uncharged self-assembled PNIPAM microgels were investigated (see Appendix A for illustrations).

(1) Direct loading during self-assembly: PNIPAM-Hzd and PNIPAM-Ald were dissolved separately at 1wt% in Milli-Q H₂O. A solution of dexamethasone was prepared in Milli-Q H₂O (solubility in water ~0.1 mg/mL) and stirred overnight. Thirty minutes prior to the self-assembly, 1 mL of the dexamethasone solution was added to PNIPAM-Hzd and stirred with a small magnetic stirrer. The self-assembly was conducted at 70°C at 350 RPM by adding 1 mL of 5 or 20 mass% of PNIPAM-Ald (relative to PNIPAM-Hzd) and allowing 15 minutes for the microgels to crosslink. The microgel suspension was cooled for 1-2 hours prior to centrifugation. The centrifugation time and speed were optimized to 18000 RPM and 20 minutes for 1-2 mL of microgel solution (total of 25 mL in each centrifuge tube, diluted with Milli-Q H₂O) to ensure efficient microgel recovery but facile redispersion of the microgels in suspension, as identified using a full factorial experimental analysis (see Supporting Information). 2 mL of supernatant was removed for drug loading analysis using high performance liquid chromatography (HPLC – see next section for details). The microgel pellet in the centrifuge tube was re-dissolved in 1 mL of 10 mM PBS for subsequent drug release studies.

(2) Conventional diffusion/partitioning-based loading following microgel fabrication: 0.05 and 0.20 Ald:Hzd self-assembled PNIPAM microgels were fabricated as previously described. 1 mL of each microgel suspension was centrifuged at 18000 RPM (20 min centrifugation time) and re-suspended in different amounts of 0.08 mg/ml dexamethasone solutions in 10 mM PBS for 24 hours. The suspensions were then centrifuged again at 18000

RPM and 20 min (total volume 25 mL, diluted with Milli-Q H₂O) to isolate the microgels from unloaded drug, and the supernatant was tested for drug loading efficiency using HPLC.

The drug loading encapsulation efficiency (EE) was calculated as follows, where C is the concentration of drug encapsulated, V is the volume of diluted nanoparticles, and T is the amount of drug added⁹⁷:

$$EE(\%) = \frac{C*V}{T} * 100\% \quad [2]$$

Preliminary drug release studies were conducted in 1 mL 3.5-5 kDa Float-a-Lyzer cellulose membranes (Spectra-Por), using 10 mM PBS as the release medium. Size and polydispersity were measured for each sample after loading with dexamethasone and after re-suspending in 10 mM PBS. Preliminary release data was collected on 0.05 Ald:Hzd microgels only using 1 mL (instead of 2 mL) of microgel suspension for centrifugation; the lower crosslink density allowed for release of dexamethasone through the semi-permeable membrane and could be detected using HPLC.

High Performance Liquid Chromatography

Quantitative determinations of dexamethasone were performed using a high-performance liquid chromatographic (HPLC) system composed of a 2707 Autosampler, 2489 UV/Visible detector and 1525 binary HPLC pump, all from Waters Corporation. Samples were analyzed using a reversed-phase Atlantis C18 column (100 mm x 4.6 mm, Waters Corporation). The mobile phase consisted of 40% acetonitrile and 60% water. A flow rate of 1.0 mL/min resulted in retention times of approximately 4 min. The absorbance was measured at 263 nm.

Results

Microgel Particle Size

The hydrodynamic radius and polydispersity of the microgels in a dilute suspension of D₂O, the layer-by-layer assembled microgels in D₂O, and the contrast-matched microgels at the relevant D₂O:H₂O ratios used for the contrast matching experiments at 25°C (T<VPTT) are listed in Table 1. Note that the solvents chosen for each listed measurement relate directly to those used in the SANS and USANS experiments, such that the sizes measured are directly comparable between the experiments. Relative to the same microgels fabricated in H₂O, the particle sizes measured in D₂O are consistently larger; this is reflective of the higher propensity of D₂O to form hydrogen bonds⁹⁸, which is the driving force for microgel hydration at T<VPTT. However, the trends in size are identical to those observed in H₂O, with lower radii observed as the relative amount of PNIPAM-Ald (crosslinker) was increased and higher radii observed when higher concentrations of the PNIPAM-Hzd polymer were used to form the initial nanoaggregate. For the covalent LbL-assembled microgels, adding one additional treatment of PNIPAM-Hzd resulted in a small but significant increase in particle size; however, adding an additional treatment of PNIPAM-Ald or adding sequential additional treatments of PNIPAM-Hzd resulted in no significant change in the particle size ($p < 0.05$ in either pair-wise comparison). This lack of an observed size change would not be anticipated if a true LbL surface assembly (akin to conventional polyelectrolyte LbL assembly) was happening. Instead, we hypothesize that the size results are indicative of a balance between additional crosslinking (restricting swelling) and the introduction of more hydrophilic hydrazide/aldehyde groups (driving swelling) upon the addition of each subsequent functional polymer. Of note, sequential additions of PNIPAM-Hzd followed by PNIPAM-Ald resulted in a much higher particle size of 268 ± 12 and substantially higher polydispersity compared to the other samples tested, suggesting significant inter-particle

aggregation in this case that was not observed with other samples. In the contrast-matched samples, the microgel size did not significantly change when deuterated d7-PNIPAM-Hzd was used as the building block of the microgel as opposed to protonated PNIPAM-Hzd ($p < 0.05$).

Table 2.1: Dynamic light scattering size and polydispersity measurements on microgels in solvents used for SANS/USANS analysis

Microgel Description	Solvent	Radius (nm)	Polydispersity
0.05 Ald:Hzd (1 wt%)	D ₂ O	162±3	0.08±0.01
0.20 Ald:Hzd (1 wt%)	D ₂ O	145±3	0.11±0.02
0.05 Ald:Hzd (2wt%)	D ₂ O	203±9	0.16±0.02
0.05 Ald:Hzd (1 wt%) + PNIPAM-Hzd	D ₂ O	176±8	0.10±0.01
0.05 Ald:Hzd (1 wt%) + PNIPAM-Hzd + PNIPAM-Hzd	D ₂ O	166±7	0.15±0.03
0.05 Ald:Hzd (1 wt%) + PNIPAM-Ald	D ₂ O	166±4	0.13±0.02
0.05 Ald:Hzd (1 wt%) + PNIPAM-Hzd + PNIPAM-Ald	D ₂ O	268±12	0.21±0.4
d-PNIPAM-Hzd 0.20 Ald:Hzd (1 wt%) (d-PNIPAM-Hzd match)	63 D ₂ O: 37 H ₂ O	183±16	0.17±0.03
d-PNIPAM-Hzd 0.20 Ald:Hzd (1 wt%) (PNIPAM-Ald match)	22 D ₂ O: 78 H ₂ O	176±8	0.15±0.04

SANS of PNIPAM-Hzd Nanoaggregates

To gain insight into the mechanism by which the sequential addition process creates self-assembled microgel particles and the structure of the thermally collapsed nanoaggregates that seed the self-assembled microgels, PNIPAM-Hzd precursor polymer solutions (prior to PNIPAM-Ald addition) were tested in D₂O using SANS at 70°C and 1 wt% or 2 wt%, the temperature and concentrations used in the self-assembly process. The majority of resulting

profiles aside from the low q regime could both be fit to the homogeneously cross-linked sphere model (i.e. $\sigma_{fuzzy} = 0$ in Eq. 1) using characteristic radii of 66 nm for 1 wt% PNIPAM-Hzd and 73 nm for 2 wt% PNIPAM-Hzd (Table 2.1; see raw data and best fit functions in Supporting Information, Figure S1.1). The higher size of the 2 wt% nanoaggregate is consistent with the larger size of the resulting microgels produced (Table 2.2), indicating some correlation between the nanoaggregate size and the resulting microgel. These sizes are however substantially smaller than those measured on the same samples via DLS (166 ± 1 nm and 176 ± 1 nm respectively), although the high measured polydispersities (~ 0.3) indicate substantial aggregation in the samples and the intensity weighting of the DLS results consistently overweights the effect of larger particles on the average particle size reported. SANS analysis similarly indicates that both precursor solutions exhibited broad polydispersities of $\sim 31\%$, with the low q region for both concentration samples showing a constant slope (the green solid lines in Fig. S1.1) indicative of large-scale aggregation⁹⁹. Interestingly, these poorly defined pre-aggregates can successfully be utilized to create relatively monodisperse microgel particles.

Table 2.2: Best fit parameters for fuzzy sphere model fit of PNIPAM-Hzd nanoaggregates at 70°C; see Supporting Information Fig. S1.1 for raw data and fit curves.

PNIPAM-Hzd Concentration (mg/mL)	σ_{fuzzy}	Radius (nm)	Polydispersity	ϵ (nm)	M
1	0	66	0.30	3.0	3.5×10^{-5}
2	0	73	0.31	3.2	6.5×10^{-5}

SANS of Self-Assembled PNIPAM Microgels

SANS experiments as a function of temperature were subsequently performed to assess the impact of the PNIPAM-Hzd starting concentration and the ratio between PNIPAM-Ald : PNIPAM-Hzd on the microgel morphology, with the results shown in Figure 2.2. The best fits accomplished with the fuzzy sphere model returned a finite shell thickness of between 2-

4 nm, a shell thickness at the extreme lower boundary of relevance for the core-shell model (Supporting Information, Figure S1.2). χ^2 values, corresponding to the goodness of fit of the model functions to the experimental data, were similar for both the homogeneously crosslinked model ($\sigma_{fuzzy} = 0$) and the core-shell Stieger model at all temperatures evaluated (Table S1); furthermore, the mid- q oscillations that are captured by the fuzzy sphere model⁷³ are not visible on the SANS profiles of the self-assembled microgels. Together these observations suggest that the additional core-shell terms in the Stieger model are unnecessary for fitting the experimental data, leading us to use the homogeneous model to fit all SANS microgel profiles presented in Figure 2.2. Note that this result lies in sharp contrast to conventionally-prepared PNIPAM microgels, in which a core-shell model with a significant shell thickness on the order of 14-30 nm (below VPTT) is required to accurately fit the SANS profiles⁷³. Figure 2.3 shows the corresponding key fitting parameters of microgel radius and mesh size as a function of temperature extracted from the homogeneous sphere fits. All fitting parameters (including a summary) for the bulk self-assembled PNIPAM microgels are included in Supporting Information Tables S3 and S4.

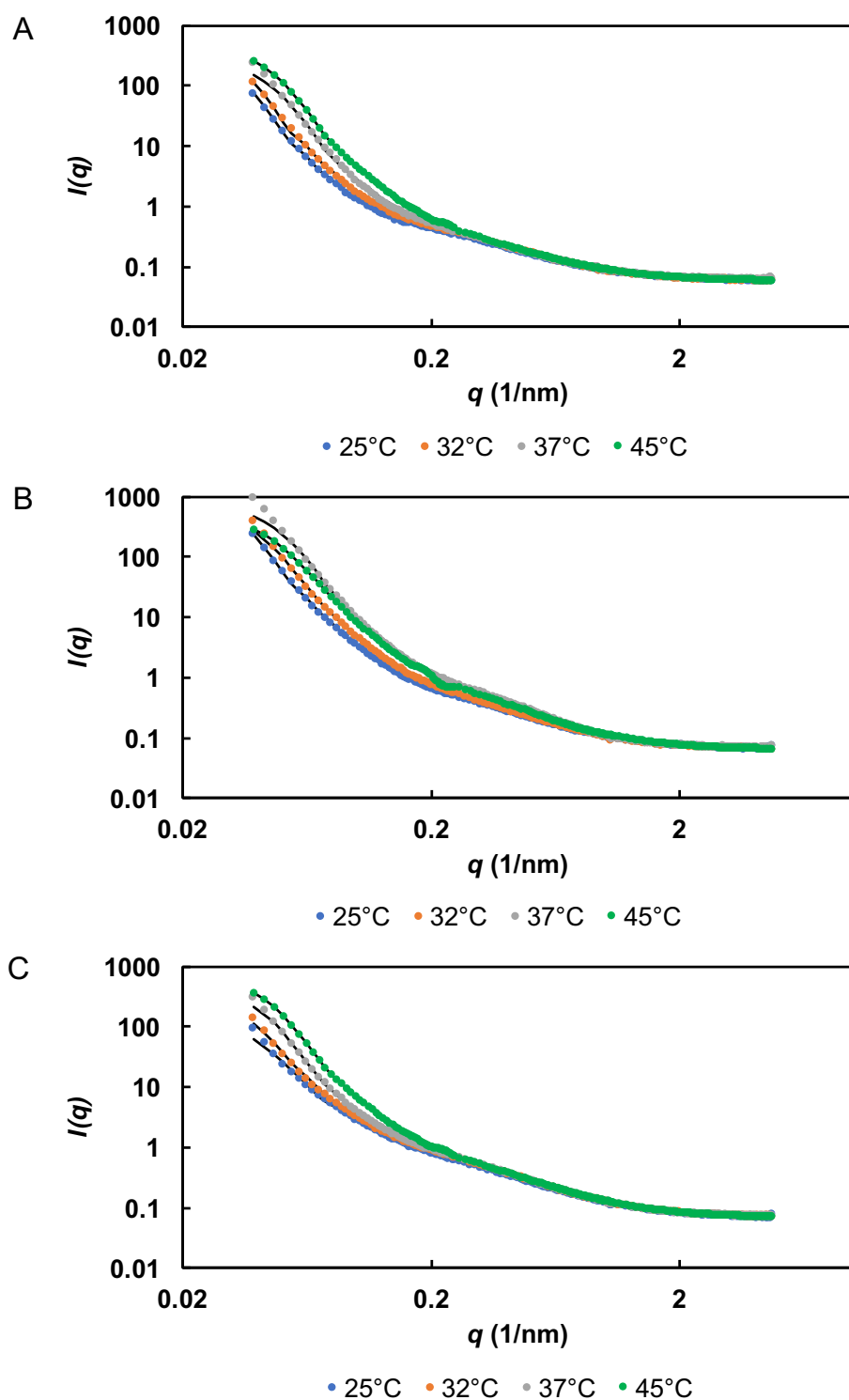


Figure 2.2: Neutron scattering intensity $I(q)$ as a function of the scattering vector (q) as a function of temperature for: (A) 0.05 Ald:Hzd microgel (1 wt% PNIPAM-Hzd); (B) 0.20 Ald:Hzd microgel (1 wt% PNIPAM-Hzd); (C) 0.05 Ald:Hzd microgel (2 wt% PNIPAM-Hzd). Solid black lines represent the fits, and standard deviations of the fits are plotted as error bars.

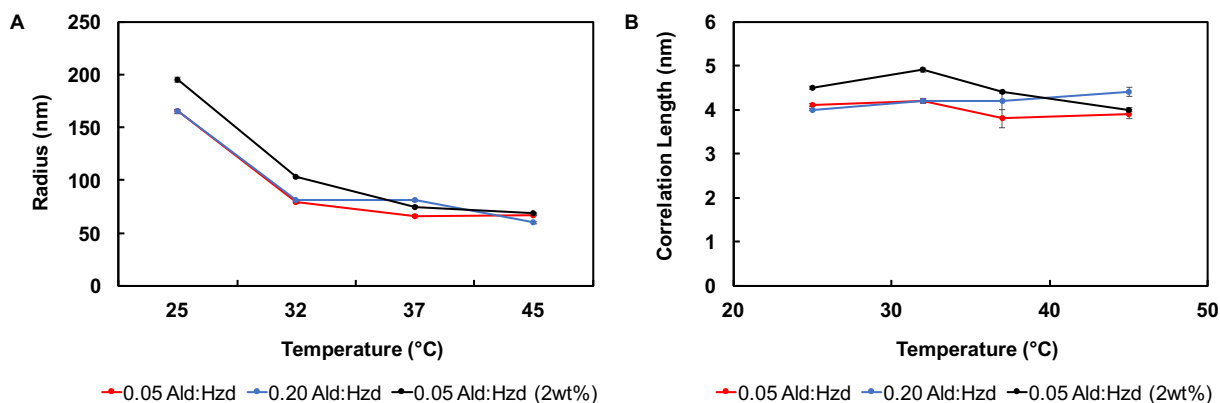


Figure 2.3: Key fitting parameters of the SANS analysis on bulk self-assembled PNIPAM microgels: (A) microgel radius versus temperature; (B) correlation length versus temperature.

In general, the scattering intensity observed increases systematically with temperature as the microgels are heated from below (25°C) to above (45°C) their VPTT, consistent with previous studies on thermoresponsive hydrogels¹⁰⁰ and microgels^{73, 75, 101}. Note that slight aggregation above the VPTT occurred particularly in the 0.20 Ald:Hzd (1 wt%) sample (Fig. 2.2B), which is reflected in the somewhat poorer fit achieved at 37°C and the lower intensity profile observed at 45°C. This increased intensity as a function of temperature correlates to a discontinuous transition in the best fit microgel radius as a function of temperature (Fig. 2.3A), consistent with (albeit slightly larger in overall magnitude compared to) the dynamic light scattering measurement of the phase transition (Supporting Information, Figure S1.3). The higher radius in the collapsed state as well as the higher temperature transition measured via DLS relative to SANS can again be attributed to the intensity weighting of the size distribution in DLS; however, the general trends measured via both techniques are highly comparable. The best fit radius of 0.05 Ald:Hzd prepared with 2 wt% PNIPAM-Hzd seed polymer also was significantly higher at lower temperatures compared to microgels prepared with a 1 wt% PNIPAM-Hzd seed polymer (Fig. 2.3A), again consistent with DLS results (Table 2.1).

Typically, decreases in microgel radius are accompanied by decreases in the correlation length (ϵ), which is conventionally attributed to represent the mesh size of the network. However, only minimal changes in the correlation length were observed as a function of temperature for the self-assembled microgels, with very slight (~ 0.5 nm) decreases observed between 32°C and 37°C for the two lower crosslink density microgels prepared with a 0.05 Ald:Hzd ratio and no significant change in correlation length observed for the more crosslinked microgel (0.20 Ald:Hzd ratio). The comparative differences between different crosslink density microgels are consistent with the DLS results and the best-fit SANS radius results, in which more crosslinked microgels exhibit broader and lower magnitude phase transitions that would result in lower changes in network mesh size as a function of temperature; this is also consistent with observations on conventional (non-homogenous) microgel particles¹⁰². However, at least some change in correlation length versus temperature was anticipated for all microgels. We hypothesize this is a result of a change in the network from being more homogeneous to featuring nanophase separated domains upon heating, the size/spacing of which may also be captured in the correlation length parameter. Given the relatively high number of polar hydrazide, aldehyde, or hydrazone functional groups present in the network, the potential for such nanoscale phase segregation is anticipated to be higher as the self-assembled microgels are heated compared to conventional microgels. As such, the correlation length may simultaneously track these different phenomena as the microgels are heated, making the trends less predictable. However, we also note that mesh size is difficult to measure accurately even with conventional PNIPAM microgels⁷³, and the aggregation noted in the 0.20 Ald:Hzd microgel may also be skewing the results for that particular sample. Regardless, a homogeneous sphere model can give good fits to the SANS profiles of self-assembled microgels over the full transition range, suggesting that the internal

morphology of these microgels is significantly more homogeneous than that of conventional microgels.

Contrast Matching Experiment

To independently track the distributions of PNIPAM-Ald and PNIPAM-Hzd within the microgel network, PNIPAM-Hzd was deuterium labeled by preparing the copolymer with d7-NIPAM as the monomer. Self-assembled microgels were then fabricated in appropriate index-matching solvents applicable to “hiding” each constituent component of the microgel network (63:37 D₂O:H₂O to hide PNIPAM-Hzd and 22:78 D₂O:H₂O to hide PNIPAM-Ald), allowing for unambiguous contrast matching of one component while preserving the scattering from the other component. USANS measurements were also performed on the same samples to allow for a further extension of the accessible q range and give additional confirmation of the quality of the model fits. Figure 2.4 shows the combined SANS and USANS curves, including the fits, for matched PNIPAM-Hzd and matched PNIPAM-Ald microgels as a function of temperature; the USANS data is highlighted with the dashed boxes to demonstrate the smooth transition at the low q region between the USANS and SANS ranges. Table 2.3 shows the key fitting parameters accessed from the resulting homogeneous sphere model fits. Refer to Supporting Information Table S1.5 for all fitting parameters used in IgorPro.

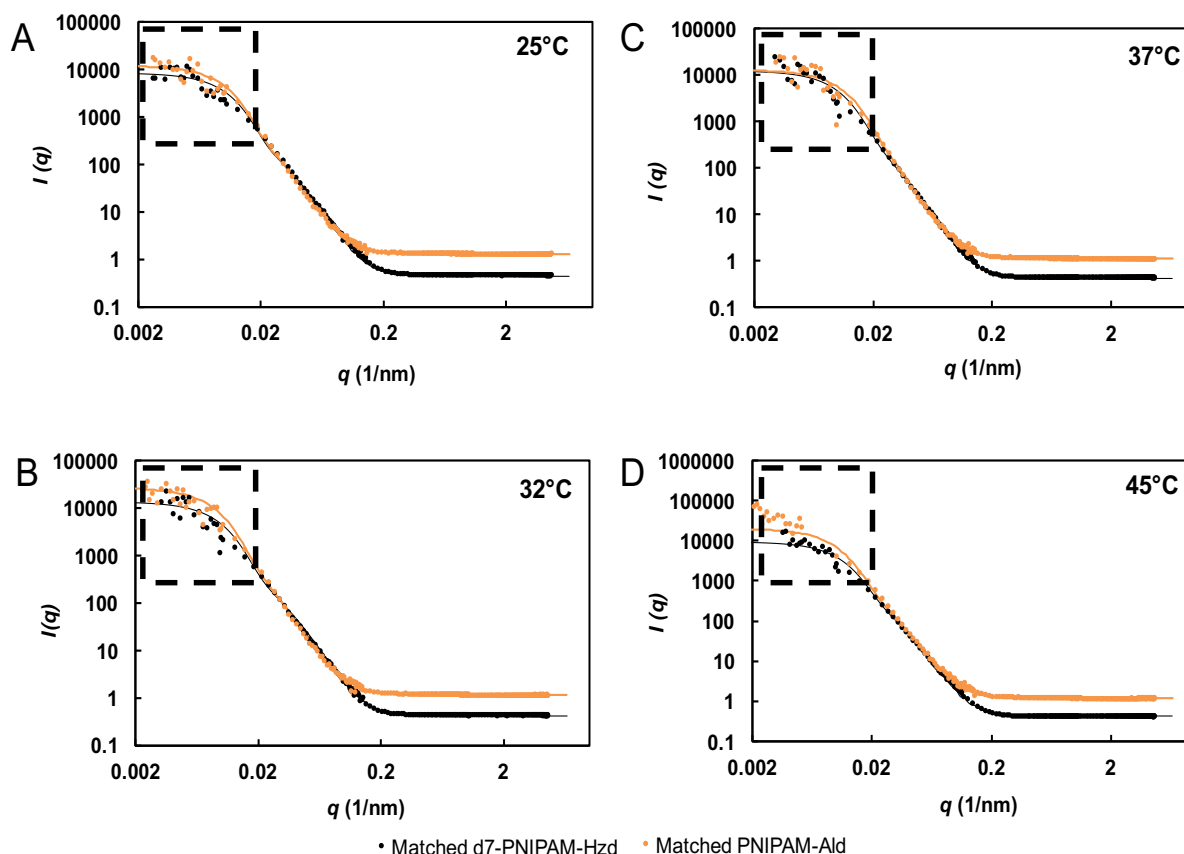


Figure 2.4: Combined SANS and USANS intensity versus q profiles (and fits) for index-matched d7-PNIPAM-Hzd (black curve) and index-matched PNIPAM-Ald (orange curve) in self-assembled microgels as a function of temperature (0.20 Ald:Hzd ratio, 1 wt% d7-PNIPAM-Hzd). USANS data are highlighted with a dotted black box. Note that while standard deviations of the fits are plotted as error bars, most error bars are too small to be visible on the graph.

Table 2.3: Best-fit parameters from homogeneous network fits of the combined USANS/SANS data for self-assembled microgels fabricated with d7-PNIPAM-Hzd and PNIPAM-Ald examined using contrast matching experiments sequentially hiding (A) the d7-PNIPAM-Hzd polymer and (B) the PNIPAM-Ald polymer

	25°C		32°C		37°C		45°C	
	(A)	(B)	(A)	(B)	(A)	(B)	(A)	(B)
Radius (nm)	120	125	118	120	88	88	81	85
Polydispersity	0.45	0.46	0.55	0.61	0.79	0.68	0.79	0.85
Mesh Size (nm)	30	34	30	34	30	34	30	32

Aside from the higher background intensity of the PNIPAM-Ald index-matched profiles (a result of the higher amount of H₂O in the solvent mixture), the scattering profiles of both index matched polymers follow a remarkably similar shape (Figure 2.4). The homogeneous sphere model ($\sigma_{fuzzy} = 0$) again gave excellent fits to both index matched polymer distributions at all temperatures studied over the full accessible USANS/SANS q range. The best-fit radii of both index-matched polymer distributions decrease with temperature (as anticipated for PNIPAM-based materials, Table 2.3) and are quantitatively matched at each temperature regardless what polymer is index-matched, suggesting that both polymers are present throughout the whole mass of the microgel. In addition, although the absolute values of the correlation lengths must be interpreted with extreme caution, as the inherent uncertainty in this value coupled with the fact that the contrast matching technique hides a significant fraction of the microgel mass in each experiment, the correlation lengths of the two contrast matched samples are very similar and again independent of temperature, suggesting that the feature sizes associated with both the d7-PNIPAM-Hzd and PNIPAM-Ald distributions are similar. All these observations are consistent with the oligomeric self-assembled microgels possessing a homogeneously crosslinked network structure.

It must be noted that the measured polydispersity values are significantly larger than those observed with the non-contrast matched experiment (Tables S1.3 and S1.4). While this result is likely in part simply a result of the contrast matching experiment itself, in which a large amount of the total mass of the microgel is “missing” in the scattering curve, the inherent differences in the LCST values between deuterated and protonated PNIPAM-Hzd may also promote larger polydispersities relative to those observed in the non-contrast matched samples. The LCST of the deuterated PNIPAM-Hzd in H₂O is ~60°C, compared to ~56°C for the protonated PNIPAM-Hzd; the addition of D₂O in the solvent (as required to index match

the deuterated polymer) further increases the LCST values by 1-3°C¹⁰³. As such, given that the assembly temperature was identical for all assemblies (70°C), the fabrication of d7-PNIPAM-Hzd-containing microgels occurred much closer to the LCST of the nanoaggregate seed polymer than assemblies using PNIPAM-Hzd. We have previously observed that assemblies performed close to the LCST of the seed polymer result in less defined nanoaggregates and thus more polydisperse microgels, as observed here²⁰. However, since the mechanism of assembly remains the same, the results extracted here remain relevant to the all-protonated microgels. It should also be noted that the polydispersity values of the overall microgels are all reasonably low (PDI<0.15) over the full size range tested for both 0.05 Ald:Hzd and 0.20 Ald:Hzd microgels in D₂O (Figure S1.4), making it more likely that this larger polydispersity is a fitting artefact rather than a real effect.

SANS of Self-Assembled Layered PNIPAM Microgels

To investigate how the addition of subsequent reactive polymers to a pre-assembled microgel (i.e. LbL modification) influences the internal morphology of the resulting microgels, SANS was used to probe the internal morphology of the resulting microgels. Table 2.4 shows the change in microgel radius as a function of adding sequential layers of PNIPAM-Hzd polymer or alternating layers of PNIPAM-Ald and PNIPAM-Hzd (see Supporting Information, Figure S1.5 for the raw SANS data and the best-fit curves). Full fitting parameters (including a summary) are provided in Supporting Information Table S1.6.

Table 2.4: Best-fit parameters from homogeneous network fits of the SANS data for layer-by-layer self-assembled microgels based on a 0.05 Ald:Hzd (1 wt % PNIPAM-Hzd) microgel core (solvent = D₂O), measured at 25°C

Microgel Description	Radius (nm)	Polydispersity (%)	Correlation length (nm)
0.05 Ald:Hzd (1 wt%)	165 ± 2	4	4.1
0.05 Ald:Hzd (1 wt%) + PNIPAM-Hzd	177 ± 1	8	4.5
0.05 Ald:Hzd (1 wt%) + PNIPAM-Hzd + PNIPAM-Hzd	178 ± 4	10	3.6
0.05 Ald:Hzd (1 wt%) + PNIPAM-Ald	167 ± 2	7	2.5
0.05 Ald:Hzd (1 wt%) + PNIPAM-Hzd + PNIPAM-Ald	176 ± 2	5	12.1

As with the self-assembled microgels themselves, no visual or quantitative (via χ^2 values, see Supporting Information Table S1.2) improvement in the quality of fit was achieved when using the fuzzy sphere model relative to a homogeneous sphere model, suggesting that the addition of the subsequent functional polymers does not substantially alter the homogeneity of the microgel network (i.e. a “shell” is not formed). However, consistent in terms of both trends as well as absolute radius values with the DLS results (Table 2.1), the best-fit radius slightly increased when an additional “layer” of PNIPAM-Hzd was added to a pre-assembled 0.05 Ald:Hzd (1 wt%) microgel. Based on these results, we hypothesize the observed size increase is a result not of the formation of a PNIPAM-Hzd-rich shell but rather a homogeneous increase in the hydrophilicity of the microgel network due to the introduction of an increasing number of unreacted polar hydrazide groups. Combined with the concurrent increase in total mass density within the microgel, the increased polarity increases the osmotic pressure inside the gel phase to drive swelling in the microgel, resulting in the larger measured size.

When a second polymer “layer” was added, the particle size did not significantly change regardless of whether the polymer was PNIPAM-Hzd or PNIPAM-Ald, although the reason behind each result is different. The original self-assembled microgels have a 20:1 excess of hydrazide versus aldehyde groups (0.05 Ald:Hzd); as such, the first PNIPAM-Hzd treatment can easily consume the available free (unreacted) aldehydes remaining from the assembly step, resulting in little if any of the additional PNIPAM-Hzd being crosslinked/immobilized into the microgel network. In contrast, the large excess hydrazide content means that the addition of further PNIPAM-Ald does result in the formation of more crosslinks (less swelling) as well as the replacement of free hydrazide groups with either aldehydes or hydrazones, both of which are less polar. These dual deswelling responses are offset by the increase in net polymer concentration within the microgel phase (driving osmotic swelling) to result in no net change in microgel particle size upon the addition of the second layer. Regardless of the mechanisms involved, these results confirm that the homogeneous sphere model can accurately fit the internal structure of oligomeric self-assembled microgels regardless of how many subsequent additions of reactive pre-polymer are performed. This result means that the pre-polymers can freely diffuse into the pre-formed microgel instead of forming the dense core-diffuse shell structure that would have been anticipated in traditional layer-by-layer assembly.

Langmuir Trough

As a complementary method to probe the internal morphology of the microgels, surface pressure measurements of 0.05 Ald:Hzd (1 wt% PNIPAM-Hzd) and 0.20 Ald:Hzd (1 wt% PNIPAM-Hzd) self-assembled microgels assembled at the n-decane/water interface were performed using a Langmuir trough. Figure 2.5 shows the normalized compression isotherms (composed from different microgel concentrations) of these two self-assembled microgels in

comparison to previously-reported isotherms related to conventionally-fabricated PNIPAM-co-methacrylic acid (PNIPAM-co-MAA) microgels that have previously been identified via SANS analysis to have a fuzzy sphere morphology⁷⁹. Note that un-normalized compression isotherms (with the corresponding amounts of 1 wt% microgel solution) are included as Supporting Information, Figure S1.6.

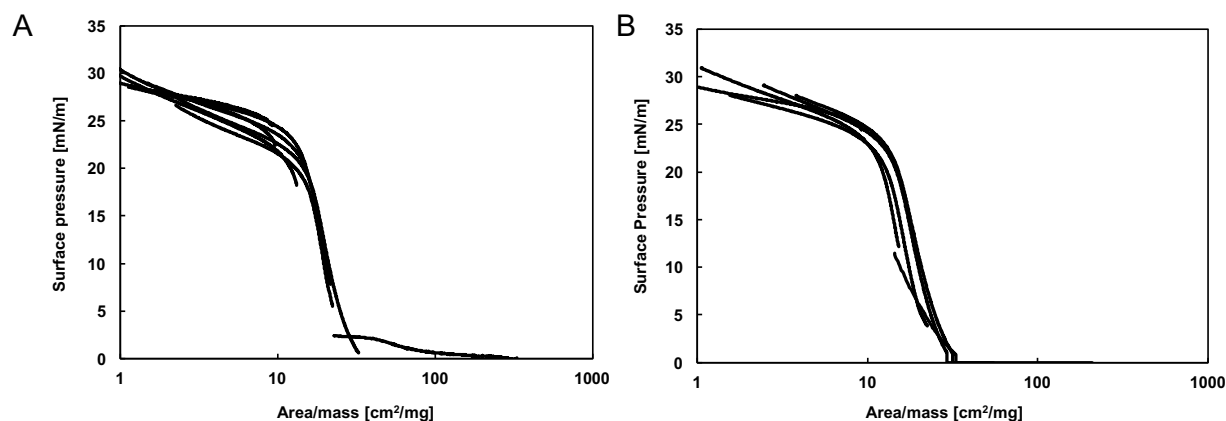


Figure 2.5: Normalized compression isotherms of self-assembled PNIPAM microgels (A) 0.05 Ald:Hzd (1 wt% PNIPAM-Hzd) and (B) 0.20 Ald:Hzd (1 wt% PNIPAM-Hzd) at the n-decane/water interface.

For the self-assembled microgels, the compression isotherms at different concentrations followed the same shape and reached a single plateau, independent of the cross-link ratio. We anticipate that the lack of difference between the 0.05 Ald:Hzd and 0.20 Ald:Hzd microgels is attributable to the reduction in the sensitivity of the Langmuir trough technique due to the moderate polydispersity of the self-assembled microgels, which cannot pack perfectly at the interface as do conventional microgels. In addition, both compression isotherms were sigmoidally shaped, with only a single plateau observed upon compression. In contrast, conventionally fabricated PNIPAM microgels with a known dense core-disperse shell structure show a distinct second plateau at the higher range of surface pressures tested¹⁰⁴⁻¹⁰⁵. This type of iso-structural transition has been attributed to the differences in compression forces measured whether the microgels are in shell-shell contact (two more

loosely crosslinked networks, compressible at lower forces) or core-core contact (two more tightly crosslinked networks, compressible only at higher forces)¹⁰⁵. The absence of this second plateau in self-assembled microgel data suggests that there is no such spatial difference in crosslinking density (i.e. no core-shell) in these microgels, again consistent with the successful SANS fits of these microgels as homogeneously cross-linked networks.

Drug Loading Efficiencies

To assess whether directly loading of the moderately hydrophobic drug (i.e. dexamethasone) is possible during the self-assembly process (a process that would have several advantages including ease of encapsulating moderately hydrophobic drugs, simple purification, and fast loading), five different concentrations of dexamethasone were loaded in 0.20 Ald:Hzd self-assembled PNIPAM microgels. Table 2.5 shows the resulting particle sizes of the microgels with and without drug loading and the encapsulation efficiency of dexamethasone at different drug concentrations. Note that 0.1 mg/mL was chosen as the upper limit for loading experiments given that this represents the aqueous solubility of dexamethasone.

Table 2.5: Drug loading efficiency for *in situ* dexamethasone loading during self-assembly

Dexamethasone Concentration (mg/mL)	Diameter without dexamethasone (nm)	Diameter with dexamethasone (nm)	Encapsulation Efficiency (%)
0.03	290 ± 8 (PDI = 0.08 ± 0.05)	261 ± 15 (PDI = 0.11 ± 0.05)	76 ± 3
0.035		275 ± 10 (PDI = 0.08 ± 0.04)	82 ± 5
0.06		265 ± 5 (PDI = 0.07 ± 0.04)	78 ± 1
0.07		280 ± 7 (PDI = 0.10 ± 0.02)	75 ± 3
0.1		264 ± 4 (PDI = 0.12 ± 0.03)	74 ± 2

The drug-loaded microgels exhibited statistically significant but relatively small decreases in size relative to microgels prepared using the same self-assembly process but without drug, consistent with the loading of a moderately hydrophobic payload into the microgel phase. However, in each case, the polydispersity of the drug-loaded microgels sample remained very low (<0.1), indicating the preservation of the monodisperse suspension of microgels important for drug delivery applications. In addition, the encapsulation efficiency over the full range of drug concentrations tested is $>75\%$; this is five times higher than the loading efficiencies achieved with the conventional diffusion-based loading method of pre-formed microgels ($15 \pm 8\%$). As such, the *in situ* loading self-assembly method is both faster (avoiding the need for microgel pre-fabrication before loading, cutting out the partitioning/diffusion equilibration time, and eliminating one centrifugation step) and significantly more effective. It is important to note that diffusion/partitioning-based loading is the only available drug loading protocol for conventional precipitation-based PNIPAM microgels, while the self-assembled microgels can be loaded either *in situ* or via passive diffusion.

Drug Release Study

A preliminary drug release study was performed with 0.05 Ald:Hzd microgels loaded using a 0.08 mg/ml dexamethasone solution, with release tracked over a duration of 12 days (Figure 2.6). Remarkably slow drug release was observed; less than 7% of the total drug was released over the 12-day experiment, indicating very slow and controlled release. To assess the mechanism of drug release in both cases, a first-order fit was plotted on the cumulative release versus time graph in Figure 2.6, while the amount of drug released as a function of sample number was plotted in Figure 2.7.

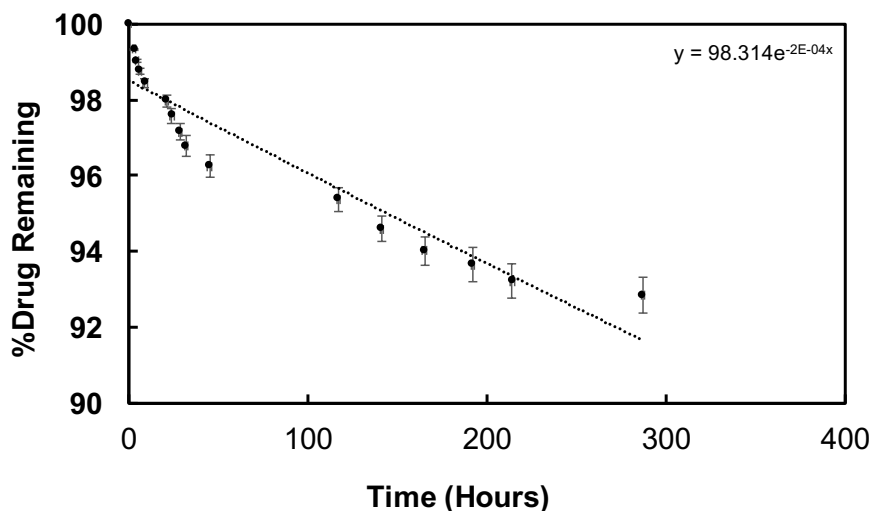


Figure 2.6: Cumulative drug release profile of dexamethasone as a function of time from 0.05 Ald:Hzd microgels (n=3). The dotted line represents a first order-fit ($R^2 = 0.91$)

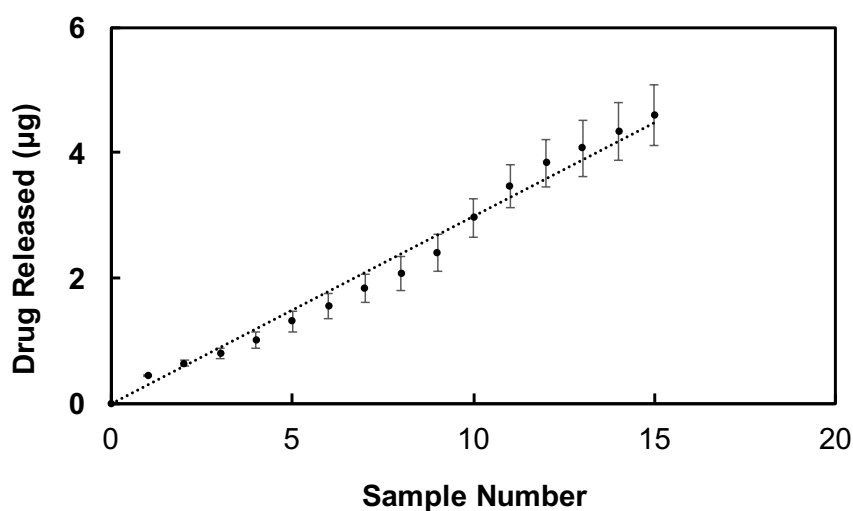


Figure 2.7: Cumulative drug release of dexamethasone as a function of sample number from 0.05 Ald:Hzd microgels (n=3). The dotted line represents a linear regression fit ($R^2 = 0.98$)

The first-order fit does not accurately describe the drug release, either qualitatively or quantitatively based on the relatively low R^2 value observed. This result suggests that the release of dexamethasone is not purely regulated by diffusion. In contrast, Figure 2.7 shows that the amount of drug released is linearly correlated with each sample number. This result suggests that the release of dexamethasone from the uncharged PNIPAM microgels is primarily due to drug partitioning (i.e. concentration gradients) between the microgel and

release phases, offering potential for longer-term drug release from microgels. A longer-term analysis is now underway to demonstrate whether or not this linearity observed between the sampling step and the cumulative drug release will remain over longer release periods/at higher cumulative drug release levels.

Discussion

Controlling the internal morphology of microgels is essential to generating the swelling, diffusive, interfacial properties, and drug loading and release properties required for specific applications. Herein, SANS (both with and without contrast matching of the constituent gel precursor polymers), USANS, and surface force measurements all suggest that our oligomeric self-assembled microgels have a homogeneously crosslinked structure, in contrast to PNIPAM microgels prepared using the conventional free radical precipitation polymerization technique. This result is somewhat unanticipated given the sequential addition synthetic procedure used to prepare the microgels starting from a pre-aggregated PNIPAM-Hzd seed above the phase transition temperature; the addition of a polymeric crosslinker to a collapsed nanoaggregate was expected to lead to the formation of a dense shell morphology based on the low anticipated diffusion of the PNIPAM-Ald crosslinker into the nanoaggregate. However, we believe the result presented is reasonable for two reasons. First, the self-assembly is conducted just above the lower critical solution temperature of what is a fairly polar starting material; ~15 mol% of the monomeric units on PNIPAM-Hzd have a highly polar hydrazide group attached. As such, while it is clear from both DLS and the SANS measurements that nanoaggregation is occurring, the nanoaggregate is likely neither highly collapsed nor highly organized, with the latter point supported by the substantial decrease in the polydispersity of the nanoaggregate upon crosslinking with PNIPAM-Ald (from ~30% for the nanoaggregate to ~10-20% for the bulk self-assembled PNIPAM

microgels, Tables S1.3 and S1.4). As such, relative to unfunctionalized PNIPAM polymers that form highly condensed aggregates, the more polar PNIPAM-Hzd nanoaggregates can likely facilitate interdiffusion of the PNIPAM-Ald crosslinking polymer. Furthermore, since the assembly temperature is also higher than the LCST of the relatively small PNIPAM-Ald oligomer ($M_n \sim 15$ kDa, LCST ~ 42 °C), the diameter of collapsed PNIPAM-Ald chains would be small and the aldehyde crosslinking groups would be less sterically accessible under the self-assembly conditions, enabling improved penetration of the polymer into the PNIPAM-Hzd nanoaggregate. Second, unlike the permanent free radical crosslinks formed using the conventional microgel fabrication technique, our use of reversible and dynamic hydrazone crosslinking chemistry enables dynamic changes in the crosslinking density over time until an equilibrium is reached. Note that the slightly acidic pH value of both the reaction mixture and obtained microgels (pH ~ 5.5 -6) is consistent with allowing such dynamic exchange on the observed time scale¹⁰⁶. Consistent with prior observations on low molecular weight polyelectrolytes, diffusion of the PNIPAM-Ald crosslinker (or any of the LbL polymer treatments) into the microgel bulk is on this basis thermodynamically favorable, given that distributing the PNIPAM-Ald polymer throughout the microgel would sterically maximize the number of hydrazone crosslinks that could be formed. Thus, the combination of these kinetic and thermodynamic contributions makes it reasonable to expect a relatively homogeneous crosslink distribution.

The homogeneous nature of these self-assembled microgels adds to the potential advantages of these microgels relative to conventional microgels in biomedical applications. In addition to the inherent degradability offered by the hydrazone crosslinks, the uniform network structure should offer more predictable drug release rates, affinities to environmental analytes, or refractive properties for biosensor applications. Specifically, the loading and

release of hydrophobic drugs, such as dexamethasone, can be improved significantly compared to conventional precipitation-based microgels by loading drug directly during the self-assembly process, not possible using conventional free radical-based microgel fabrication techniques. Ocular inflammatory diseases including age-related macular degeneration, diabetic retinopathy and glaucoma require the controlled delivery of dexamethasone to the posterior segment of the eye that avoid frequent drug dosages and thus lead to poor patient compliance¹⁰⁷. Degradable microgels offer a potential solution to this challenge which are minimally invasive but still effective in terms of enabling controlled drug delivery. It must be emphasized that the self-assembly loading method requires that the drug to be loaded is thermally stable at the assembly conditions ($\sim 70^{\circ}\text{C}$ over at most one hour between the pre-heating and assembly steps); while this is not to be problematic for many drugs of interest, drug stability must be considered to ensure the efficacy of this method.

Conclusion

A combination of surface force measurements, small angle neutron scattering (SANS), and ultra-small angle neutron scattering (USANS) was used to demonstrate that self-assembled microgels based on hydrazide and aldehyde-functionalized poly(N-isopropylacrylamide) oligomers have a homogeneously cross-linked internal structure. This structure is hypothesized to form as a result of the combination of the dynamic nature of the hydrazone crosslinking chemistry and the assembly conditions used that promote polymer interdiffusion. In contrast, conventional precipitation polymerization-derived PNIPAM microgels have a diffuse shell-dense core structure. As such, we anticipate that these well-defined degradable and homogeneous nanoscale gel networks offer opportunities for addressing challenges in drug delivery, biosensing, and optics by exploiting the predictable diffusive and refractive properties of the homogeneous microgel networks. In particular, herein we demonstrate successful co-self-assembly of a moderately hydrophobic anti-inflammatory drug

(dexamethasone) with five-fold higher efficacy in drug encapsulation (75-80%) relative to the conventional partition/diffusion-based drug loading processes using a much faster, single-step process (suitable if drug is stable at assembly temperature).

Acknowledgements: Funding from the Natural Sciences and Engineering Research Council of Canada (NSERC, Discovery Grant Program RGPIN 356693) and the Ontario Early Researcher Awards (Ontario Ministry of Research and Innovation, ERA ER09-06-185) is gratefully acknowledged. Access to USANS BT5 and NGB30SANS was provided by the Center for High Resolution Neutron Scattering, a partnership between the National Institute of Standards and Technology and the National Science Foundation under Agreement No. DMR-1508249. EM acknowledges the receipt of the Ronald William Merkel Travel Scholarship and the Engineering Student Mobility Award from McMaster University to facilitate her travel to Germany as well as and Nadine Daleiden for help with the Langmuir trough experiments. AS acknowledges funding the Alexander von Humboldt Foundation. WR thanks the Deutsche Forschungsgemeinschaft for support within SFB 985 "Functional microgels and microgel systems".

Chapter 3: Fabrication and Characterization of Charged and Amphoteric Self-Assembled PNIPAM Microgels

Cationic, anionic, and amphoteric dual pH/temperature-responsive degradable microgels via self-assembly of functionalized oligomeric precursor polymers

Eva Mueller, Madeline Simpson, Sebastian Himbert, Michael Majcher, Todd Hoare

To be submitted August 2018

Summary

Multi-responsive smart materials with the capacity to reversibly change properties (i.e. size, charge) upon the application of more than one stimulus (i.e. temperature, pH) offer potential in numerous biotechnology and biomedical applications due to their ability to offer amplified responses to multiple “on” stimuli and/or respond to specific biological niches. Herein, we demonstrate the use of an aqueous thermally-driven self-assembly approach based on hydrazide and aldehyde-functionalized poly(N-isopropylacrylamide) (PNIPAM) oligomers functionalized with cationic and/or anionic comonomers for the fabrication of degradable temperature/pH dual responsive microgels. The self-assembled microgels show properties analogous to conventional cationic or anionic PNIPAM microgels, retaining their thermal responsiveness while exhibiting pH-driven swelling upon functional comonomer ionization. Amphoteric microgels can similarly be produced by mixing cationic and anionic-functionalized precursor polymers during the self-assembly process, reproducing the high pH/low pH parabolic swelling response observed in conventional amphoteric microgels. Coupling the precise dual responsive swelling responses achievable with the degradability of the hydrazone crosslinks, self-assembled charged PNIPAM microgels offer potential for

improved performance in drug delivery applications demanding dual pH/temperature specific delivery (e.g. infection sites or cancer).

Literature Review

Stimulus-responsive or ‘smart’ polymers are increasingly attracting interest in biotechnology and medicine, especially in the development of drug-delivery systems, given their fast changes from a hydrophilic to a more hydrophobic state when exposed to only small changes in their environment (e.g. pH, temperature, ionic strength)¹⁰⁸. These changes are reversible, allowing the system to return to its initial state when the environmental trigger is removed. The development of smart polymeric systems originated from the idea to imitate the behavior of DNA and proteins, the building blocks of life, which have the ability to respond to very small changes in chemical signals to perform necessary metabolic processes within the body¹⁰⁹. Using the same concept for drug delivery applications, smart polymers offer potential to be an innovative approach for treating many life-threatening diseases and improve the standard of living for patients.

Drug delivery is the transportation of pharmaceutical components to target sites within the human body while maintaining the optimum therapeutic activity and minimizing any unwanted side effects. Available drug delivery systems include liposomes, gels and nanoparticles, among many others¹¹⁰⁻¹¹¹. Hydrogels are water-swollen polymer crosslinked networks that can be classified based on their synthesis method, type of ionic charges present in the polymer network and physical structures¹⁰⁹. Hydrogels have several advantages relative to other types of materials including high hydrophilicity, flexibility, high water absorptivity and generally good cytocompatibility. One of the most valuable characteristics of a hydrogel in the context of their use as a drug delivery system is their ability to respond to external stimuli¹⁰⁹. For example, with the presence of ionic charges in the hydrogel matrix,

the internal mesh size (also known as the distance between cross-links) of the polymeric network can change with small pH variations in the environment.

In comparison to macroscopic hydrogels, microgels are three-dimensional, covalently crosslinked polymer networks on the size range of 10 nm to 1 μm ¹. Microgels have the advantages of responding to external stimuli much faster compared to bulk gels and allowing for minimally invasive administration due to their nanoscale size. As with conventional bulk hydrogels, microgels can be described in terms of their water content, average crosslink density and characteristic swelling and de-swelling behaviour. Furthermore, in the context of drug delivery, microgels offer the key advantages of facile control over particle size and charge, ease of synthesis and easy functionalization allowing for stimulus-responsive behaviour¹¹². The high water content and thus low interfacial tension also offers the ability for a long-term circulation and the possibility of being actively or passively targeted to the desired location within the body, i.e. tumour sites⁵⁴.

Stimuli-responsive microgels (also referred to as “smart” microgels) have attracted the interest of many research groups, resulting in a vast array of applications including sensors¹¹³⁻¹¹⁴, optics¹¹⁵ and loading/release applications^{112, 116}. Microgels have been designed that can change their properties in response to physical (temperature, light, electric and magnetic fields) or chemical (pH, ionic strength, and the presence of chemical or biological compounds)¹¹² stimuli. The latter is more common in terms of targeting delivery sites within the body. Thermoresponsive poly(N-isopropylacrylamide) (PNIPAM) microgels are perhaps the best-known smart soft nanomaterial. PNIPAM microgels have a volume phase transition temperature (VPTT), a direct result of the lower critical solution temperature (LCST) of the PNIPAM polymer ($\sim 32^\circ\text{C}$)⁷. PNIPAM microgels are swollen at room temperature but, when

heated above the VPTT, they discontinuously shrink in size. This phase transition is commonly related to the breaking of hydrogen bonds between water and amide bonds in PNIPAM as the hydrophobic interactions between the isopropyl groups become stronger at higher temperatures. Due to their high stability relative to other drug loaded carriers such as liposomes or micelles, PNIPAM microgels have been widely investigated as a drug delivery vehicle, particularly for anticancer drugs given that their small tunable size (<200 nm) allows for relatively efficient uptake into tumours^{63, 117-118}.

The swelling behaviour of PNIPAM microgels can be tuned by co-polymerizing monomers with different affinities for water, in particular organic acids or bases⁷. NIPAM has been successfully copolymerized with acrylic acid, methacrylic acid, maleic acid, vinylacetic acid, allyl-acetic acid, and dimethylaminoethyl methacrylate, among many others¹⁸. These co-monomers are of special interest as they introduce charges into the polymer network that will significantly influence the overall swelling and shrinking behaviour of the microgel particles in different ways. Co-polymerization can increase or decrease the LCST of the PNIPAM polymer, which consequently changes the VPTT by varying the hydrophilic-hydrophobic balance in the microgel. Moreover, the addition of these monomers allows the already thermo-responsive PNIPAM microgels to also exhibit responsiveness to pH and ionic strength, which alter the charge density of the polymer network and the Debye screening length (and thus Donnan equilibrium-driven swelling of the microgel network)¹¹⁹.

In the conventional precipitation-based microgel synthesis, the minimum reactants required for polymerizing a charged microgel are a free radical initiator, a monofunctional monomer (giving the linear segments), a bifunctional monomer (giving crosslinks) and a charged monomer (providing the pH-ionizable behaviour). Crosslink and charge densities can vary

for each copolymerization. This strategy has demonstrated potential to produce well-defined microgels with highly tunable charge densities and thus pH-induced swelling responses¹²⁰. Such responses have significant potential in biomedical applications. Drug loading and release profiles of in particular charged drugs can be significantly altered by introducing partitioning effects beyond simple diffusion-controlled release⁶⁴. In addition, pH-responsive microgels have been fabricated for highly specific targeting of cancer cells, leveraging the pH changes in the intracellular environment for targeted delivery of anticancer drugs into tumor cells¹²¹. The dual temperature/pH responsiveness of charged PNIPAM microgels offers further opportunities in this context given the typically slightly higher temperature observed at rapidly growing tumour or infection sites⁴⁷, enabling the design of microgels that could release their cargo specifically in cancer and/or infection microenvironments.

However, to use such microgels for biomedical applications, degradability remains an issue. Most microgel preparations use a non-degradable crosslinker; even if the crosslinker is degradable, the molecular weights of the degradation products are often not controllable and thus may not be cleared following gel degradation. To address this degradability issue in the context of biomedical applications, a novel thermally-driven self-assembly approach has been developed in the Hoare group²⁰. In this method, a hydrazide-functionalized PNIPAM polymer is heated above the LCST of the polymer to form un-crosslinked nanoaggregates in solution. With the addition of an aldehyde-functionalized PNIPAM polymer, an acid-labile hydrazone bond is formed between the hydrazide and aldehyde groups to fabricate colloiddally stable PNIPAM microgels in solution. These microgels are degradable, monodisperse, and stable over months, while retaining their responsiveness to temperature due to the presence of PNIPAM²⁰. The properties of such self-assembled microgels can be designed to be identical

to precipitation-based PNIPAM microgels with the added advantage of degradability into polymers with known molecular weights below the kidney clearance limit.

To date, only thermo-responsive self-assembled PNIPAM microgels have been fabricated and characterized. By adding charge into the precursor polymers used in self-assembly, pH tunability (and different swelling behaviors) can be achieved that may be of significant interest for a number of applications ranging from sensors to drug delivery. Of particular interest are amphoteric microgels, a special subcategory of pH-responsive microgels that have both cationic and anionic charges incorporated into their crosslinked polymeric network. Amphoteric hydrogels have been demonstrated to offer superior repellency to protein adsorption^{24, 122}, key for promoting long circulation times *in vivo* and thus more effective drug delivery. In addition, amphoteric microgels have different swelling/de-swelling behaviours compared to single-charged microgels, opening them up to be utilized for specific drug delivery applications. For example, Taira et al. demonstrated the use of amphoteric microgels as DNA scavengers that can trap ssDNA at neutral pH due to the formation of an ion complex between negatively charged DNA and positively charged microgels; in alkaline pH, ssDNA was released due to the electrostatic repulsion forces induced by the change of the microgel charge¹²³.

Amphoteric microgels are typically prepared using the same precipitation polymerization process used to fabricate conventional thermoreponsive microgels¹²³⁻¹²⁴. Introducing both cationic and anionic charges directly in the precipitation polymerization of microgels has been well studied. For example, Richtering's group prepared amphoteric microgels by the copolymerization of NIPAAm with acrylic acid and vinylimidazole¹²⁵ and designed methods to prepare amphoteric microgels with temperature-sensitive properties and a controlled

distribution of charged groups¹²⁴. However, self-assembly/crosslinking methods for introducing both charges into the microgel system are less common and not as well understood in literature.

Objective

Charged microgels have many applications in ion exchange¹²⁶, drug delivery¹²⁷ and environmental sorption¹²⁸ due to their ability to improve loading and/or mediate release of charged species and de-swell and/or aggregate at a specific pH/temperature combinations, However, conventional precipitation-based PNIPAM microgels are non-degradable. Our novel self-assembly process allows for the fabrication of charged PNIPAM microgels because the precursor polymers can be easily functionalized to incorporate both cationic and anionic charges. As such, the objective of this Chapter is to fabricate and characterize the physical properties of single-charged and amphoteric self-assembled PNIPAM microgels that offer both desirable biological charge-switching properties as well as degradability and clearance in biomedical applications.

Experimental Section

Materials

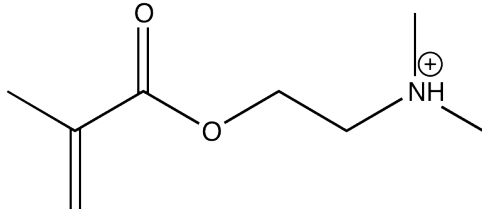
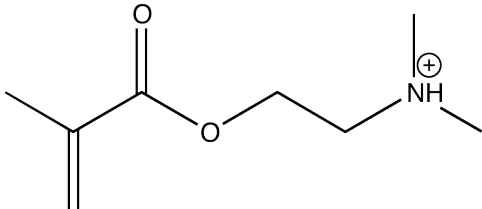
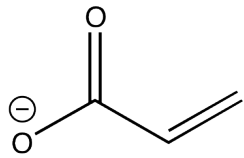
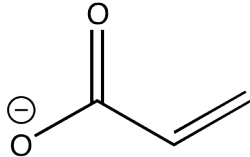
N-isopropylacrylamide (NIPAM, 99%), acrylic acid (AA, 99%), 2-(dimethylamino) ethyl methacrylate (DMAEMA, 98%), thioglycolic acid (98%), aminoacetaldehyde dimethyl acetal (99%), sodium cyanoborohydride (95%), 2,2,6,6-tetramethyl-1-piperidinyloxy (TEMPO, 98%), methacryloyl chloride (purum), acryloyl chloride (97%) and tert-butyl carbazate (98%) were purchased from Sigma Aldrich (Oakville, ON). NIPAM was purified by dissolving 1 g/mL in toluene at 60°C, adding a 2:3 ratio of hexane to toluene, placing the solution in an ice bath for 1-2 hours, filtering/rinsing with hexanes, and drying the recrystallized NIPAM monomer under N₂ overnight. Adipic acid dihydrazide (ADH, Alfa Aesar, 98%), *N*'-ethyl-*N*-(3-dimethylaminopropyl)-carbodiimide (EDC, Carbosynth, Compton CA, commercial grade), 2,2-azobisisobutyric acid dimethyl ester (AIBMe, Wako Chemicals, 98.5%), and ethanol (Commercial Alcohols, Brampton, ON) were purchased and used without further purification. Milli-Q grade distilled deionized water (DIW) was used for all experiments.

The hydrazide acrylate monomer was synthesized by adding Et₃N (2.40 mL, 17.3 μmoles, 1.1 eq) to a solution of boc-carbazate (2.07 g, 15.7 μmoles) in CH₂Cl₂ (75 mL) under a nitrogen atmosphere and the solution was cooled to 0°C. Acryloyl chloride (1.27 mL, 15.7 μmoles) was added dropwise over 5 min and the reaction was allowed to stir at 0°C for 30 min. The crude reaction mixture was filtered to remove the triethylamine hydrochloride salt and the filtrate was concentrated by rotary evaporation. The product was purified via silica gel column chromatography (2:1 to 1:1 Hex/EtOAc) to give 1.52 g of the desired product (52 % yield). The reaction scheme and NMRs (¹H NMR and ¹³C NMR) confirming the successful synthesis of the monomer are provided in Appendix B (Figures S2.1 and S2.2).

Prepolymer Synthesis

All polymers were prepared via free radical copolymerization of NIPAM (4.5 g) in 20 mL of ethanol using thioglycolic acid (TGA, 80 μ L) as the chain transfer agent and 2,2-azobisisobutyric acid dimethyl ester (AIBME, 0.056 g) as the initiator (reaction temperature = 60°C). Functional comonomers appropriate for both facilitating hydrazone crosslinking and introducing charge into the microgels were added as described case-by-case below. For reference, the chemical structures of the charged co-monomers in the PNIPAM polymerizations are highlighted in Table 3.1.

Table 3.1: Chemical structures of charged co-monomers in PNIPAM polymerizations

	PNIPAM-Hzd	PNIPAM-Ald
Cationic		
Anionic		

(1) Cationic hydrazide-functionalized PNIPAM ((+)-PNIPAM-Hzd):

The base recipe was used together with 0.5 g AA and 2 mL DMAEMA. The acrylic acid residues were subsequently converted to hydrazide groups by dissolving 1 g of PNIPAM-co-AA-DMAEMA, 20 g of adipic acid dihydrazide (ADH, 5-fold molar excess), and 11 g of EDC in 200 mL of Milli-Q water. The pH was adjusted to 4.75 and maintained throughout the reaction (4-5 hours) via the addition of 1 M HCl as required to facilitate conjugation of

ADH to the acrylic acid residues. The resulting solution was dialyzed against Milli-Q water over six 6 h cycles (12–14 kDa MWCO) and lyophilized.

(2) Anionic hydrazide-functionalized PNIPAM ((-)-PNIPAM-Hzd):

The base recipe was used together with a 1.3 g of the hydrazide acrylate monomer and 0.5 g of AA. After the overnight polymerization, the polymer was dissolved in 50:50 DCM:TFA for 2-3 hours to remove the t-butyl protecting group and expose the hydrazide group. Once the solvent was blown off with air in the fumehood overnight, the polymer was dissolved in water and dialyzed over 6 cycles against Milli-Q water in 12-14 MWCO. See Appendix B (Figure S2.3) for ¹H NMR confirmation of the production of a pure protected hydrazide acrylate monomer.

(3) Cationic aldehyde-functionalized PNIPAM ((+)-PNIPAM-Ald):

The base recipe was used together with 2.10 mL of DMAEMA and 0.95 g of N-(2,2-dimethoxyethyl)methacrylamide (DMEMAm, synthesized as previously described in⁴). After the overnight polymerization, the polymer was dissolved in 1 M HCl for 24 hours to hydrolyze the pendant acetal group in DMEMAm into aldehyde groups. The resulting solution was dialyzed against Milli-Q water over six 6 h cycles (12–14 kDa MWCO) and lyophilized.

(4) Anionic aldehyde-functionalized PNIPAM ((-)-PNIPAM-Ald):

The base recipe was used together with 0.5 g of AA and 0.95 g of N-(2,2-dimethoxyethyl)methacrylamide (DMEMAm). Polymerization and work-up was conducted analogously to that described for the cationic PNIPAM-Ald polymer.

Prepolymer Characterization

Base-into-acid conductometric titration (ManTech Associates) using 0.1 M NaOH as the titrant and 50 mg of the functionalized microgel suspended in 1 mM NaCl as the sample was used to measure the stoichiometric incorporation of the titratable comonomers AA and DMAEMA (mol%) into the polymer. Nuclear magnetic resonance spectroscopy (^1H NMR, Bruker AV600 in deuterated DMSO) was used to confirm the identity and composition of the functional groups incorporated (see Appendix B for ^1H NMR of all charged PNIPAM polymers produced, S2.3-6).

Microgel Particle Size and Charge

Dynamic light scattering measurements were performed with a Brookhaven 90Plus particle analyzer running Particle Solutions Software (Version 2.6, Brookhaven Instruments Corporation), using a 659 nm laser and a 90 degree detection angle. Each measurement was performed at a count rate between 200-500 kilocounts/s for 2 minutes. The intensity-weighted particle sizes and polydispersities were reported as averages of the replicate measurements, with the reported error representing the standard deviation of these replicates.

Electrophoretic mobility was measured using a ZetaPlus zeta potential analyser (Brookhaven Instrument Corporation) operating in PALS (phase analysis light scattering) mode with polystyrene cuvettes. Samples were prepared in 10 mM NaCl and done in triplicate, with each run consisting of 15 cycles; the experimental uncertainties represent the standard deviation of the replicate measurements.

Both the diameter and the zeta potential/mobility of the microgels were investigated as a function of pH. Adjustments to the pH of the microgel solution was made using 0.1 M NaOH and 0.1 M HCl, and the pH was measured using a micro pH probe.

LCST Measurements

The lower critical solution temperature (LCST) of the functionalized PNIPAM polymers was measured using UV-visible spectrophotometry (Variant Cary Bio 100) by performing transmittance measurements over a temperature range of 25 to 80°C (2°C intervals, 1°C/min ramp rate). The onset LCST was defined as the temperature at which the transmittance of the sample was 95%.

Microgel Fabrication

All charged microgels were fabricated using the self-assembly process previously reported²⁰. In short, the hydrazide-functionalized PNIPAM polymer (with or without cationic or anionic charge) was dissolved at 1 wt% in water (without any pH adjustment) and heated to 70°C. The precursor polymer with an LCST below 70°C switched from transparent to cloudy, confirming the generation of nanoaggregates upon heating. Upon this phase change (~3-5 minutes), the aldehyde functionalized polymer (also dissolved in 1 wt% in water, again without pH adjustment) was added dropwise over 1-2 minutes, and the reaction was allowed to continue for 15 minutes in the heated oil bath. To fabricate amphoteric microgels, cationic and anionic PNIPAM-Hzd polymers were mixed at the desired charge ratio of the ultimate microgel but at the same overall mass concentration (1 wt%) used for the single-charge microgels, using 10 mM NaCl instead of water as the assembly solvent to partially screen the opposite charges in the pre-polymer solution. The solution was then heated to form the nanoaggregate as per the single-charge microgels, followed by addition of neutral PNIPAM-Ald to facilitate crosslinking (Figure 3.1). This seed polymer blending approach was used

instead of chemically synthesizing a PNIPAM polymer with both cationic and anionic charges such that the same polymers used in the single-charged microgel fabrication can be used to fabricate amphoteric microgels any desired charge ratio by simple mixing.

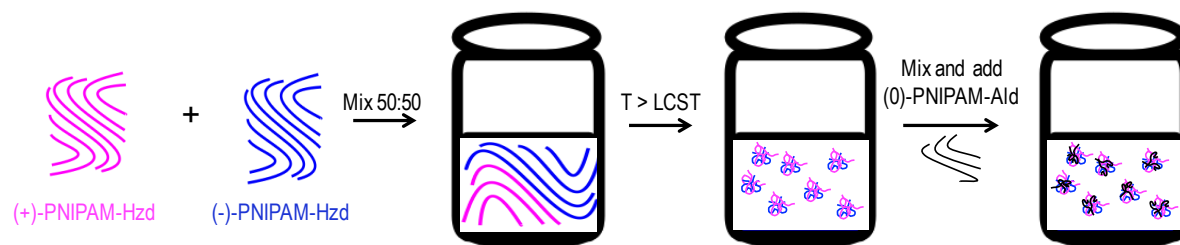


Figure 3.1: Schematic for amphoteric self-assembly, illustrating the blending technique. The different colors represent cationic and anionic PNIPAM-Hzd polymers.

Results and Discussion

Polymer Characterization

Titration characterization data for the charged precursor PNIPAM polymers is summarized in Table 3.2.

Table 3.2: Charged PNIPAM polymer characterization

Polymer	Mol% Charged Comonomer Incorporation
(+)-PNIPAM-Hzd	19 ± 2
(-)-PNIPAM-Hzd	17 ± 3
(+)-PNIPAM-Ald	21 ± 1
(-)-PNIPAM-Ald	17 ± 2

Each charged polymer is functionalized with close to the target (20 mol%) cationic or anionic functional group, such that mass-by-mass mixing of the polymers (in particular, the two hydrazide polymers used for fabricating amphoteric microgels) will yield near-stoichiometric charge balances.

The LCST values for the seed PNIPAM polymers (1 wt%) at different pH values are summarized in Table 3.3. LCST values for the charged PNIPAM-Ald were included for reference, but are not as important to the ultimate success of the self-assembly fabrication process; we have previously demonstrated that the proximity of the self-assembly temperature to the LCST of the seed precursor polymer (in this case, the hydrazide-functionalized polymer(s)) is the key driver to forming monodisperse microgels²⁷.

Table 3.3: LCST for functionalized PNIPAM polymers at different pH values

Seed Polymer	pH 4	pH 7	pH 10
(0)-PNIPAM-Hzd	58°C	58°C	58°C
(-)-PNIPAM-Hzd	52°C	75°C	>80°C
(+)-PNIPAM-Hzd	>80°C	70°C	57°C
(-/+)-PNIPAM-Hzd (1:1)	62°C	N/A	62°C
(0)-PNIPAM-Ald	45°C	45°C	45°C
(-)-PNIPAM-Ald	43°C	55°C	>80°C
(+)-PNIPAM-Ald	70°C	49°C	42°C

When the charged hydrazide precursor polymers were in the ionized state (pH 10 for (-)-PNIPAM-Hzd and pH 4 for (+)-PNIPAM-Hzd), no measurable LCST was observed up to 80°C, as the ionization of the functional comonomer shifts the hydrophilic/hydrophobic balance as to make the polymers functionally non-thermoresponsive in water. Conversely, when the charged hydrazide precursor polymers were neutralized (pH 4 for (-)-PNIPAM-Hzd and pH 10 for (+)-PNIPAM-Hzd), measurable LCST values in the 50-60°C were observed. A similar general trend was observed with the charged aldehyde precursor polymers. When the anionic and cationic hydrazide pre-polymers were mixed in equal ratios, the LCST is

equivalent both at pH 4 ((+)-PNIPAM-Hzd charged, (-)-PNIPAM-Hzd uncharged) and pH 10 ((-)-PNIPAM-Hzd charged, (+)-PNIPAM-Hzd uncharged), consistent with a roughly equal amount of both acidic and basic copolymer present in the mixture. Note that blending of cationic and anionic PNIPAM at pH 7 resulted in macroscopic polymer aggregation, such that no LCST could not be measured; no self-assemblies were subsequently performed at this pH value.

Single Charged Microgels

Single charged cationic and anionic microgels were fabricated using the self-assembly method at a constant temperature of 70°C in H₂O without any additional pH adjustments (resulting in assembly pH values of pH ~7.2 for (+)-PNIPAM-Hzd and pH ~4.8 for (-)-PNIPAM-Hzd). It is of important to note that as a result of the fixed assembly temperature (independent of the actual LCST of the seed precursor polymer(s)) and the varying pH values and seed polymer concentrations used for self-assemblies (known to strongly influence particle properties)²⁰, it is not possible to unambiguously compare the absolute particle sizes or polydispersities achieved between the cationic and anionic microgel assemblies; these factors will be considered and controlled in future experiments. However, the general swelling trends observed (the key novel aspect of this chapter) are not dependent on the consistency of the assembly conditions and can be qualitatively compared with high confidence.

Cationic self-assembled microgels, (+)-PNIPAM-Hzd and (0)-PNIPAM-Ald were fabricated at different Ald:Hzd ratios using the self-assembly method at a constant temperature of 70°C in H₂O, no pH adjustment and a seed polymer concentration of 5 mg/ml. All self-assemblies were performed at a pH of ~7.2 supporting ~70% ionization in the (+)-PNIPAM-Hzd

precursor seed polymer (as per potentiometric titration). Figure 3.2 shows the diameter as a function of pH for self-assembled cationic-functionalized microgels prepared with (+)-PNIPAM-Hzd and (0)-PNIPAM-Ald at different Ald:Hzd ratios.

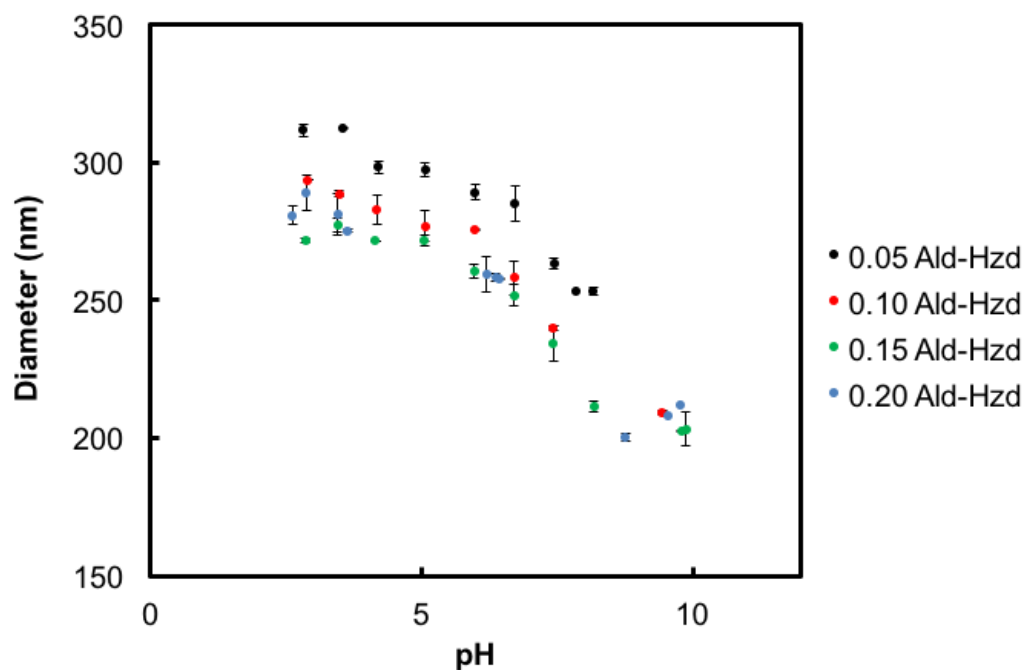


Figure 3.2: Diameter as a function of pH for single-charged cationic self-assembled PNIPAM microgels with (+)-PNIPAM-Hzd and (0)-PNIPAM-Ald

The diameter decreased with any cross-link ratio as the pH increased from acidic to basic conditions. Given that the pK_a of DMAEMA is ~ 8 , the microgels become positively charged at low pH, allowing the diameter to increase due to Donnan equilibrium swelling. The diameter also decreased as the Ald:Hzd ratio (i.e. degree of cross-linking) increased, consistent with more cross-linking elastically hindering the pH-dependent swelling of the microgels. Both these behaviours are directly analogous with conventional cationic non-degradable microgel behaviours¹²⁹.

Analogous to the cationic self-assembled PNIPAM microgels, anionic self-assembled PNIPAM microgels were fabricated using the self-assembly method at 70°C. The seed polymer concentration was 10 mg/ml for all anionic self-assembled PNIPAM microgels. All self-assemblies were performed in H₂O without any pH adjustment of the seed PNIPAM-Hzd polymer solution, with the resulting pH of ~4.8 supporting ~0% ionization in the (-)-PNIPAM-Hzd precursor seed polymer (as per potentiometric titration). Figure 3.3 shows the diameter as a function of pH for the self-assembled anionic-functionalized microgels prepared with (-)-PNIPAM-Hzd and (0)-PNIPAM-Ald at 0.10 and 0.20 Ald:Hzd ratios.

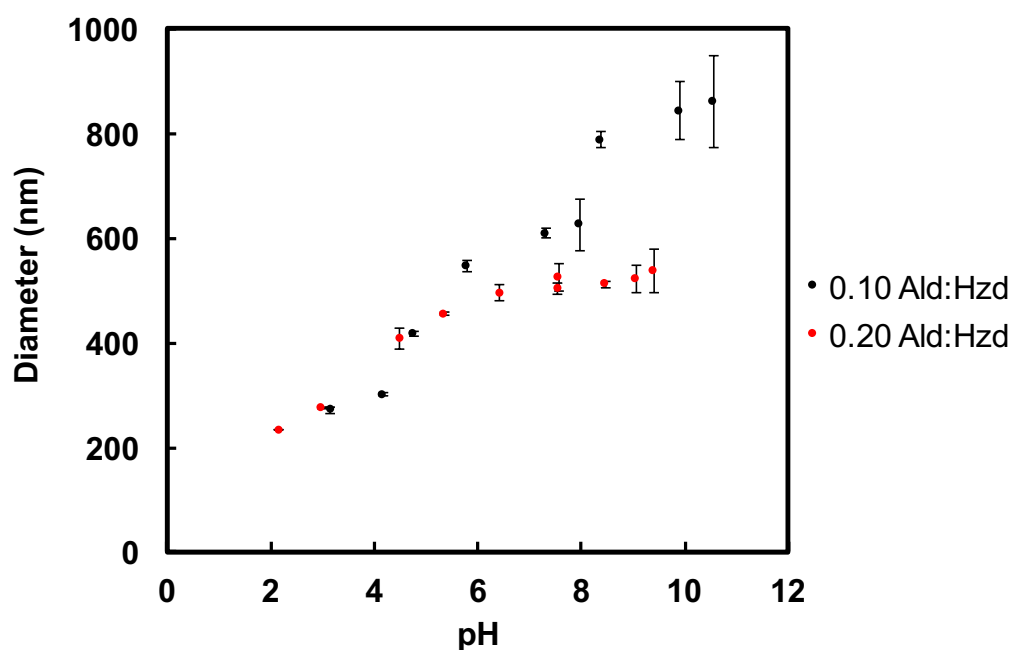


Figure 3.3: Diameter as a function of pH for single-charged anionic self-assembled PNIPAM microgels at 0.10 and 0.20 Ald:Hzd

In contrast to the cationic microgels, the diameter increased for both crosslink ratios as the pH increased from acidic to basic conditions. With the pK_a of AA being ~4.25, the microgels become negatively charged at high pH, resulting in an increase in microgel diameter due to Donnan equilibrium swelling. Similar to the cationic microgels, the diameter decreased as the Ald:Hzd ratio increased from 0.1 to 0.2, consistent with more cross-linking elastically

hindering the pH-dependent swelling of the microgels. Again, this result is directly analogous to observations with anionic conventional microgels¹³⁰.

The potential to tune microgel charge by altering the charge of both the seed and crosslinking polymer used is demonstrated in Figure 3.4, which shows pH-induced swelling results for self-assembled anionic-functionalized microgels prepared by mixing: (a) (0)-PNIPAM-Hzd and (-)-PNIPAM-Ald (neutral seed, anionic crosslinker) (b) (-)-PNIPAM-Hzd and (0)-PNIPAM-Ald (anionic seed, neutral crosslinker), and (c) (-)-PNIPAM-Hzd and (-)-PNIPAM-Ald (anionic seed, anionic crosslinker), all using a 0.20 Ald:Hzd ratio.

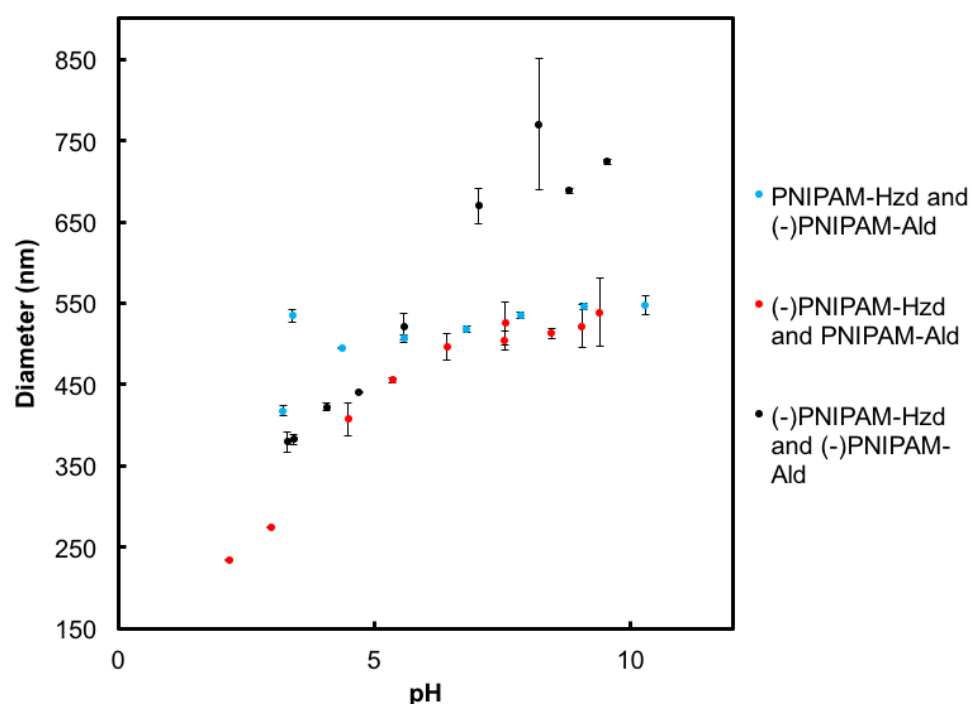


Figure 3.4: Diameter as a function of pH for single-charged anionic self-assembled PNIPAM microgels prepared by adding anionic charge in the seed, crosslinker, or both precursor polymer(s). All microgels prepared using a 0.20 Ald:Hzd ratio.

As anticipated, the diameter increased as a function of pH for all anionic-functionalized microgels. However, the degree of swelling is determined by the amount of charge incorporated into the microgel. When both the seed and cross-linking polymers were anionic,

the largest swelling ratio was observed, consistent with the most charge being present in that system. When only the seed polymer was anionic, significant swelling was still observed since the seed polymer accounts for 83% of the total polymer added (i.e. (-)PNIPAM-Hzd/PNIPAM-Ald has 83% of the total charge of (-)PNIPAM-Hzd/(-)PNIPAM-Ald). When only the cross-linking polymer was anionic, significantly less swelling was observed given that the aldehyde polymer accounts for a much lower percentage of the total polymer added during self-assembly (i.e. PNIPAM-Hzd/(-)PNIPAM-Ald has only 17% of the charge of (-)PNIPAM-Hzd/(-)PNIPAM-Ald). Thus, the degree of swelling can be controlled based on the amount of charged precursor polymer added to the self-assembly. Again, this behaviour is consistent with conventional precipitation-based microgels¹³⁰.

Amphoteric Microgels

Cationic, anionic and 50:50 amphoteric self-assembled PNIPAM microgels were fabricated in 10 mM NaCl at 70°C without further pH adjustment during assembly. Figure 3.5 shows the electrophoretic mobility as a function of pH for the resulting cationic, anionic, and amphoteric (50:50) self-assembled microgels using (0)-PNIPAM-Ald as the crosslinker and a 0.20 Ald:Hzd ratio.

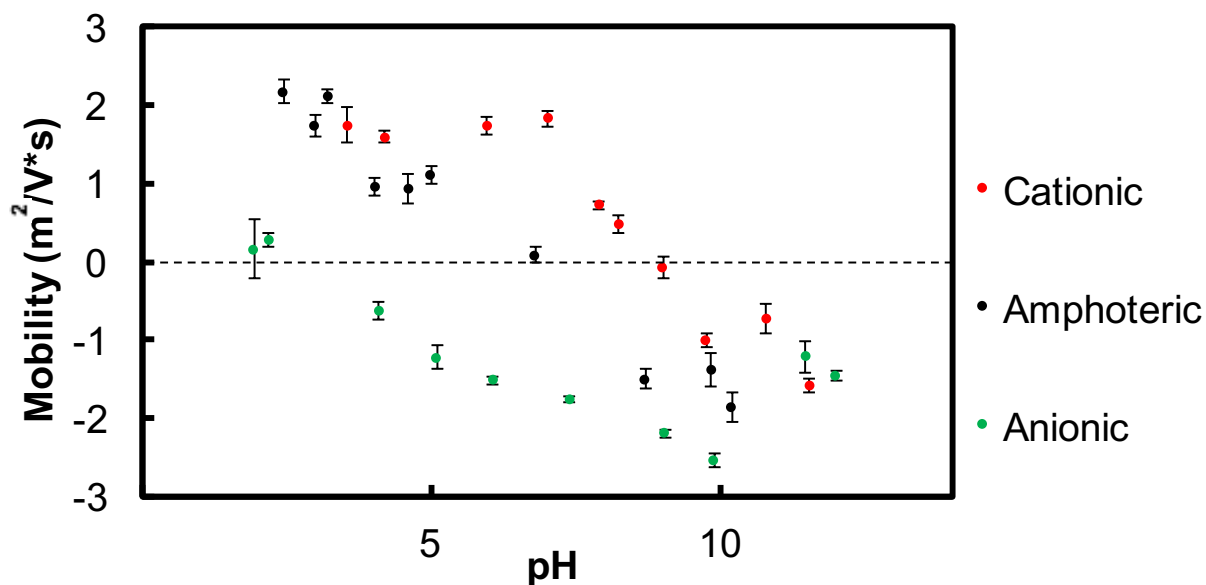


Figure 3.5: Electrophoretic mobility versus pH measurements for cationic, anionic and amphoteric self-assembled PNIPAM microgels prepared at a 0.20 Ald:Hzd ratio in 10 mM NaCl

Cationic microgels were fully charged at low pH while anionic microgels were fully charged at high pH, consistent with the different pK_a values of the co-monomers. Note that negative mobilities were observed for cationic microgels at high pH because of the charge screening with hydroxyl ions in solution¹³¹. The self-assembled amphoteric PNIPAM microgels had intermediate mobility values with an isoelectric point of ~ 7 , highlighting the successful incorporation of a roughly equal number of cationic and anionic charges by simple mixing of cationic and anionic hydrazide-functionalized precursor polymers as the seed.

To change the isoelectric point of the system, amphoteric microgels were fabricated with different ratios of (+)-PNIPAM-Hzd and (-)-PNIPAM-Hzd, using (0)-PNIPAM-Ald as the crosslinker and a 0.20 Ald:Hzd crosslinking ratio. Figure 3.6 shows the electrophoretic mobility as a function of pH for five different (+)-PNIPAM-Hzd to (-)-PNIPAM-Hzd ratios (i.e. 0:1 represents 100% anionic charge, 1:4 represents 20% cationic charge and 80% anionic charge, etc.).

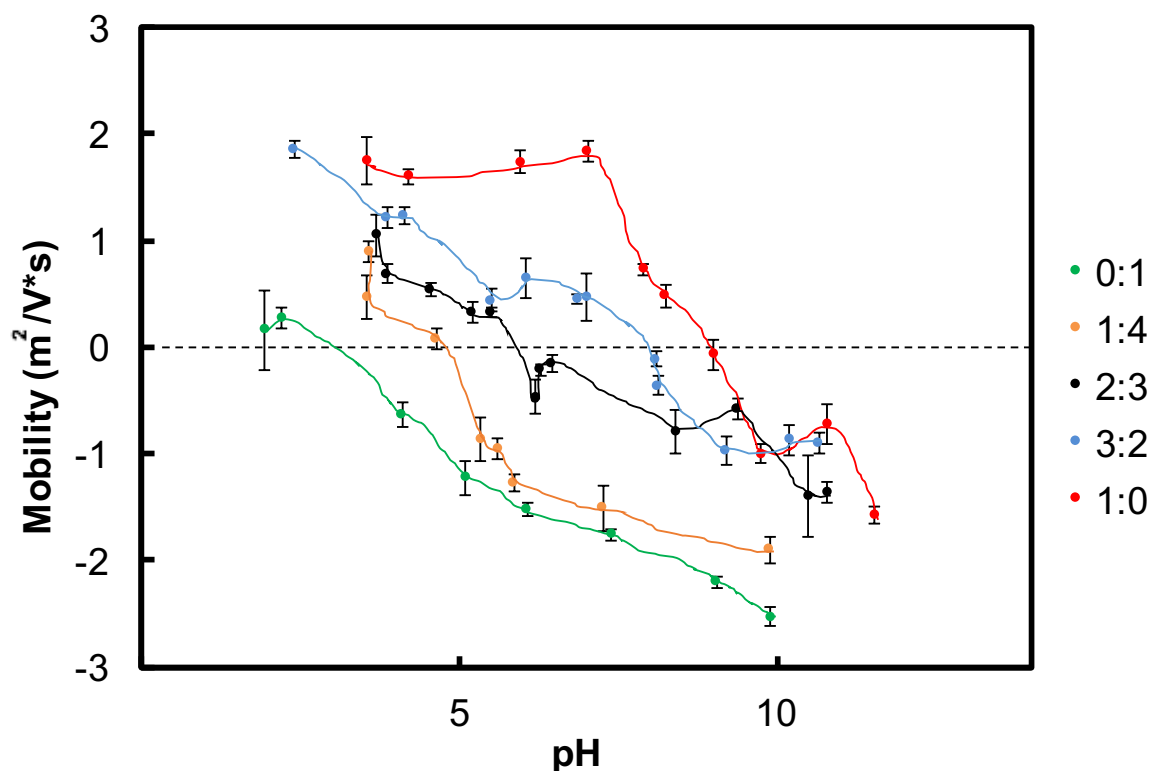


Figure 3.6: Electrophoretic mobility versus pH measurements for amphoteric self-assembled PNIPAM microgels prepared at a 0.20 Ald:Hzd ratio in 10 mM NaCl using different mass ratios of (+)-PNIPAM-Hzd to (-)-PNIPAM-Hzd

Different isoelectric points could be achieved by simply changing the ratio of (+)-PNIPAM-Hzd to (-)-PNIPAM-Hzd in the seed polymer solution, with isoelectric points of 4.6, 6.3, and 8.1 observed for the (+)/(-) charge ratios 1:4, 2:3 and 3:2 respectively. With a higher amount of (+)-PNIPAM-Hzd, the isoelectric point increased accordingly, while the lowest isoelectric point was achieved with 100% anionic charge in the system (Figure S2.7). Consequently, instead of synthesizing a conventional microgel with defined amounts of anionic and cationic charges for each desired charge ratio, self-assembly of varying ratios of cationic and anionic seed polymer can achieve well-controlled amphoteric microgels of any charge density/ratio based on mixing a defined number of functionalized precursor polymers.

The diameter of amphoteric microgels as a function of both pH and the starting self-assembly pH is shown in Figure 3.7.

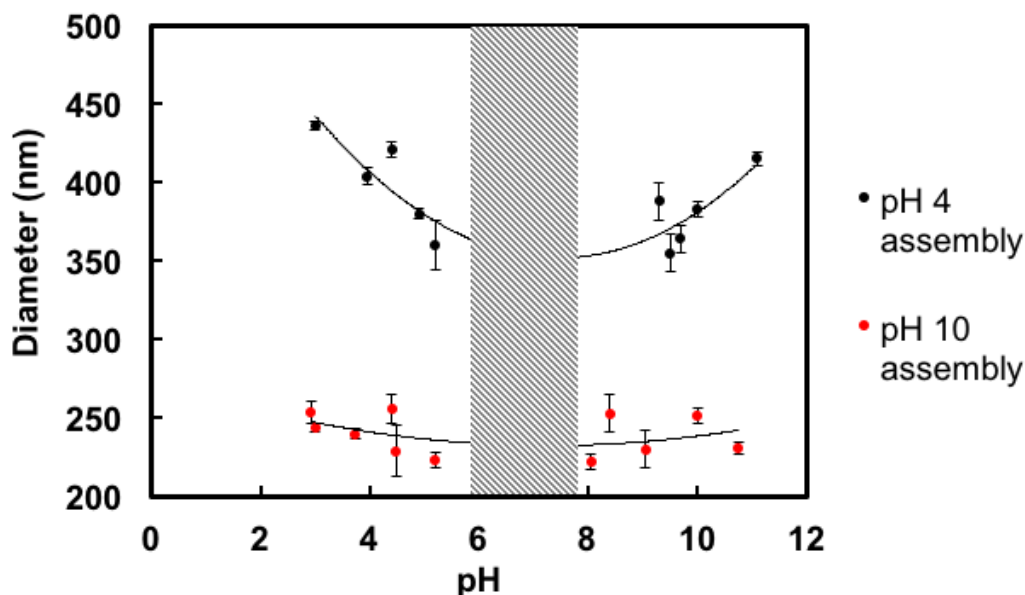


Figure 3.7: Hydrodynamic diameter as a function of pH for amphoteric self-assembled PNIPAM microgels prepared in 10 mM NaCl with pH adjusted to either acidic (pH 4) or basic (pH 10) conditions in the seed polymer solution.

For self-assembly conducted at pH 4, the diameter followed a U-shaped profile as a function of pH, analogous to conventional precipitation PNIPAM microgels. While a similar U-shaped function is indicated by the raw data for self-assemblies conducted at pH 10, the trend is significantly shallower such that within error there is no significant pH response. Irreversible aggregation between pH 6 and 8 was found consistently between all experiments (as indicated by the grey box), a function of the formation of charged coacervates at this intermediate pH at which both precursor polymers are ionized. Note that fabrication attempts at pH 7 resulted in aggregation of the cationic and anionic PNIPAM-Hzd polymers for the same reason, resulting in an inability to create the seed nanoaggregate required to enable microgel fabrication through this pathway. This window of aggregation is expected to decrease with a higher salt concentration (>10 mM NaCl), and will be investigated further in

future experiments. The reason for the significantly different diameters depending on assembly pH (despite the identical measured LCSTs of the 50:50 cationic/anionic polymer mixture at pH 4 and pH 10, Table 3.3) are not clear) and will be investigated further in future experiments.

Conclusion

Charged self-assembled PNIPAM microgels can be successfully fabricated by functionalizing the precursor hydrazide and aldehyde PNIPAM polymers with DMAEMA and AA to introduce cationic and anionic charges, respectively. Cationic single-charged PNIPAM microgels deswell as a function of pH while the anionic single-charged PNIPAM microgels swell as a function of pH, consistent with the pK_a values of the respective functional monomers and analogous to observations with conventional precipitation-based PNIPAM microgels. Amphoteric self-assembled PNIPAM microgels can similarly be fabricated by using a blend of cationic and anionic PNIPAM-Hzd as the seed polymer in the self-assembly. The diameter for these amphoteric microgels followed a U-shape curve as a function of pH with an isoelectric point of $pH \sim 7$, again analogous to conventional microgels. This combination of desirable pH swelling responses and degradability suggests the potential use of these charged self-assembled PNIPAM microgels in applications including ion exchange, drug delivery and environmental sorption. In particular, due to their pH-tunability coupled with their retained thermoresponsiveness, amphoteric microgels are able to de-swell and/or aggregate at a specific pH/temperature combination, advantageous for targeting of cancer and/or infection microenvironments in the human body.

Chapter 4: Conclusion and Future Outlook

Conclusions

The purpose of the presented research was to develop the platform of self-assembled PNIPAM microgels to address challenges in drug delivery applications. The work was divided into two distinct chapters focusing on (1) the structural analysis (and direct drug loading) of uncharged self-assembled PNIPAM microgels and (2) the fabrication and characterization of charged self-assembled PNIPAM microgels.

In **Chapter 2**, a combination of small angle neutron scattering, ultra-small angle neutron scattering, and surface force measurements were applied to determine that the self-assembly method fabricates microgels with homogeneously crosslinked internal structures. This was a surprising result given the sequential addition method used to fabricate microgels via oligomeric self-assembly, which was expected to result in a dense shell-diffuse core structure (i.e. the opposite of conventional precipitation-based microgels) due to limited diffusion of the crosslinking aldehyde-functionalized oligomer into the collapsed hydrazide-functionalized nanoaggregate. These well-defined degradable and homogeneous nanoscale gel networks are anticipated to offer opportunities for addressing challenges in drug delivery, biosensing, and optics by exploiting the predictable diffusive and refractive properties of homogeneous microgel networks. To illustrate the applicability of these microgels, a moderately hydrophobic anti-inflammatory drug (dexamethasone) was co-assembled during the self-assembly process, resulting in a five-fold higher efficiency in drug encapsulation (75-80%) relative to the conventional partition/diffusion-based drug loading processes.

Chapter 3 discussed the successful incorporation of charged co-monomers into the backbone of the hydrazide/aldehyde-functionalized precursor polymers, allowing for the fabrication of

both single charged cationic and anionic and amphoteric self-assembled PNIPAM microgels. Charge was introduced into the precursor polymers by co-polymerizing acrylic acid and 2-dimethylaminoethylmethacrylate to incorporate anionic and cationic charge, respectively. Compared to conventional precipitation-based microgels, it is very simple to incorporate well-defined amphoteric charge densities in particular because the cationic and anionic hydrazide functionalized PNIPAM polymers can be synthesized independently and then mixed at any desired mass (and thus charge) ratio, avoiding the inherent constraints of copolymerization kinetics in controlling the number and distribution of charges in microgels using the conventional free radical precipitation approach. Charged and amphoteric self-assembled PNIPAM microgels showed analogous behaviour to conventional precipitation-based PNIPAM microgels.

In conclusion, the oligomeric self-assembly method is demonstrated to be an adaptable method to fabricate monodisperse, colloidally stable and degradable microgels. The internal structure of these microgels has been determined, and the capacity for creating multi-responsive pH/temperature-responsive microgels has been demonstrated. In addition, the degradability of the microgels coupled with the extremely high encapsulation efficiencies achieved using self-assembly versus conventional diffusion-based loading are of great promise for clinical drug delivery applications.

Future Experiments

The applicability of the uncharged self-assembled PNIPAM microgels for potential clinical applications needs to be investigated more in detail. These experiments can be divided into *in vitro* and *in vivo* studies:

Drug Release Studies: The release profile of dexamethasone needs to be assessed over a longer time period with repeat experiments to confirm whether or not the release is due to drug partitioning or diffusion. Different drugs (or even proteins) with varying hydrophobicities (as judged by the $\log P$ octanol-water partition coefficient), molecular weights, and charges should be studied using both uncharged and charged microgel carriers to assess the limits of the simultaneous drug loading/self-assembly approach. Examples of model drugs that would be of interest in this research (using both uncharged and charged self-assembled PNIPAM microgels) are included in Table 4.1.

Table 4.1: Drugs to be tested in future drug loading and release experiments

Drug Name	Description	log <i>P</i> value	p <i>K</i> _a	Physiological charge	Solubility in water (mg/ml)
Dibucaine ¹³²	A local anesthetic of the amide type now generally used for surface anesthesia; charged and hydrophobic	4.4 (base)	8.9	cationic	0.042
Dexamethasone ¹³³	A synthetic adrenal corticosteroid with anti-inflammatory properties; uncharged and hydrophobic	1.83	N/A	neutral	<1
Naproxen ¹³⁴	An anti-inflammatory agent with analgesic and antipyretic properties; anionic and hydrophobic	3.18 (acid)	4.2	anionic	0.016
Acetaminophen ¹³⁵	An analgesic and antipyretic medication for mild-to-moderate pain and fever; cationic and hydrophilic	0.46 (base)	9.4	cationic	14
Doxorubicin ¹³⁶	An anthracycline antibiotic that prevents DNA replication and inhibits protein synthesis; cationic and hydrophilic	1.27 (base)	7.34, 8.46, 9.46	cationic	2.6

***In Vivo* Studies:** To date, self-assembled PNIPAM microgels have not been tested *in vivo*.

These studies (including biodistribution) should be conducted after finalizing the *in vitro* release profiles to determine if localized drug delivery can be achieved without any cytotoxic side effects.

The single-charged and amphoteric self-assembled PNIPAM microgels need to be characterized in more detail before carrying out the required *in vitro* and *in vivo* studies.

These future experiments can be categorized into three areas:

Structural Analysis using SANS/uSANS: Previous results (Chapter 2) have proven that the uncharged self-assembled PNIPAM microgels have a homogeneously cross-linked internal structure. Having been awarded more time at the National Institute of Standards of Technology (NIST, Gaithersburg), we are interested in how the incorporation of charge (Chapter 3) affects the cross-link density and internal morphology. For example, if an anionic aldehyde polymer is used to crosslink an anionic hydrazide polymer (or, analogously, two cationic polymers are used), will a homogeneously internal structure result or would charge repulsion create the dense shell-diffuse core structure we expected with the neutral microgels? Conversely, if oppositely charged precursor polymers are used for assembly, would the dual reversible chemical (hydrazone bonds) and physical (charge-charge) interactions between precursor polymers promote or hinder the formation of a homogeneously crosslinked structure?

The objective of this SANS/uSANS experiment is to probe the morphology of the self-assembled charged PNIPAM microgels using various charged precursor polymer addition sequences. Table 4.2 outlines the samples that will be measured (and analyzed) using SANS and uSANS. The design of this experiment will give key insight into how charge interactions influence the equilibrium morphology of charged microgels, with the hope to design longer-term drug release vehicles, more selective biosensors and other microgel-based technologies.

Table 4.2: Samples to be measured and analyzed using SANS and uSANS

Sample Name	Self-assembly pH	Measurement pH
Anionic core-neutral shell (-/0)	4, 7, 10	4, 10
Neutral core-anionic shell (0/-)	4, 7, 10	4, 10
Anionic core-anionic shell (-/-)	4, 7, 10	4, 10
Cationic core-neutral shell (+/0)	4, 7, 10	4, 10
Neutral core-cationic shell (0/+)	4, 7, 10	4, 10
Cationic core-cationic shell (+/+)	4, 7, 10	4, 10
Anionic/cationic core (1:1)-neutral shell	4, 10	4, 10

The self-assembly temperature will be set at $5^{\circ}\text{C} + \text{LCST}$ of the core polymer at the given self-assembly pH, and the self-assembly will be performed in 10 mM NaCl D_2O adjusted to the appropriate pH (using NaOH and HCl). Previous results have shown that performing the self-assembly at a temperature 5°C above the LCST of the seed polymer results in the most monodisperse microgel suspension²⁷. The diameter of each sample will be measured on the DLS prior to the neutron scattering experiment, while the pH will be carefully measured and adjusted as required 1-2 hours prior to the individual measurements. The data will be fit first with a homogeneously crosslinked sphere model to see if similar homogenous crosslink distributions are observed as compared to the neutral, uncharged microgels. If necessary, models developed by Berndt et al. for dense shell/diffuse core microgels¹³⁷, Stieger et al. for diffuse shell/dense core microgels⁷³, or the simpler thermoresponsive nanogel models proposed by Kratz et al.⁷⁶ will also be evaluated, with goodness of fits between models compared to extract the morphology of each microgel tested.

pH and Zeta Potential Titrations: It is of importance to repeat all single-charged and amphoteric microgels (as listed in Table 4.1) in 10 mM NaCl and with the appropriate self-assembly temperatures ($5^{\circ}\text{C} + \text{LCST}$), as we expect some of the unusual trends observed (i.e. the significantly higher particle size of cationic versus anionic seed self-assembled microgels) may be attributable to comparing the microgel properties across different pH conditions. With all samples, the diameter and zeta potential (or electrophoretic mobility) as a function of pH will be measured to have complete characterization for the self-assembled charged PNIPAM microgels.

Degradation and Stability Experiments: Degradation studies (performed by exposing the self-assembled microgels to 0.1 M HCl and tracking the molecular weight of the resulting degradation products using GPC) will be performed on the charged self-assembled PNIPAM microgels to confirm that the molecular weights of the degradation products is comparable to the precursor polymers (similarly to the uncharged microgels). Stability studies will also be performed on these microgels as a function of time at different physiologically-relevant pH values to determine the approximate time for which the microgels are stable. Uncharged self-assembled PNIPAM microgels are stable up to 120 days with only a small increase in diameter due to the reversible hydrazone bond allowing water to penetrate into the internal structure²⁰. Since hydrazone bonds are acid-labile, the stability of the charged self-assembled microgels both at low self-assembly pH and low measured pH is expected to decrease. Such behavior may also be useful for the use of such materials as drug delivery vehicles that can both swell and degrade faster in slightly acidic sites in the body (e.g. infections, cancer) and/or once taken up into cells (i.e. intracellular versus intercellular delivery of drugs).

Loading and Release of Charged Drugs: The loading of charged drugs (and temperature-stable proteins) into these charged self-assembled PNIPAM microgels will be investigated (Table 4.1). Both the encapsulation efficiency and the drug release kinetics of these therapeutics into/from self-assembled microgels will be compared to that achieved using the conventional diffusion-based loading method (the only loading method accessible for precipitation-based PNIPAM microgels). Based on results to-date, we hypothesize that the charged self-assembled PNIPAM microgels will both encapsulate a higher amount of drug (or protein) and slow the release, ideal properties for *in vivo* applications.

References

1. Hoare, T. R.; Kohane, D. S., Hydrogels in drug delivery: Progress and challenges. *Polymer* **2008**, *49* (8), 1993-2007.
2. Sinha, V.; Trehan, A., Biodegradable microspheres for protein delivery. *J. of controlled release* **2003**, *90* (3), 261-280.
3. Berger, J.; Reist, M.; Mayer, J. M.; Felt, O.; Peppas, N.; Gurny, R., Structure and interactions in covalently and ionically crosslinked chitosan hydrogels for biomedical applications. *Europ. J. of Pharmaceutics and Biopharmaceutics* **2004**, *57* (1), 19-34.
4. Patenaude, M.; Campbell, S.; Kinio, D.; Hoare, T., Tuning Gelation Time and Morphology of Injectable Hydrogels Using Ketone–Hydrazide Cross-Linking. *Biomacromolecules* **2014**, *15* (3), 781-790.
5. Smeets, N. M.; Bakaic, E.; Patenaude, M.; Hoare, T., Injectable and tunable poly (ethylene glycol) analogue hydrogels based on poly (oligoethylene glycol methacrylate). *Chemical Comm.* **2014**, *50* (25), 3306-3309.
6. Pelton, R., Temperature-sensitive aqueous microgels. *Adv. in colloid and interface science* **2000**, *85* (1), 1-33.
7. Guan, Y.; Zhang, Y., PNIPAM microgels for biomedical applications: from dispersed particles to 3D assemblies. *Soft Matter* **2011**, *7* (14), 6375-6384.
8. Berndt, I.; Richtering, W., Doubly Temperature Sensitive Core– Shell Microgels. *Macromolecules* **2003**, *36* (23), 8780-8785.
9. Heskins, M.; Guillet, J. E., Solution properties of poly (N-isopropylacrylamide). *J. of Macromolecular Science—Chemistry* **1968**, *2* (8), 1441-1455.
10. Pelton, R.; Chibante, P., Preparation of aqueous latices with N-isopropylacrylamide. *Colloids and Surfaces* **1986**, *20* (3), 247-256.
11. Schild, H. G., Poly (N-isopropylacrylamide): experiment, theory and application. *Progress in polymer science* **1992**, *17* (2), 163-249.
12. Hoare, T.; Pelton, R., Characterizing charge and crosslinker distributions in polyelectrolyte microgels. *Curr. Opin. Coll. Interface Science* **2008**, *13* (6), 413-428.
13. Kureha, T.; Sato, T.; Suzuki, D., Relationship between Temperature-Induced Changes in Internal Microscopic Structures of Poly (N-isopropylacrylamide) Microgels and Organic Dye Uptake Behavior. *Langmuir* **2014**, *30* (29), 8717-8725.
14. Dai, Z.; Ngai, T., Microgel particles: The structure-property relationships and their biomedical applications. *J. Poly. Sci.: Polym. Chem.* **2013**, *51* (14), 2995-3003.
15. Virtanen, O.; Brugnoli, M.; Kather, M.; Pich, A.; Richtering, W., The next step in precipitation polymerization of N-isopropylacrylamide: particle number density control by monochain globule surface charge modulation. *Poly. Chem.* **2016**, *7* (32), 5123-5131.
16. Das, M.; Sanson, N.; Fava, D.; Kumacheva, E., Microgels loaded with gold nanorods: photothermally triggered volume transitions under physiological conditions. *Langmuir* **2007**, *23* (1), 196-201.
17. Ma, X.; Xi, J.; Huang, X.; Zhao, X.; Tang, X., Novel hydrophobically modified temperature-sensitive microgels with tunable volume-phase transition temperature. *Materials Letters* **2004**, *58* (27-28), 3400-3404.
18. Ahiabu, A.; Serpe, M. J., Rapidly Responding pH-and Temperature-Responsive Poly (N-Isopropylacrylamide)-Based Microgels and Assemblies. *ACS Omega* **2017**, *2* (5), 1769-1777.
19. Garbern, J. C.; Hoffman, A. S.; Stayton, P. S., Injectable pH-and temperature-responsive poly (N-isopropylacrylamide-co-propylacrylic acid) copolymers for delivery of angiogenic growth factors. *Biomacromolecules* **2010**, *11* (7), 1833-1839.

20. Sivakumaran, D.; Mueller, E.; Hoare, T., Temperature-induced assembly of monodisperse, covalently cross-linked, and degradable poly (N-isopropylacrylamide) microgels based on oligomeric precursors. *Langmuir* **2015**, *31* (21), 5767-5778.
21. Oh, J. K.; Siegwart, D. J.; Lee, H.-i.; Sherwood, G.; Peteanu, L.; Hollinger, J. O.; Kataoka, K.; Matyjaszewski, K., Biodegradable nanogels prepared by atom transfer radical polymerization as potential drug delivery carriers: synthesis, biodegradation, in vitro release, and bioconjugation. *J. Am. Chem. Society* **2007**, *129* (18), 5939-5945.
22. Aleksanian, S.; Khorsand, B.; Schmidt, R.; Oh, J. K., Rapidly thiol-responsive degradable block copolymer nanocarriers with facile bioconjugation. *Polymer Chemistry* **2012**, *3* (8), 2138-2147.
23. Murthy, N.; Thng, Y. X.; Schuck, S.; Xu, M. C.; Frechet, J. M., A novel strategy for encapsulation and release of proteins: hydrogels and microgels with acid-labile acetal cross-linkers. *J. Am. Chem. Society* **2002**, *124* (42), 12398-12399.
24. Bakaic, E.; Smeets, N. M.; Badv, M.; Dodd, M.; Barrigar, O.; Siebers, E.; Lawlor, M.; Sheardown, H.; Hoare, T., Injectable and Degradable Poly (Oligoethylene glycol methacrylate) Hydrogels with Tunable Charge Densities as Adhesive Peptide-Free Cell Scaffolds. *ACS Biomaterials Science & Engineering* **2017**.
25. Smeets, N.; Hoare, T., Designing responsive microgels for drug delivery applications. *Journal of Polymer Science Part A: Polymer Chemistry* **2013**, *51* (14), 3027-3043.
26. Mueller, E.; Alsop, R. J.; Scotti, A.; Bleuel, M.; Rheinstadter, M. C.; Richtering, W.; Hoare, T., Dynamically Cross-Linked Self-Assembled Thermoresponsive Microgels with Homogeneous Internal Structures. *Langmuir* **2018**, *34* (4), 1601-1612.
27. Simpson, M. J.; Corbett, B.; Arezina, A.; Hoare, T., Narrowly Dispersed, Degradable, and Scalable Poly (oligoethylene glycol methacrylate)-Based Nanogels via Thermal Self-Assembly. *Industrial & Engineering Chemistry Research* **2018**.
28. Sun, M.; Zhu, A.; Zhang, Q.; Ye, M.; Liu, Q., Smart shape-controlled synthesis of poly (N-isopropylacrylamide)/chitosan/Fe₃O₄ microgels. *European Polymer Journal* **2015**, *66*, 569-576.
29. Silva, C. S.; Baptista, R. P.; Santos, A. M.; Martinho, J. M.; Cabral, J. M.; Taipa, M. Â., Adsorption of human IgG on to poly (N-isopropylacrylamide)-based polymer particles. *Biotechnology letters* **2006**, *28* (24), 2019-2025.
30. Hoare, T.; Santamaria, J.; Goya, G. F.; Irusta, S.; Lin, D.; Lau, S.; Padera, R.; Langer, R.; Kohane, D. S., A magnetically triggered composite membrane for on-demand drug delivery. *Nano letters* **2009**, *9* (10), 3651-3657.
31. Ogawa, K.; Wang, B.; Kokufuta, E., Enzyme-regulated microgel collapse for controlled membrane permeability. *Langmuir* **2001**, *17* (16), 4704-4707.
32. Morones, J. R.; Frey, W., Room temperature synthesis of an optically and thermally responsive hybrid PNIPAM–gold nanoparticle. *Journal of Nanoparticle Research* **2010**, *12* (4), 1401-1414.
33. Plamper, F. A.; Richtering, W., Functional Microgels and Microgel Systems. *Accounts of Chemical Research* **2017**, *50* (2), 131-140.
34. Lu, Y.; Mei, Y.; Ballauff, M.; Drechsler, M., Thermosensitive core– shell particles as carrier systems for metallic nanoparticles. *The Journal of Physical Chemistry B* **2006**, *110* (9), 3930-3937.
35. Davies, J.; Davies, D., Origins and evolution of antibiotic resistance. *Microbiology and molecular biology reviews* **2010**, *74* (3), 417-433.
36. Saltzman, W. M., *Drug delivery: engineering principles for drug therapy*. Oxford University Press: 2001.
37. Langer, R., New methods of drug delivery. *Science* **1990**, *249* (4976), 1527-1533.

38. Desai, M. P.; Labhassetwar, V.; Amidon, G. L.; Levy, R. J., Gastrointestinal uptake of biodegradable microparticles: effect of particle size. *Pharmaceutical research* **1996**, *13* (12), 1838-1845.
39. Ensign, L. M.; Cone, R.; Hanes, J., Oral drug delivery with polymeric nanoparticles: the gastrointestinal mucus barriers. *Adv. drug delivery reviews* **2012**, *64* (6), 557-570.
40. Santini, J., John T; Richards, A. C.; Scheidt, R.; Cima, M. J.; Langer, R., Microchips as controlled drug-delivery devices. *Angew. Chem. Int.* **2000**, *39* (14), 2396-2407.
41. Parmar, R. D.; Parikh, R. K.; Vidyasagar, G.; Patel, D. V.; Patel, C. J.; Patel, B. D., Pulsatile drug delivery systems: an overview. *Int J Pharm Sci Nanotechnol* **2009**, *2*, 605-614.
42. Bhusal, P.; Harrison, J.; Sharma, M.; Jones, D. S.; Hill, A. G.; Svirskis, D., Controlled release drug delivery systems to improve post-operative pharmacotherapy. *Drug delivery and translational research* **2016**, *6* (5), 441-451.
43. Joshi, N.; Yan, J.; Levy, S.; Bhagchandani, S.; Slaughter, K. V.; Sherman, N. E.; Amirault, J.; Wang, Y.; Riegel, L.; He, X., Towards an arthritis flare-responsive drug delivery system. *Nature comm.* **2018**, *9* (1), 1275.
44. Yu, J.; Zhang, Y.; Bomba, H.; Gu, Z., Stimuli-responsive delivery of therapeutics for diabetes treatment. *Bioengineering & translational medicine* **2016**, *1* (3), 323-337.
45. Luo, Z.; Jin, K.; Pang, Q.; Shen, S.; Yan, Z.; Jiang, T.; Zhu, X.; Yu, L.; Pang, Z.; Jiang, X., On-Demand Drug Release from Dual-Targeting Small Nanoparticles Triggered by High-Intensity Focused Ultrasound Enhanced Glioblastoma-Targeting Therapy. *ACS applied materials & interfaces* **2017**, *9* (37), 31612-31625.
46. Jain, D.; Raturi, R.; Jain, V.; Bansal, P.; Singh, R., Recent technologies in pulsatile drug delivery systems. *Biomatter* **2011**, *1* (1), 57-65.
47. Lawson, R. N.; Chughtai, M., Breast cancer and body temperature. *Canadian Medical Association Journal* **1963**, *88* (2), 68.
48. Kato, Y.; Ozawa, S.; Miyamoto, C.; Maehata, Y.; Suzuki, A.; Maeda, T.; Baba, Y., Acidic extracellular microenvironment and cancer. *Cancer cell int.* **2013**, *13* (1), 89.
49. Rovers, S. A.; Hoogenboom, R.; Kemmere, M. F.; Keurentjes, J. T., Repetitive on-demand drug release by magnetic heating of iron oxide containing polymeric implants. *Soft Matter* **2012**, *8* (5), 1623-1627.
50. Rabinow, B. E., Nanosuspensions in drug delivery. *Nature Reviews Drug Discovery* **2004**, *3* (9), 785.
51. Loftsson, T.; Hreinsdóttir, D.; Másson, M., The complexation efficiency. *Journal of Inclusion Phenomena and Macrocyclic Chemistry* **2007**, *57* (1-4), 545-552.
52. WebMD. Dexamethasone <https://www.webmd.com/drugs/2/drug-1027-5021/dexamethasone-oral/dexamethasone-oral/details>.
53. Geroski, D. H.; Edelhauer, H. F., Drug delivery for posterior segment eye disease. *Investigative ophthalmology & visual science* **2000**, *41* (5), 961-964.
54. Wilhelm, S.; Tavares, A. J.; Dai, Q.; Ohta, S.; Audet, J.; Dvorak, H. F.; Chan, W. C., Analysis of nanoparticle delivery to tumours. *Nature Rev. Mat.* **2016**, *1* (5), 16014.
55. Jabir, N. R.; Anwar, K.; Firoz, C. K.; Oves, M.; Kamal, M. A.; Tabrez, S., An overview on the current status of cancer nanomedicines. *Current medical research and opinion* **2018**, *34* (5), 911-921.
56. Sigurdsson, H. H.; Konráðsdóttir, F.; Loftsson, T.; Stefansson, E., Topical and systemic absorption in delivery of dexamethasone to the anterior and posterior segments of the eye. *Acta Ophthalmologica* **2007**, *85* (6), 598-602.
57. Wu, X.; Pelton, R. H.; Hamielec, A. E.; Woods, D. R.; McPhee, W., The kinetics of poly(N-isopropylacrylamide) microgel latex formation. *Coll. Polym. Sci.* **1994**, *272* (4), 467-477.

58. Hoare, T.; Pelton, R., Highly pH and temperature responsive microgels functionalized with vinylacetic acid. *Macromolecules* **2004**, *37* (7), 2544-2550.
59. Ngai, T.; Behrens, S. H.; Auweter, H., Novel emulsions stabilized by pH and temperature sensitive microgels. *Chemical communications* **2005**, (3), 331-333.
60. Karg, M.; Pastoriza-Santos, I.; Rodriguez-Gonzalez, B.; von Klitzing, R.; Wellert, S.; Hellweg, T., Temperature, pH, and ionic strength induced changes of the swelling behavior of PNIPAM– poly (allylacetic acid) copolymer microgels. *Langmuir* **2008**, *24* (12), 6300-6306.
61. Jones, C. D.; Lyon, L. A., Synthesis and characterization of multiresponsive core–shell microgels. *Macromolecules* **2000**, *33* (22), 8301-8306.
62. Zhang, Q.; Colazo, J.; Berg, D.; Mugo, S. M.; Serpe, M. J., Multiresponsive Nanogels for Targeted Anticancer Drug Delivery. *Molecular Pharmaceutics* **2017**.
63. Yallapu, M. M.; Jaggi, M.; Chauhan, S. C., Design and engineering of nanogels for cancer treatment. *Drug discovery today* **2011**, *16* (9-10), 457-463.
64. Hoare, T.; Pelton, R., Impact of Microgel Morphology on Functionalized Microgel–Drug Interactions. *Langmuir* **2008**, *24* (3), 1005-1012.
65. Ungaro, F.; Giovino, C.; Catanzano, O.; Miro, A.; Mele, A.; Quaglia, F.; La Rotonda, M. I., Use of cyclodextrins as solubilizing agents for simvastatin: effect of hydroxypropyl- β -cyclodextrin on lactone/hydroxyacid aqueous equilibrium. *International journal of pharmaceutics* **2011**, *404* (1), 49-56.
66. Acciaro, R.; Gilányi, T.; Varga, I., Preparation of monodisperse poly (N-isopropylacrylamide) microgel particles with homogenous cross-link density distribution. *Langmuir* **2011**, *27* (12), 7917-7925.
67. Tan, B. H.; Tam, K. C., Review on the dynamics and micro-structure of pH-responsive nano-colloidal systems. *Adv. Coll. Int. Science* **2008**, *136* (1), 25-44.
68. Jones, C. D.; Lyon, L. A., Shell-restricted swelling and core compression in poly (N-isopropylacrylamide) core– shell microgels. *Macromol.* **2003**, *36* (6), 1988-1993.
69. Sanson, N.; Rieger, J., Synthesis of nanogels/microgels by conventional and controlled radical crosslinking copolymerization. *Polym. Chem.* **2010**, *1* (7), 965-977.
70. Sivakumaran, D.; Maitland, D.; Hoare, T., Injectable microgel-hydrogel composites for prolonged small-molecule drug delivery. *Biomacromolecules* **2011**, *12* (11), 4112-4120.
71. Pich, A.; Richtering, W., Microgels by Precipitation Polymerization: Synthesis, Characterization, and Functionalization. In *Chemical Design of Responsive Microgels*, Pich, A.; Richtering, W., Eds. Springer Berlin Heidelberg: Berlin, Heidelberg, 2011; pp 1-37.
72. Richtering, W.; Berndt, I.; Pedersen, J. S., Determination of Microgel Structure by Small-Angle Neutron Scattering. *Microgel Suspensions: Fundamentals and Applications* **2011**, 117-132.
73. Stieger, M.; Pedersen, J. S.; Lindner, P.; Richtering, W., Are thermoresponsive microgels model systems for concentrated colloidal suspensions? A rheology and small-angle neutron scattering study. *Langmuir* **2004**, *20* (17), 7283-7292.
74. Berndt, I.; Pedersen, J. S.; Richtering, W., Temperature-Sensitive Core–Shell Microgel Particles with Dense Shell. *Angewandte Chemie* **2006**, *118* (11), 1769-1773.
75. Saunders, B. R., On the structure of poly (N-isopropylacrylamide) microgel particles. *Langmuir* **2004**, *20* (10), 3925-3932.
76. Kratz, K.; Hellweg, T.; Eimer, W., Structural changes in PNIPAM microgel particles as seen by SANS, DLS, and EM techniques. *Polymer* **2001**, *42* (15), 6631-6639.

77. Meyer, S.; Richtering, W., Influence of polymerization conditions on the structure of temperature-sensitive poly (N-isopropylacrylamide) microgels. *Macromolecules* **2005**, *38* (4), 1517-1519.
78. Hoare, T.; McLean, D., Kinetic prediction of functional group distributions in thermosensitive microgels. *The Journal of Physical Chemistry B* **2006**, *110* (41), 20327-20336.
79. Geisel, K.; Isa, L.; Richtering, W., The Compressibility of pH-Sensitive Microgels at the Oil–Water Interface: Higher Charge Leads to Less Repulsion. *Angewandte Chemie International Edition* **2014**, *53* (19), 4905-4909.
80. Hoare, T.; Pelton, R., Functionalized microgel swelling: comparing theory and experiment. *The Journal of Physical Chemistry B* **2007**, *111* (41), 11895-11906.
81. Xue, J.; Zhang, Z.; Nie, J.; Du, B., Formation of Microgels by Utilizing the Reactivity of Catechols with Radicals. *Macromolecules* **2017**, *50* (14), 5285-5292.
82. Sheikholeslami, P.; Ewaschuk, C. M.; Ahmed, S. U.; Greenlay, B. A.; Hoare, T., Semi-batch control over functional group distributions in thermoresponsive microgels. *Colloid and Polymer Science* **2012**, *290* (12), 1181-1192.
83. Vo, C. D.; Kuckling, D.; Adler, H.-J.; Schönhoff, M., Preparation of thermosensitive nanogels by photo-cross-linking. *Coll. and Polymer Science* **2002**, *280* (5), 400-409.
84. Kuckling, D.; Vo, C. D.; Wohlrab, S. E., Preparation of nanogels with temperature-responsive core and pH-responsive arms by photo-cross-linking. *Langmuir* **2002**, *18* (11), 4263-4269.
85. Cao, Z.; Du, B.; Chen, T.; Nie, J.; Xu, J.; Fan, Z., Preparation and properties of thermo-sensitive organic/inorganic hybrid microgels. *Langmuir* **2008**, *24* (22), 12771-12778.
86. Oh, J. K.; Tang, C.; Gao, H.; Tsarevsky, N. V.; Matyjaszewski, K., Inverse miniemulsion ATRP: a new method for synthesis and functionalization of well-defined water-soluble/cross-linked polymeric particles. *Journal of the American Chemical Society* **2006**, *128* (16), 5578-5584.
87. Oh, J. K.; Bencherif, S. A.; Matyjaszewski, K., Atom transfer radical polymerization in inverse miniemulsion: a versatile route toward preparation and functionalization of microgels/nanogels for targeted drug delivery applications. *Polymer* **2009**, *50* (19), 4407-4423.
88. Duncanson, W. J.; Lin, T.; Abate, A. R.; Seiffert, S.; Shah, R. K.; Weitz, D. A., Microfluidic synthesis of advanced microparticles for encapsulation and controlled release. *Lab on a Chip* **2012**, *12* (12), 2135-2145.
89. Wong, J. E.; Richtering, W., Layer-by-layer assembly on stimuli-responsive microgels. *Current Opinion in Colloid & Interface Science* **2008**, *13* (6), 403-412.
90. Kleinen, J.; Klee, A.; Richtering, W., Influence of architecture on the interaction of negatively charged multisensitive poly (N-isopropylacrylamide)-co-methacrylic acid microgels with oppositely charged polyelectrolyte: absorption vs adsorption. *Langmuir* **2010**, *26* (13), 11258-11265.
91. Kleinen, J.; Richtering, W., Rearrangements in and release from responsive microgel– polyelectrolyte complexes induced by temperature and time. *The Journal of Physical Chemistry B* **2011**, *115* (14), 3804-3810.
92. Deng, X.; Smeets, N. M.; Sicard, C. m.; Wang, J.; Brennan, J. D.; Filipe, C. D.; Hoare, T., Poly (oligoethylene glycol methacrylate) Dip-Coating: Turning Cellulose Paper into a Protein-Repellent Platform for Biosensors. *Journal of the American Chemical Society* **2014**, *136* (37), 12852-12855.
93. Azuah, R. T.; Kneller, L. R.; Qiu, Y.; Tregenna-Piggott, P. L.; Brown, C. M.; Copley, J. R.; Dimeo, R. M., DAVE: a comprehensive software suite for the reduction,

- visualization, and analysis of low energy neutron spectroscopic data. *Journal of Research of the National Institute of Standards and Technology* **2009**, *114* (6), 341.
94. Kline, S. R., Reduction and analysis of SANS and USANS data using IGOR Pro. *Journal of applied crystallography* **2006**, *39* (6), 895-900.
 95. Liu, Y.; Yuan, G.; Bleuel, M., Gelation of spherical colloidal systems with bridging attractions. *Phys. Rev.* **2016**, *94* (4), 040601.
 96. Pedersen, J. S.; Posselt, D.; Mortensen, K., Analytical treatment of the resolution function for small-angle scattering. *J. Appl. Crystallography* **1990**, *23* (4), 321-333.
 97. Piazza, J.; Hoare, T.; Molinaro, L.; Terpstra, K.; Bhandari, J.; Selvaganapathy, P. R.; Gupta, B.; Mishra, R. K., Haloperidol-loaded intranasally administered lectin functionalized poly(ethylene glycol)-block-poly(d,l)-lactic-co-glycolic acid (PEG-PLGA) nanoparticles for the treatment of schizophrenia. *European Journal of Pharmaceutics and Biopharmaceutics* **2014**, *87* (1), 30-39.
 98. Horkay, F.; Hammouda, B., Small-angle neutron scattering from typical synthetic and biopolymer solutions. *Colloid and Polymer Science* **2008**, *286* (6-7), 611-620.
 99. Grobelny, S.; Hofmann, C. H.; Erlkamp, M.; Plamper, F. A.; Richtering, W.; Winter, R., Conformational changes upon high pressure induced hydration of poly (N-isopropylacrylamide) microgels. *Soft Matter* **2013**, *9* (25), 5862-5866.
 100. Smeets, N. M.; Bakaic, E.; Yavitt, F. M.; Yang, F.-C.; Rheinstädter, M. C.; Hoare, T., Probing the Internal Morphology of Injectable Poly (oligoethylene Glycol Methacrylate) Hydrogels by Light and Small-Angle Neutron Scattering. *Macromolecules* **2014**, *47* (17), 6017-6027.
 101. Höfl, S.; Zitzler, L.; Hellweg, T.; Herminghaus, S.; Mugele, F., Volume phase transition of “smart” microgels in bulk solution and adsorbed at an interface: a combined AFM, dynamic light, and small angle neutron scattering study. *Polymer* **2007**, *48* (1), 245-254.
 102. Varga, I.; Gilányi, T.; Meszaros, R.; Filipcsei, G.; Zrínyi, M., Effect of cross-link density on the internal structure of poly (N-isopropylacrylamide) microgels. *The Journal of Physical Chemistry B* **2001**, *105* (38), 9071-9076.
 103. Crowther, H. M.; Saunders, B. R.; Mears, S. J.; Cosgrove, T.; Vincent, B.; King, S. M.; Yu, G.-E., Poly (NIPAM) microgel particle de-swelling: a light scattering and small-angle neutron scattering study. *Colloids and Surfaces A: Physicochemical and Engineering Aspects* **1999**, *152* (3), 327-333.
 104. Pinaud, F.; Geisel, K.; Massé, P.; Catargi, B.; Isa, L.; Richtering, W.; Ravaine, V.; Schmitt, V., Adsorption of microgels at an oil-water interface: correlation between packing and 2D elasticity. *Soft Matter* **2014**, *10* (36), 6963-6974.
 105. Rey, M.; Fernández-Rodríguez, M. Á.; Steinacher, M.; Scheidegger, L.; Geisel, K.; Richtering, W.; Squires, T. M.; Isa, L., Isostructural solid-solid phase transition in monolayers of soft core-shell particles at fluid interfaces: structure and mechanics. *Soft Matter* **2016**, *12* (15), 3545-3557.
 106. Rodriguez-Docampo, Z.; Otto, S., Orthogonal or simultaneous use of disulfide and hydrazone exchange in dynamic covalent chemistry in aqueous solution. *Chemical Communications* **2008**, (42), 5301-5303.
 107. Patel, A.; Cholkar, K.; Agrahari, V.; Mitra, A. K., Ocular drug delivery systems: an overview. *World journal of pharmacology* **2013**, *2* (2), 47.
 108. Galaev, I. Y.; Mattiasson, B., ‘Smart’ polymers and what they could do in biotechnology and medicine. *Trends in biotechnology* **1999**, *17* (8), 335-340.
 109. Vashist, A.; Ahmad, S., Hydrogels: smart materials for drug delivery. *Oriental Journal of Chemistry* **2013**, *29* (3), 861-870.

110. Wilczewska, A. Z.; Niemirowicz, K.; Markiewicz, K. H.; Car, H., Nanoparticles as drug delivery systems. *Pharmacological reports* **2012**, *64* (5), 1020-1037.
111. Kraft, J. C.; Freeling, J. P.; Wang, Z.; Ho, R. J., Emerging research and clinical development trends of liposome and lipid nanoparticle drug delivery systems. *Journal of pharmaceutical sciences* **2014**, *103* (1), 29-52.
112. Klinger, D.; Landfester, K., Stimuli-responsive microgels for the loading and release of functional compounds: Fundamental concepts and applications. *Polymer* **2012**, *53* (23), 5209-5231.
113. Wang, D.; Liu, T.; Yin, J.; Liu, S., Stimuli-responsive fluorescent poly (N-isopropylacrylamide) microgels labeled with phenylboronic acid moieties as multifunctional ratiometric probes for glucose and temperatures. *Macromolecules* **2011**, *44* (7), 2282-2290.
114. Hu, J.; Liu, S., Responsive polymers for detection and sensing applications: current status and future developments. *Macromolecules* **2010**, *43* (20), 8315-8330.
115. Gao, Y.; Li, X.; Serpe, M. J., Stimuli-responsive microgel-based etalons for optical sensing. *RSC Advances* **2015**, *5* (55), 44074-44087.
116. Pan, Y.-J.; Chen, Y.-Y.; Wang, D.-R.; Wei, C.; Guo, J.; Lu, D.-R.; Chu, C.-C.; Wang, C.-C., Redox/pH dual stimuli-responsive biodegradable nanohydrogels with varying responses to dithiothreitol and glutathione for controlled drug release. *Biomaterials* **2012**, *33* (27), 6570-6579.
117. McMasters, J.; Poh, S.; Lin, J. B.; Panitch, A., Delivery of anti-inflammatory peptides from hollow PEGylated poly (NIPAM) nanoparticles reduces inflammation in an ex vivo osteoarthritis model. *Journal of Controlled Release* **2017**, *258*, 161-170.
118. Xu, W.; Zhang, Y.; Gao, Y.; Serpe, M. J., Electrically Triggered Small Molecule Release from Poly (N-Isopropylacrylamide-co-Acrylic Acid) Microgel-Modified Electrodes. *ACS applied materials & interfaces* **2018**, *10* (15), 13124-13129.
119. Karg, M.; Hellweg, T., New “smart” poly (NIPAM) microgels and nanoparticle microgel hybrids: Properties and advances in characterisation. *Current Opinion in Colloid & Interface Science* **2009**, *14* (6), 438-450.
120. Hoare, T.; Pelton, R., Titrametric characterization of pH-induced phase transitions in functionalized microgels. *Langmuir* **2006**, *22* (17), 7342-7350.
121. Das, M.; Mardyani, S.; Chan, W. C.; Kumacheva, E., Biofunctionalized pH-responsive microgels for cancer cell targeting: rational design. *Advanced Materials* **2006**, *18* (1), 80-83.
122. Damodaran, V. B.; Murthy, N. S., Bio-inspired strategies for designing antifouling biomaterials. *Biomaterials research* **2016**, *20* (1), 18.
123. Taira, S.; Du, Y. Z.; Kodaka, M., Trap and release of oligonucleotide using pH-responsive amphoteric particle prepared by interfacial polymerization in W/O miniemulsion system. *Biotechnology and bioengineering* **2006**, *93* (2), 396-400.
124. Schachschal, S.; Balaceanu, A.; Melian, C.; Demco, D. E.; Eckert, T.; Richtering, W.; Pich, A., Polyampholyte microgels with anionic core and cationic shell. *Macromolecules* **2010**, *43* (9), 4331-4339.
125. Pich, A.; Richtering, W., Microgels by precipitation polymerization: synthesis, characterization, and functionalization. In *Chemical Design of Responsive Microgels*, Springer: 2010; pp 1-37.
126. Li, P.; SenGupta, A. K., Intraparticle diffusion during selective ion exchange with a macroporous exchanger. *Reactive and Functional Polymers* **2000**, *44* (3), 273-287.
127. Lee, E. S.; Gao, Z.; Bae, Y. H., Recent progress in tumor pH targeting nanotechnology. *Journal of Controlled Release* **2008**, *132* (3), 164-170.

128. Sigolaeva, L. V.; Gladyr, S. Y.; Gelissen, A. P.; Mergel, O.; Pergushov, D. V.; Kurochkin, I. N.; Plamper, F. A.; Richtering, W., Dual-stimuli-sensitive microgels as a tool for stimulated spongelike adsorption of biomaterials for biosensor applications. *Biomacromolecules* **2014**, *15* (10), 3735-3745.
129. Hu, X.; Tong, Z.; Lyon, L. A., Synthesis and physicochemical properties of cationic microgels based on poly (N-isopropylmethacrylamide). *Colloid and polymer science* **2011**, *289* (3), 333-339.
130. Xiong, W.; Gao, X.; Zhao, Y.; Xu, H.; Yang, X., The dual temperature/pH-sensitive multiphase behavior of poly (N-isopropylacrylamide-co-acrylic acid) microgels for potential application in in situ gelling system. *Colloids and Surfaces B: Biointerfaces* **2011**, *84* (1), 103-110.
131. Bernal, J. D.; Fowler, R. H., A theory of water and ionic solution, with particular reference to hydrogen and hydroxyl ions. *The Journal of Chemical Physics* **1933**, *1* (8), 515-548.
132. National Center for Biotechnology Information. PubChem Compound Database; CID=3025, <https://pubchem.ncbi.nlm.nih.gov/compound/3025>
133. National Center for Biotechnology Information. PubChem Compound Database; CID=5743, <https://pubchem.ncbi.nlm.nih.gov/compound/5743>
134. National Center for Biotechnology Information. PubChem Compound Database; CID=156391, <https://pubchem.ncbi.nlm.nih.gov/compound/156391>
135. National Center for Biotechnology Information. PubChem Compound Database; CID=1983, <https://pubchem.ncbi.nlm.nih.gov/compound/1983>
136. National Center for Biotechnology Information. PubChem Compound Database; CID=31703, <https://pubchem.ncbi.nlm.nih.gov/compound/31703>
137. Berndt, I.; Pedersen, J. S.; Richtering, W., Temperature-Sensitive Core-Shell Microgel Particles with Dense Shell. *Angewandte Chemie* **2006**, *118* (11), 1769-1773.

Appendices

Appendix A: Chapter 2 Supplementary Information

Raw and best-fit SANS profiles for all data presented, hydrodynamic diameter versus temperature profiles of the microgels collected in the SANS solvent(s), raw (un-normalized) Langmuir Trough compression data, full tables summarizing the SANS best-fit parameters, and centrifugation optimization parameters and drug loading methods are available below:

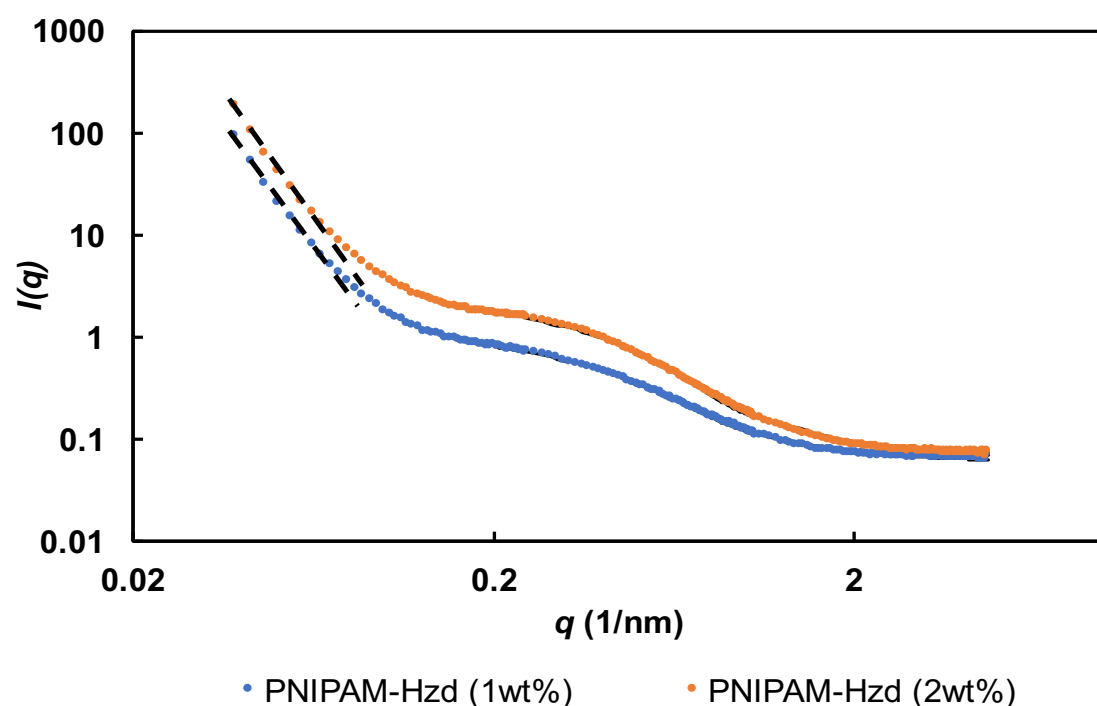


Figure S1.1: Scattering intensity as a function of the scattering vector of hydrazide-functionalized PNIPAM precursors (PNIPAM-Hzd) dissolved in water at (A) 1 wt% and (B) 2 wt%, measured at 70°C (the temperature used for microgel self-assembly based on these PNIPAM-Hzd nanoaggregates). The homogeneously crosslinked model fits are shown as black lines (up to $q=0.2 \text{ nm}^{-1}$). The dotted black lines represent aggregation and are fit to a $M \cdot X^{-4.5}$, where M (amplitude of intensity in arbitrary units) is 3.5×10^{-5} for (A) and 6.5×10^{-5} for (B).

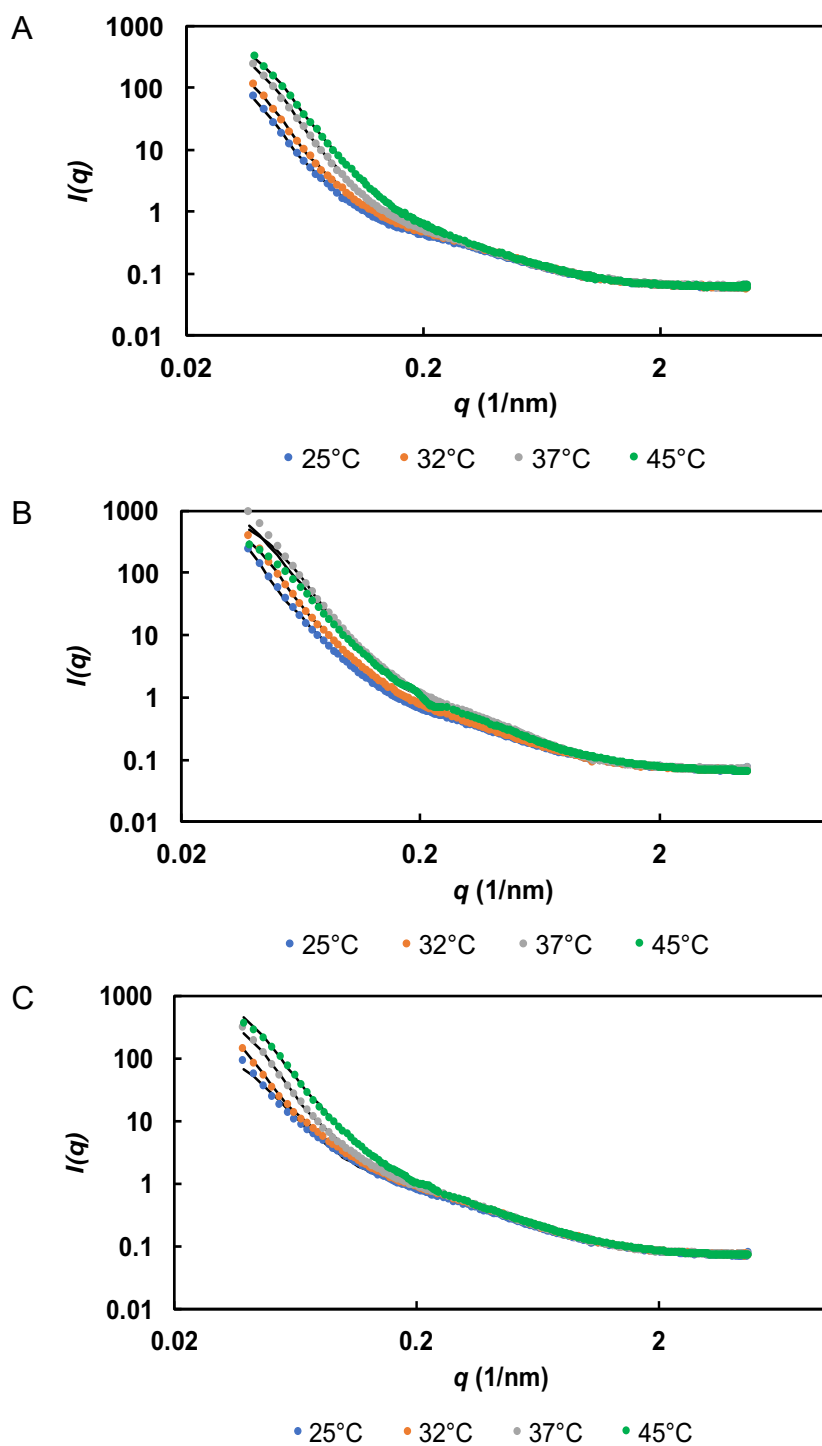


Figure S1.2: Neutron scattering intensity $I(q)$ as a function of the scattering vector (q) as a function of temperature for: (A) 0.05 Ald:Hzd microgel (1 wt% PNIPAM-Hzd); (B) 0.20 Ald:Hzd microgel (1 wt% PNIPAM-Hzd); (C) 0.05 Ald:Hzd microgel (2 wt% PNIPAM-Hzd), using the Stieger model. Solid black lines represent the fits and standard deviations of the fits are plotted as error bars.

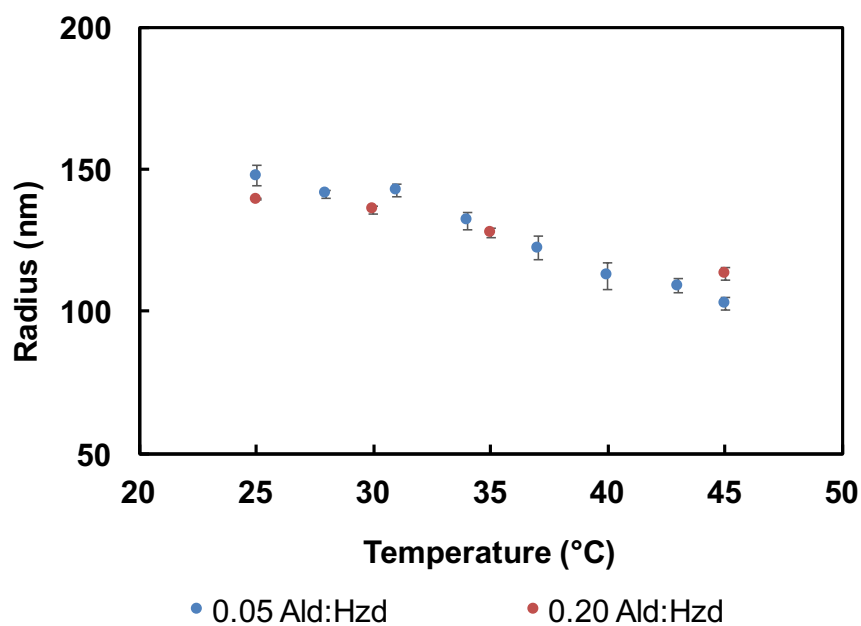


Figure S1.3: Hydrodynamic radius obtained from dynamic light scattering versus temperature for 0.05 Ald:Hzd and 0.20 Ald:Hzd microgels

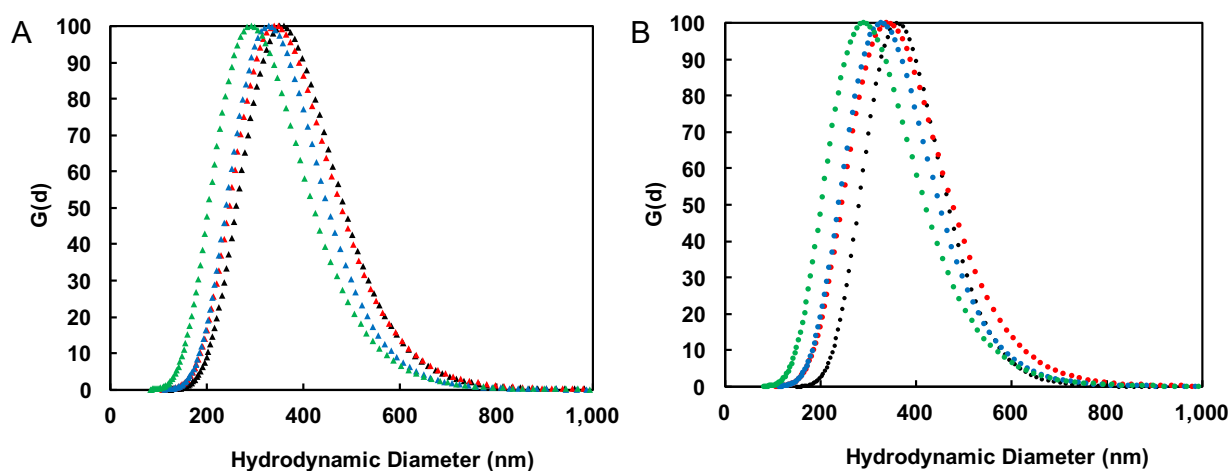


Figure S1.4: Particle size distributions from dynamic light scattering measurements of (A) 0.05 Ald:Hzd (▲) and (B) 0.20 Ald:Hzd (●), fabricated and measured in D₂O, as a function of temperature: black (25°C), red (32°C), blue (37°C), green (45°C)

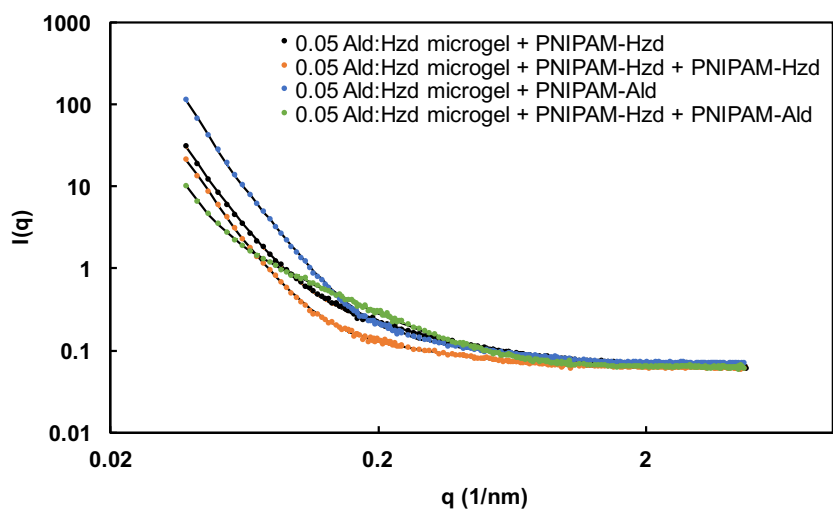


Figure S1.5: Scattering intensity as a function of the scattering vector for 0.05 Ald:Hzd (1 wt% PNIPAM-Hzd) self-assembled microgels subsequently mixed with additional PNIPAM-Hzd and/or PNIPAM-Ald polymers (treatment sequences as indicated in legend). Scattering profiles were measured in D_2O at 25°C . Solid black lines represent the fits, while the standard deviations of the fits are plotted as error bars.

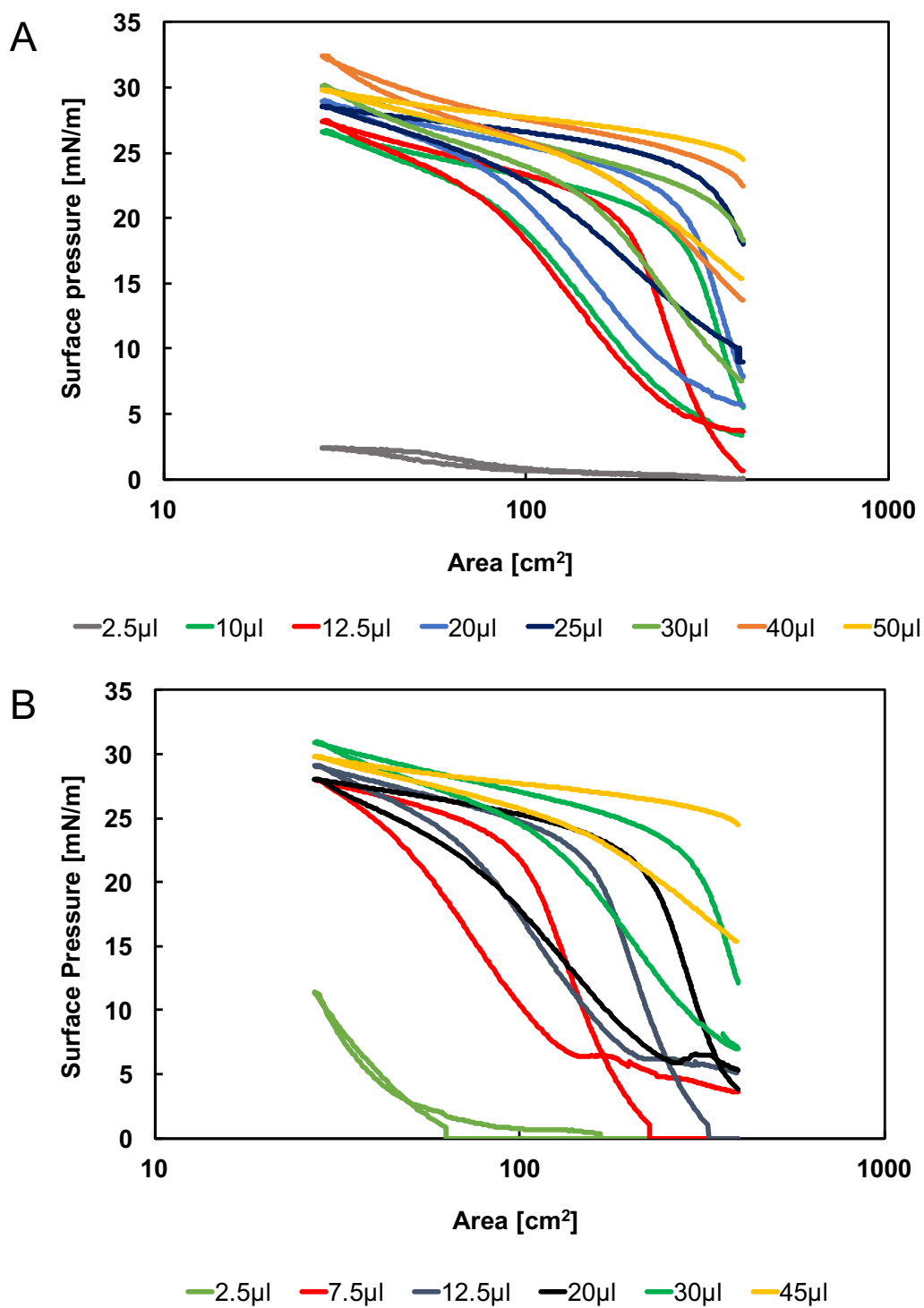


Figure S1.6: Surface pressure as a function of un-normalized area for (a) 0.05 Ald:Hzd (1 wt% PNIPAM-Hzd) and (b) 0.20 Ald:Hzd (1 wt% PNIPAM-Hzd) self-assembled microgels

Table S1.1: Chi squared (χ^2) goodness of fit parameters for the homogeneously cross-linked model and the Stieger model for three bulk self-assembled PNIPAM microgels, measured at 25°C. The similarity between the χ^2 values for both fits suggests the additional complexity of the Stieger model is not necessary to fit the data accurately, suggesting that the self-assembled microgels are internally homogeneous.

	χ^2 (homogeneously cross-linked model)	χ^2 (Stieger model)
0.05 Ald:Hzd (1 wt% PNIPAM-Hzd)	0.359	1.043
0.20 Ald:Hzd (1 wt% PNIPAM-Hzd)	0.618	0.594
0.05 Ald:Hzd (2 wt% PNIPAM-Hzd)	13.172	8.799

Table S1.2: Chi squared (χ^2) goodness of fit parameters for the homogeneously cross-linked model and the Stieger model for four layered self-assembled PNIPAM microgels, measured at 25°C. As in Table S1, no significant difference exists between the quality of the model fits using the two models, suggesting the added complexity of the core-shell model is unnecessary to fit.

	χ^2 (homogeneously cross-linked model)	χ^2 (Stieger model)
0.05 Ald:Hzd microgel + PNIPAM-Hzd	0.076	0.069
0.05 Ald:Hzd microgel + PNIPAM-Ald	0.400	0.600
0.05 Ald:Hzd microgel + PNIPAM-Hzd + PNIPAM-Hzd	0.076	0.032
0.05 Ald:Hzd microgel + PNIPAM-Hzd + PNIPAM-Ald	0.048	0.053

Table S1.3: Summary of fitting parameters for bulk self-assembled PNIPAM microgels using the homogeneous sphere model ($\sigma_{fuzzy} = 0$): (a) 0.05 Ald:Hzd (1 wt% PNIPAM-Hzd); (b) 0.20 Ald:Hzd (1 wt% PNIPAM-Hzd); (c) 0.05 Ald:Hzd (2 wt% PNIPAM-Hzd)

(a) 0.05 Ald:Hzd (1 wt% PNIPAM-Hzd)

Temperature (°C)	Radius (nm)	Polydispersity (%)	Correlation Length (nm)
25	165	4	4.1
32	79	18	4.2
37	66	18	3.8
45	67	19	3.9

(b) 0.20 Ald:Hzd (1 wt% PNIPAM-Hzd)

Temperature (°C)	Radius (nm)	Polydispersity (%)	Correlation Length (nm)
25	165	5	4.0
32	81	20	4.2
37	81	20	4.2
45	60	18	4.4

(c) 0.05 Ald:Hzd (2 wt% PNIPAM-Hzd)

Temperature (°C)	Radius (nm)	Polydispersity (%)	Correlation Length (nm)
25	195	22	4.5
32	103	19	4.9
37	75	18	4.4
45	69	19	4.0

Table S1.4: Fitting parameters for bulk self-assembled PNIPAM microgels using the homogeneous sphere model ($\sigma_{fuzzy} = 0$), using IDL for analysis: (a) 0.05 Ald:Hzd (1 wt% PNIPAM-Hzd); (b) 0.20 Ald:Hzd (1 wt% PNIPAM-Hzd); (c) 0.05 Ald:Hzd (2 wt% PNIPAM-Hzd)

(a) 0.05 Ald:Hzd (1 wt% PNIPAM-Hzd)

Temperature (°C)	25	32	37	45
Mean Radius (nm)	165	79	65	67.3
Polydispersity (%)	4.3	18.4	18.1	18.8
Scale	12018.3	572.8	553.3	1022.4
Correlation Length (nm)	4.1	4.2	3.8	3.9
Scale	0.54	0.60	0.49	0.52
Background	0.058	0.058	0.059	0.059

(b) 0.20 Ald:Hzd (1 wt% PNIPAM-Hzd)

Temperature (°C)	25	32	37	45
Mean Radius (nm)	165	81	81.3	60
Polydispersity (%)	5.4	19.9	19.9	18.6
Scale	39475.1	1936.5	4383.1	1387.9
Correlation Length (nm)	4.0	4.2	4.2	4.4
Scale	0.73	0.81	1.07	1.15
Background	0.064	0.061	0.055	0.062

(c) 0.05 Ald:Hzd (2 wt% PNIPAM-Hzd)

Temperature (°C)	25	32	37	45
Mean Radius (nm)	195	103	75	69
Polydispersity (%)	21.9	19.4	18.3	19.0
Scale	16858.3	2383.9	1178.9	1563.3
Correlation Length (nm)	4.5	4.9	4.4	4.0
Scale	1.17	1.42	1.02	1.06
Background	0.068	0.069	0.068	0.069

Table S1.5: Fitting parameters for contrast-matched self-assembled PNIPAM microgels using the homogeneous sphere model ($\sigma_{fuzzy} = 0$), using IgorPro for analysis: (a) index-matched d7-PNIPAM-Hzd; (b) index-matched PNIPAM-Ald

(a) Index-matched d7-PNIPAM-Hzd (only PNIPAM-Ald signal measured)

Temperature (°C)	25	32	37	45
Volume Fraction (scale)	0.00055	0.00055	0.000735	0.00065
Mean Radius (nm)	120	118	88	80
Polydispersity (sig/avg)	0.45	0.55	0.765	0.79
Interface Thickness (nm)	0	0	0	0
SLD Sphere (\AA^{-2})	6.00E-07	4.00E-07	6.00E-07	5.15E-07
SLD Solvent (\AA^{-2})	3.00E-06	3.00E-06	3.00E-06	3.00E-06
Lorentzian Scale	100	95	80	85
Lorentzian Exponent	3.9	3.84	3.8	4.1
Lorentzian Correlation Length (nm)	30	30	30	30
Background ($\text{cm}^{-1} \text{sr}^{-1}$)	0.447	0.415	0.43	0.42

(b) Index-matched PNIPAM-Ald (only d7-PNIPAM-Hzd signal measured)

Temperature (°C)	25	32	37	45
Volume Fraction (scale)	0.00064	0.00095	0.00092	0.00099
Mean Radius (nm)	125	120	88	85
Polydispersity (sig/avg)	0.46	0.61	0.68	0.85
Interface Thickness (nm)	0	0	0	0
SLD Sphere (\AA^{-2})	5.50E-07	5.20E-07	5.20E-07	5.10E-07
SLD Solvent (\AA^{-2})	3.00E-06	3.00E-06	3.00E-06	3.00E-06
Lorentzian Scale	100	80	75	70
Lorentzian Exponent	3.85	3.7	3.76	3.8
Lorentzian Correlation Length (nm)	34	34	34	32
Background ($\text{cm}^{-1} \text{sr}^{-1}$)	1.28	1.15	1.12	1.19

Table S1.6: Fitting parameters for layered self-assembled PNIPAM microgels using the homogeneous sphere model ($\sigma_{fuzzy} = 0$), using IDL for analysis: (a) 0.05 Ald:Hzd microgel + PNIPAM-Hzd; (b) 0.05 Ald:Hzd microgel + PNIPAM-Ald; (c) 0.05 Ald:Hzd microgel + PNIPAM-Hzd + PNIPAM-Hzd; (d) 0.05 Ald:Hzd microgel + PNIPAM-Hzd + PNIPAM-Ald

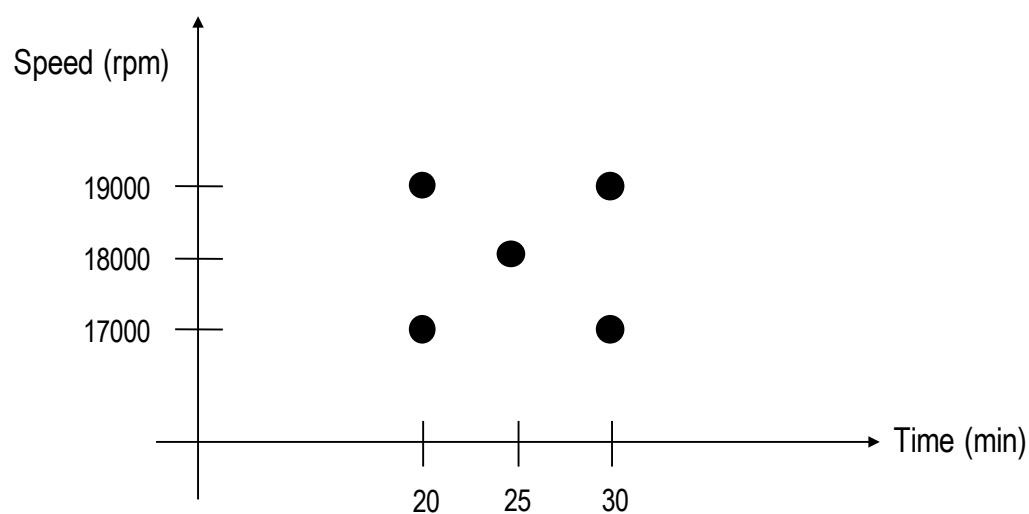
Addition Sequence	(a)	(b)	(c)	(d)
Mean Radius (nm)	177	167	178	176
Polydispersity (%)	7.9	7.2	10	5.3
Scale	8375	20872	4363	2357
Correlation Length (nm)	4.5	2.5	3.6	12.1
Scale	0.24	0.07	0.08	1.49
Background	0.066	0.068	0.061	0.061

Centrifugation Optimization for Drug Loading

Optimization of centrifuge speed and time was required to facilitate the loading and release of dexamethasone using uncharged self-assembled PNIPAM microgels. Specifically, microgels must be (1) fully isolated from suspension (to enable accurate drug loading measurements and (2) fully redispersible following centrifugation (to allow for drug release kinetics assessments). A simple factorial experimental design was designed, as seen below, to answer three questions:

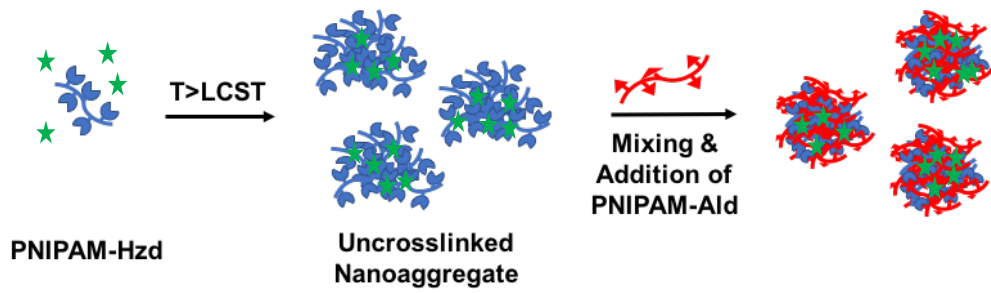
- (1) Does the pellet re-suspend in 10 mM PBS? (*Qualitative*)
- (2) How much polymer and remaining drug is in the supernatant? (*Quantitative* – measure mass of 20 mL supernatant in aluminum weigh boat in oven overnight)
- (3) How much drug is loaded? (*Quantitative* – testing supernatant using HPLC)

The final centrifugation parameters used in subsequent experiments were **18000 RPM and 20 minutes**.

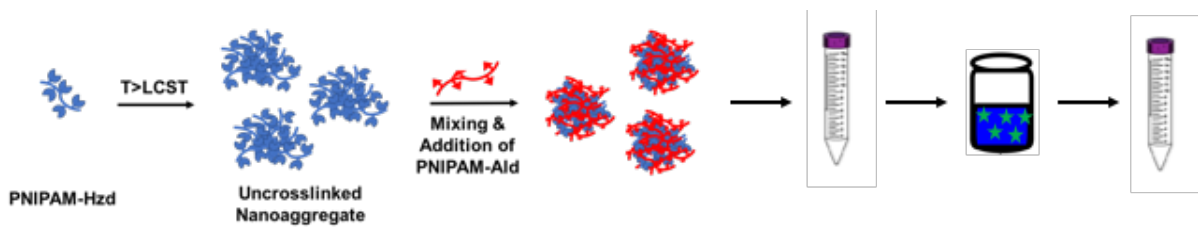


Two Drug Loading Methods:

(1) Directly into the self-assembly process



(2) Passive diffusion



Appendix B: Chapter 3 Supplementary Information

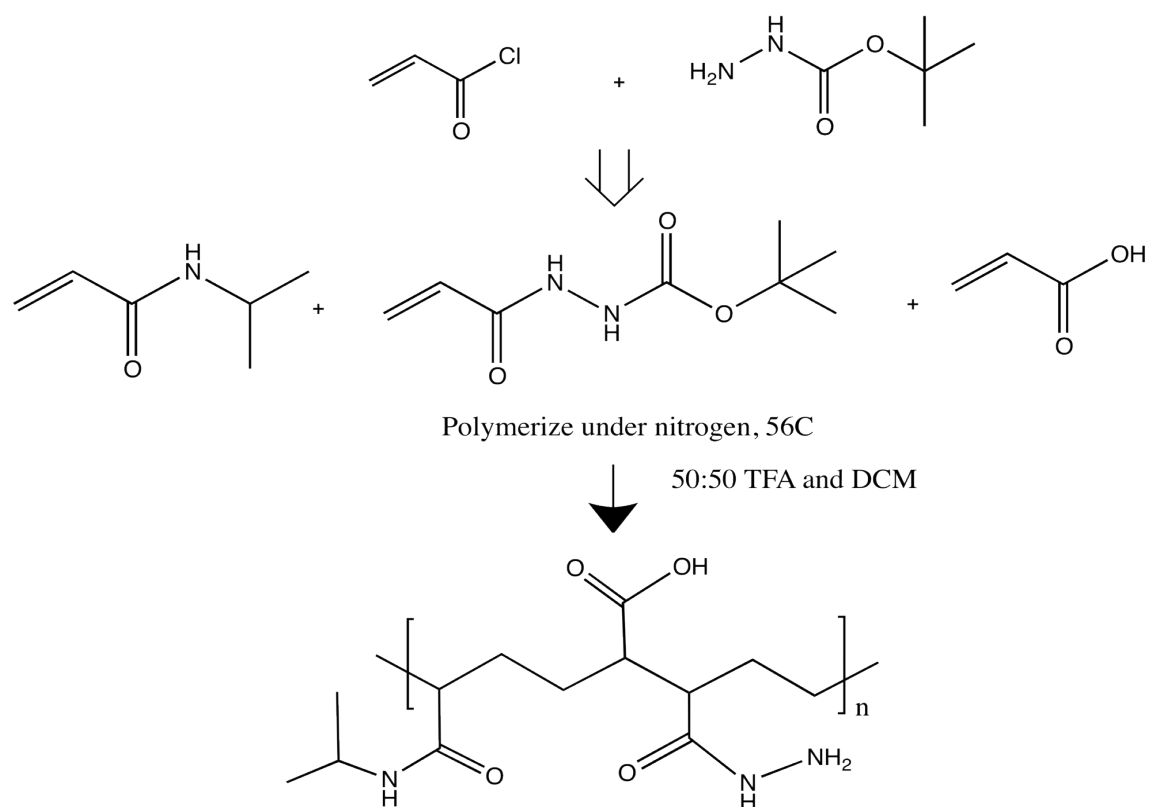


Figure S2.1: Reaction mechanism for (-)-PNIPAM-Hzd

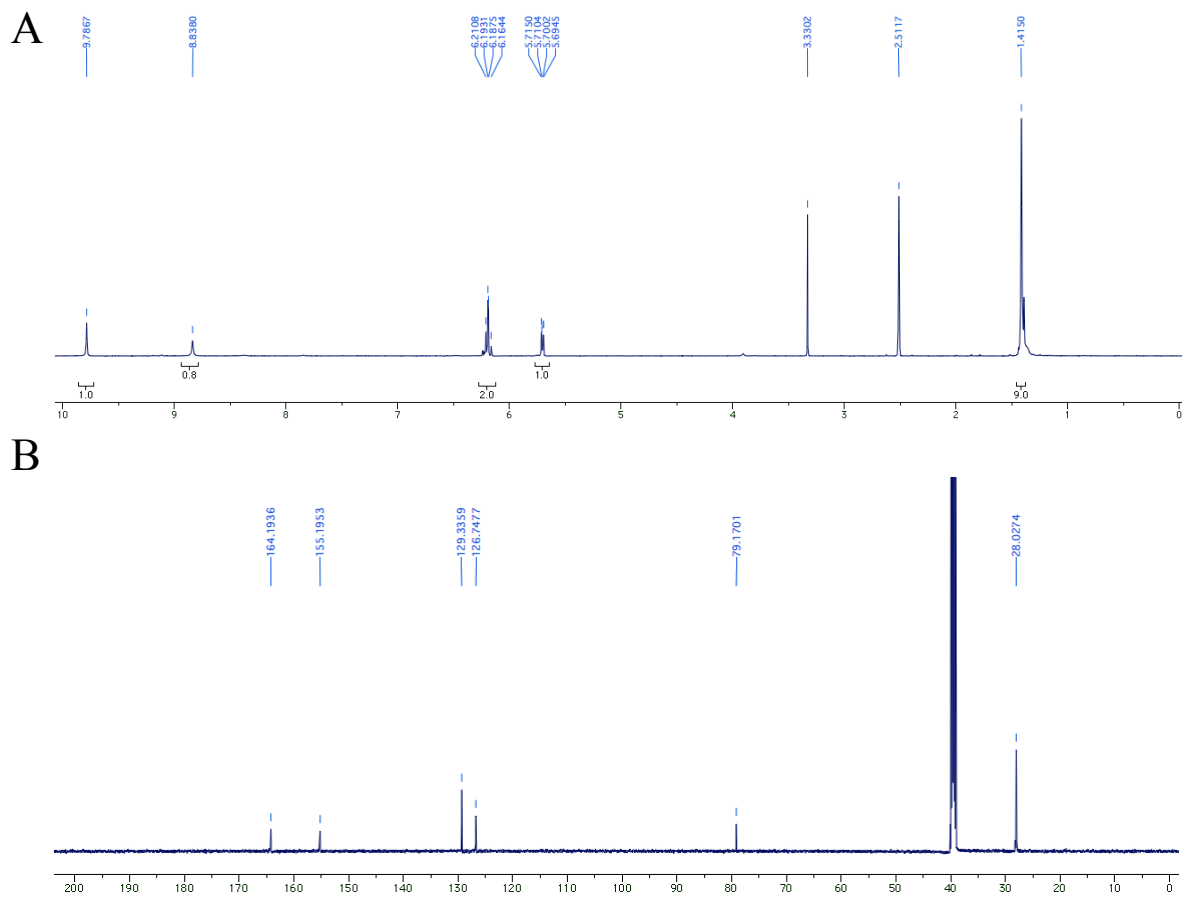


Figure S2.2: NMR spectra for acrylate hydrazide monomer: (A) ^1H NMR (600 MHz; DMSO): δ 9.79 (s, 1H), 8.84 (s, 1H), 6.21-6.16 (m, 2H), 5.71 (dd, $J = 9.2, 3.1$, 1H), 1.41 (s, 9H), (B) ^{13}C NMR (150 MHz; DMSO): 164.19, 155.20, 129.34, 126.75, 79.17, 28.03.

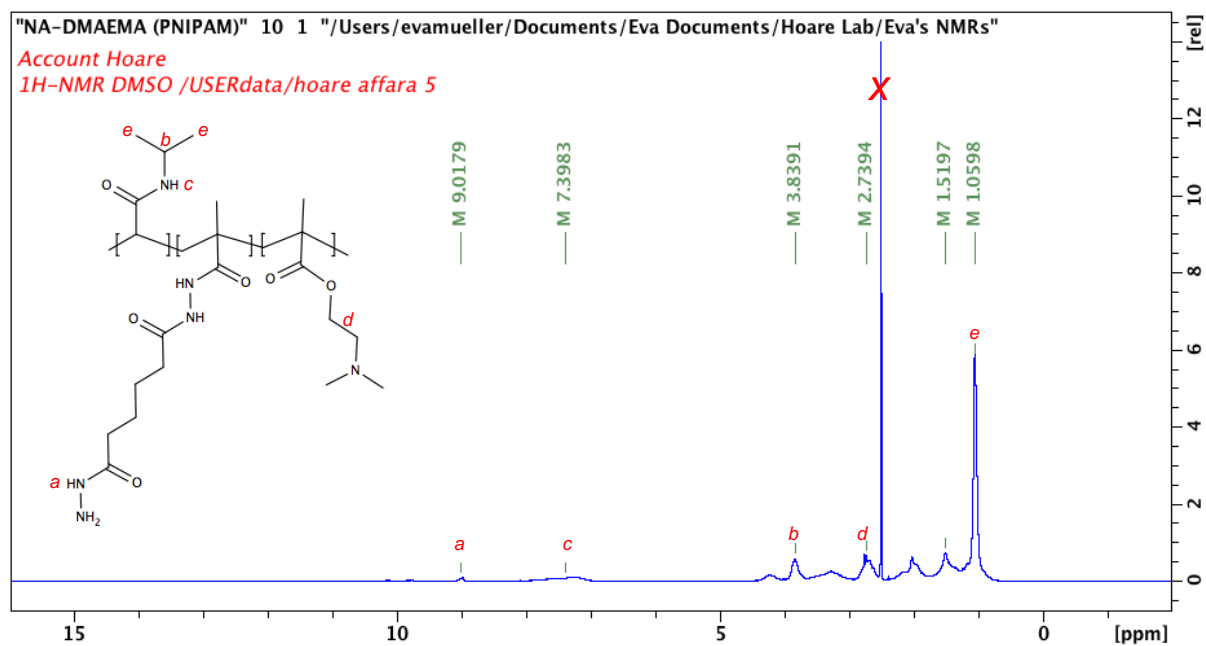


Figure S2.3: ¹H NMR for (+)-PNIPAM-Hzd

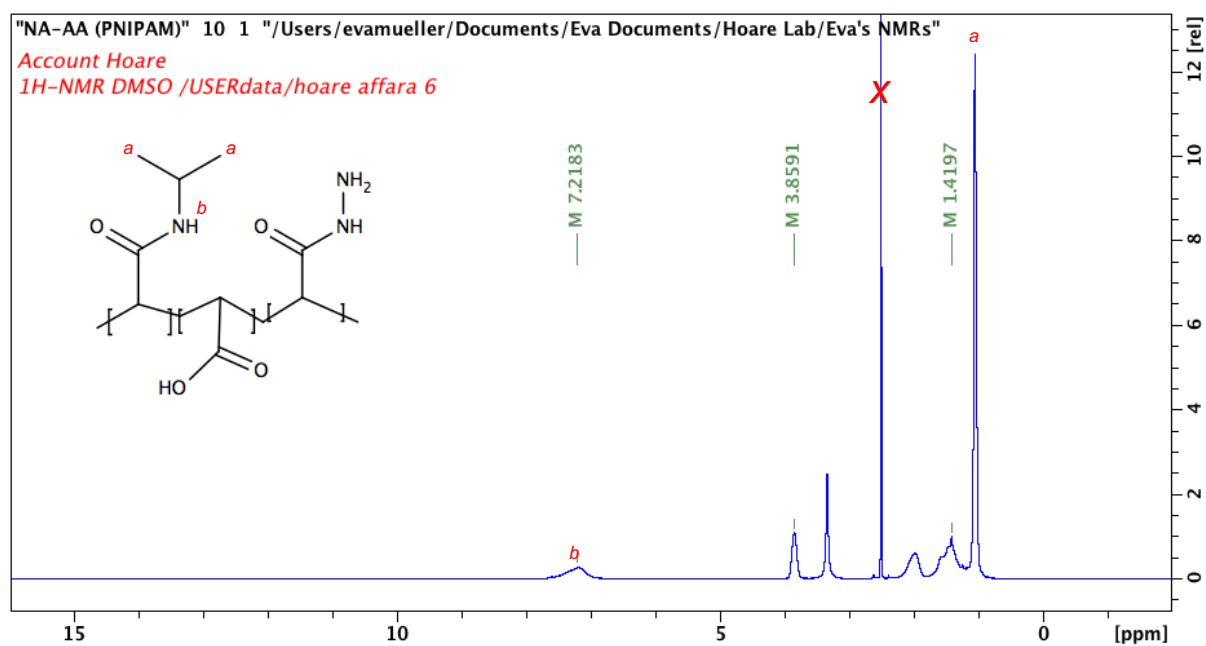


Figure S2.4: ¹H NMR for (-)-PNIPAM-Hzd

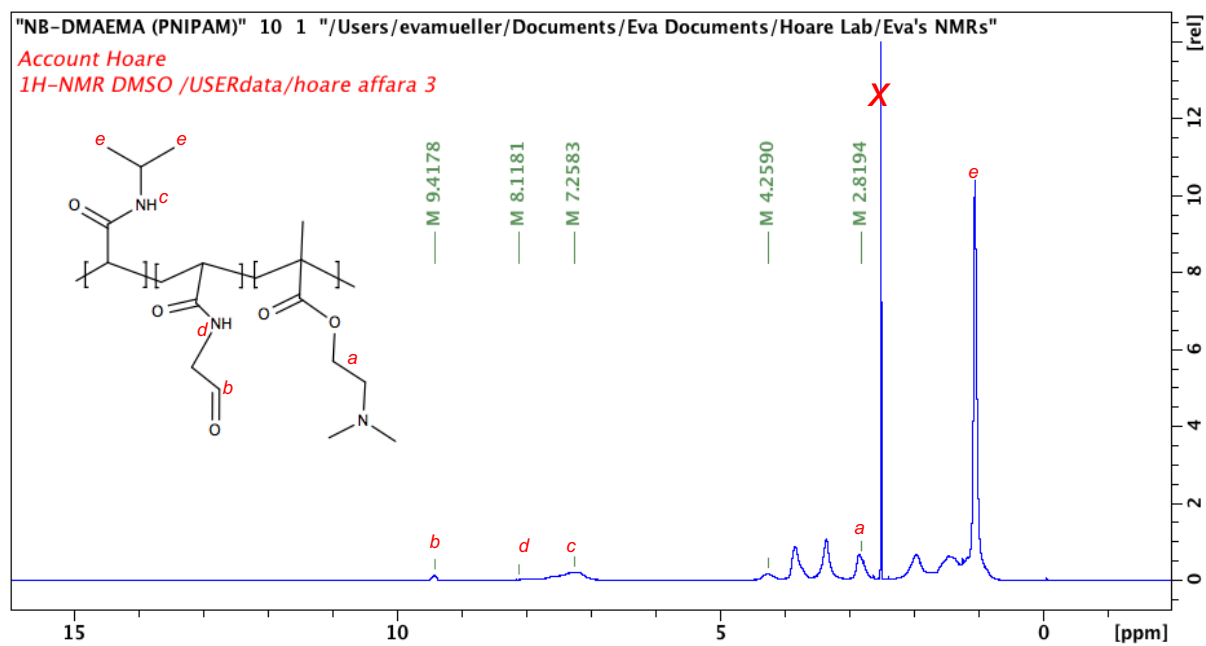


Figure S2.5: ^1H NMR for (+)-PNIPAM-Ald

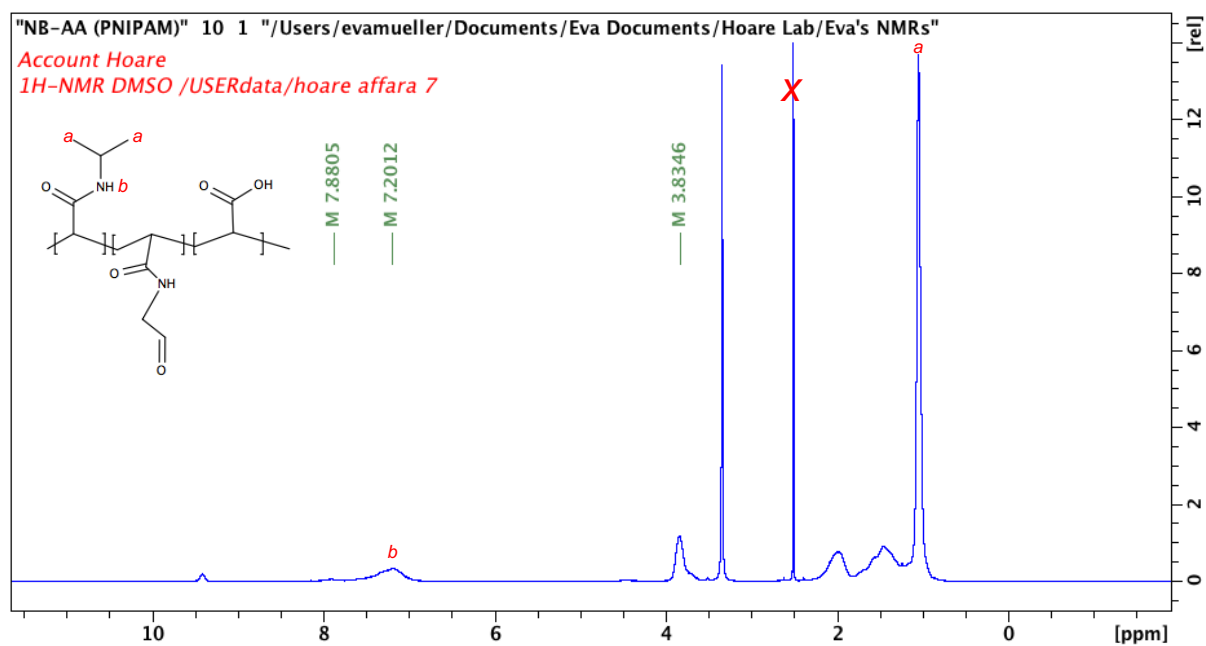


Figure S2.6: ^1H NMR for (+)-PNIPAM-Ald

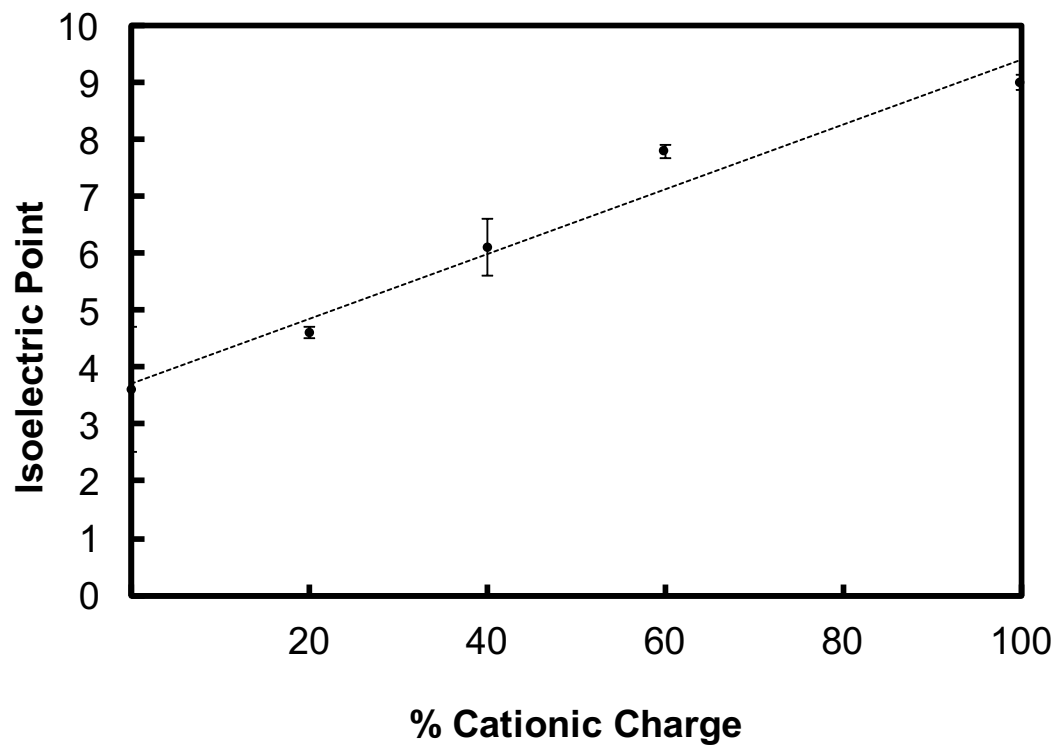


Figure S2.7: Isoelectric point as a function of % cationic charge in amphoteric self-assembled PNIPAM microgels